LUND UNIVERSITY

Multiple Antenna Terminals in Realistic Environments - A Composite Channel Modeling Approach

Harrysson, Fredrik

Published: 2012-01-01

Link to publication

Citation for published version (APA):
Harrysson, F. (2012). Multiple Antenna Terminals in Realistic Environments - A Composite Channel Modeling Approach Lund University

Multiple Antenna Terminals in Realistic Environments

A Composite Channel Modeling Approach

Doctoral Thesis

Fredrik Harrysson

Lund University
Lund, Sweden
2012

to my family and parents

Abstract

For evaluation of specific antenna arrangements in wireless communication systems we need physical channel models that take into account also the directional domain of the propagation channel. In this thesis we investigate, validate and propose a practical approach to wireless channel modeling and, particularly, to mobile communication systems. For this we make the assumption that the channel can be divided into separate parts, or regions that can be treated and modeled separately. The basic idea is that the antenna parts of the channel is the parts considered in the design of base station antennas and user equipments and can be characterized by a single measurement of each design, while the propagation part of the channel can be characterized separately, independent of the specific installed base station antenna or the user equipment, but based on generic channel sounder measurements with, as far as possible, open areas around the transmitter and the receiver antennas. For more complex antenna environments we may imagine intermediate scattering regions of the channel model between the antenna parts and the propagation part, that can or cannot be handled separately, e.g., the body of a mobile phone user, an office desk, a vehicle, surroundings of base station antennas in dense deployments, etc.

A first step in evaluating such a composite channel modeling approach is to verify the validity of communication link simulations were the mobile phone antennas together with the user can be treated as a *super-antenna* with its aggregate far-field pattern to be combined with a directional channel model in a classical way. This is first presented in Paper II, and the method is in its extensible form here referred to as a *composite channel method*. It is found that this method, as we expected, work well for statistical performance evaluation of diversity and spatial multiplexing.

An extension of the composite approach is outlined with an attempt to find a simple yet accurate directional scattering model for, firstly, the user body, and, secondly, a car environment with the user inside. A simple model that still catch the proper influence of antenna efficiency, fading statistics, and

correlation at the mobile side.

In Paper I a first investigation of user influence on an indoor 2×2 multiple-input multiple-output (MIMO) link is performed based on a narrowband measurement setup and the diversity performance is evaluated. In Paper II, the first step of the composite channel approach is evaluated with respect to MIMO by channel measurements including user influence in two static outdoor-to-indoor and indoor-to-indoor scenarios. The approach is verified for statistical properties such as antenna correlation and MIMO eigenvalue distributions. It is found, with extended detail given in Paper III that the presence of the user, apart from introducing hand and body absorption and mismatch that increases the path loss, also increases the correlation between the antenna branch signals and, thus, slightly decreases potential MIMO capacity. In Paper IV and Paper V the investigation is extended to the scenario were the user is located inside a family car (station wagon). In Paper IV a first analysis of an outdoor MIMO measurements campaign with the user outside and inside the car is presented. The results show an increased scattering inside the car that improves mainly the potential diversity gain, and to some extent also the potential MIMO capacity gain, to the cost of higher path loss (lower SNR) due to car penetration loss. An important observation is the dependency of this penetration loss on the directional properties of the outer propagation channel, which indicates a possible need for scenario dependent penetration loss in general channel modeling. In Paper V this is further verified with directional estimation of the propagation channel both outside and inside the car. We also find that the composite channel method with the inherit assumption of plane-waves impinging on the mobile terminal, actually does produce good results even in this close near-field environment inside the car with the nearby scatterers within the far-field (Rayleigh) distance of the probe antenna array.

Preface

After a Master of Science degree in electrical engineering, with a tint of semi-conductor and microwave technology, and ten years of industrial research work that took me from airborne radar antennas to mobile communication radio propagation modeling and antennas, I got the fantastic opportunity to do an industrial doctoral thesis work. An opportunity that gave me the chance to recapture and deepen my knowledge in the fields of probability theory and random processes, signal processing, communication and information theory, and much more, during my graduate studies.

The practical research work was set up to fit my present research with focus on channel modeling at the mobile or user side of cellular mobile systems. At this time, the promising potential of multiple antennas for diversity and spatial multiplexing, or MIMO, was theoretically well established and had been shown possible also in practice by various channel measurement campaigns. Results that lead to the development of MIMO channel models, e.g., the COST 259 directional channel model (DCM). However, there still remained some doubts or questions about how reliable these performance results were, and what should one expect if truly realistic environments were considered, like the hands and body of users, indoors with nearby furniture, or inside vehicles? Do we still get the high spatial multiplexing gain using MIMO that we have seen in simulations and more idealized channel measurement scenarios, how is the communication channel affected, better or worse? And, if this is important, how do we analyze it, and is it possible to model such specific environments in a simple manner that can be combined with existing directional channel models? At the time when this work started these questions were still mainly unanswered, and thus, with a little help from colleagues and supervisors, I set off a journey with the goal to find tools and answers to at least some of these questions.

The results and findings of this research journey are presented in this doctorate thesis that is comprised of two parts. The first part gives a brief introduction to the field of research, our research approach, and a summary of our scientific contributions. The second part contains three published conference

papers and two journal papers (one not yet published at the writing of this thesis). The papers included in the thesis are:

[1] F. Harrysson, H. Asplund, M. Riback, and A. Derneryd, "Dual antenna terminals in an indoor scenario," in *IEEE Veh. Technol. Conf. VTC 2006-Spring*, vol. 6, pp. 2737–2741, Melbourne, Australia, May 2006.

[2] F. Harrysson, J. Medbo, A. F. Molisch, A. J. Johansson, and F. Tufvesson, "Efficient experimental evaluation of a MIMO handset with user influence," in *IEEE Trans. Wireless Commun.*, vol. 9, no. 2, pp. 853–863, Feb. 2010.

[3] F. Harrysson, A. Derneryd, and F. Tufvesson, "Evaluation of user hand and body impact on multiple antenna handset performance," in *IEEE Int. Symp. on Antennas and Propagation AP-S 2010*, Toronto, Canada, July 2010.

[4] F. Harrysson, T. Hult, and F. Tufvesson, "Evaluation of an outdoor-to-in-car radio channel with a four-antenna handset and a user phantom," in *IEEE Veh. Technol. Conf. VTC 2011-Fall*, San Francisco, CA, Sept. 2011.

[5] F. Harrysson, J. Medbo, T. Hult, and F. Tufvesson, "Experimental investigation of the directional outdoor-to-in-car propagation channel," (Submitted to *IEEE Trans. Veh. Technol.*, April 2012).

Before and during my graduate studies, I have also contributed to the following publications, though they are not included in the thesis:

[7] F. Harrysson, "Analysis of a large array antenna with circular waveguide elements," in *IEEE Int. Symp. on Antennas and Propagation AP-S 1998*, vol. 2, pp. 1016-1019, Atlanta, GA, June 1998.

[8] F. Harrysson and J.-E. Berg, "Propagation prediction at 2.5 GHz close to a roof mounted antenna in an urban environment," in *Proc. IEEE Veh. Technol. Conf. VTC 2001-Fall*, vol. 3, pp. 1261–1263, Atlantic City, NJ, Oct. 2001.

[9] F. Harrysson, "A simple directional path loss model for a terminal inside a car," in *Proc. IEEE Veh. Technol. Conf. VTC 2003-Fall*, vol. 1, pp. 119–122, Boston, MA, Oct. 2003.

[10] J. Medbo, F. Harrysson, H. Asplund, and J.-E. Berg, "Measurements and analysis of a MIMO macrocell outdoor-indoor scenario at 1947 MHz," in *Proc. IEEE Veh. Technol. Conf. VTC 2004-Spring*, vol. 1, pp. 261–265, Milan, Italy, May 2004.

[11] J. Medbo, J.-E. Berg, and F. Harrysson, "Temporal radio channel variations with stationary terminal," in *Proc. IEEE Veh. Technol. Conf. VTC 2004-Fall*, vol. 1, pp. 91–95 Vol. 1, Los Angeles, CA, Sept. 2004.

[12] M. Riback, J. Medbo, J.-E. Berg, F. Harrysson, and H. Asplund, "Carrier frequency effects on path loss," in *Proc. IEEE Veh. Technol. Conf. VTC 2006-Spring*, vol. 6, pp. 2717–2721, Melbourne, Australia, May 2006.

[13] F. Harrysson, L. Manholm, H. Asplund, M. Riback, and A. Derneryd, "Performance of two test terminals with dual antennas in an office environment," in *Antenn 06-The Nordic Antenna Symposium*, Linköping, Sweden, May 30 – June 1 2006.

[14] F. Harrysson, J. Medbo, and A. F. Molisch, "Performance of a MIMO terminal including a user phantom in a stationary micro-cell scenario with comparison between a ray-based method and direct measurements," TD (07) 379, COST 2100, Duisburg, Germany, Sept. 2007.

[15] H. Asplund, J.-E. Berg, F. Harrysson, J. Medbo, and M. Riback, "Propagation characteristics of polarized radio waves in cellular communications," in *Proc. IEEE Veh. Technol. Conf. VTC 2007-Fall*, pp. 839–843, Baltimore, MD, Sept. 2007.

[16] F. Harrysson, J. Medbo, A. F. Molisch, A. J. Johansson, and F. Tufvesson, "The composite channel method: Efficient experimental evaluation of a realistic MIMO terminal in the presence of a human body," in *Veh. Technol. Conf. VTC 2008-Spring*, pp. 473–477, Singapore, May 2008.

[17] F. Harrysson, J. Medbo, and A. F. Molisch, "Indoor performance of a MIMO handset including user influence by comparing a composite channel method with direct measurements," TD (08) 661, COST 2100, Lille, France, Oct. 2008.

[18] F. Harrysson, A. Derneryd, and F. Tufvesson, "Evaluation of user hand and body impact on multiple antenna handset performance," TD (10) 12035, COST 2100, Bologna, Italy, Nov. 2010.

[19] J. Medbo, and F. Harrysson, "Efficiency and accuracy enhanced super resolved channel estimation," Proceedings of the 6th European Conference on Antennas and Propagation (EuCAP), Prague, Czech Republic, March 2012.

Acknowledgments

I would like to express my deepest gratitude to a number of people of great importance for this work.

First of all my main advisor Dr. Fredrik Tufvesson and my former main advisor Prof. Andreas F. Molisch for giving me the opportunity to work under their supervision. Their wide knowledge of wireless communication provides great inspiration. You have taught me a great deal about scientific work and not least about scientific writing. I am also grateful to my co-advisors Dr. Anders J. Johansson and Prof. Ove Edfors, who has provided vital support in scientific matters and also in numerous administrative issues.

I also would like to specifically recognize my co-advisor and colleague at Ericsson Research, Prof. Anders Derneryd who encouraged me to embark this journey and always seem to have time for support and discussions, and my manager Björn Johannisson together with Jan-Erik Berg, who both supported the idea. Anders and Jan-Erik has through my years at Ericsson been great sources of inspiration and motivation.

Thanks also to my other colleagues at Ericsson Research; Dr. Jonas Medbo who put in a lot of effort into the channel measurements and channel analyses, Henrik Asplund and Mathias Riback who also helped with channel measurements, Dr. Jonas Fridén, Dr. Anders Stjernman, Lars Manholm, Dr. Fredrik Athley, Dr. Martin Johansson, Martin Siegbahn and many more, and at the university; Dr. Shurjeel Wyne, Dr. Johan Kåredal, Dr. Tommy Hult, Dr. Vanja Plicanic Samuelsson, Dr. Buon Kiong Lau, Dr. Andrés Alayon Glazunov, Dr. Peter Almers, Gunnar Eriksson, Dr Ruiyuan Tien, and many more, for help and many discussions from which I have gained a lot. A special thanks also to Lars Hedenstjerna for the excellent measurement fixtures, Martin Nilsson for electronic masterpieces, and to Birgitta Holmgren, Pia Bruhn, and Doris Glöck for help with administrative matters.

I would also like to express my gratitude to Thomas Bolin, Zhinong Ying and Dmytro Pugachov at Sony-Ericsson Mobile Communications AB who helped me with the terminal antenna measurements and let me use their measurement range, and to Thomas Kornback at RUAG Space AB for help with the mea-

surement of the cylindrical array antenna. Thanks also to professors and PhD students of the Institution for Signals and Systems at Chalmers University for letting me take some of my courses there.

Furthermore, I would like to thank Dr Tim Brown for taking the time to be the faculty opponent at my thesis defence, Prof. Alain Sibille, Prof. Jan Carlsson, and Prof. Anders Sunesson for agreeing to be the members of the examination board.

This work has been financed within my employment at Ericsson AB, and was supported by a grant from the Swedish Science Council (Vetenskapsrådet).

Finally, I am also eternally grateful for the support and patience of my family - my wife Katarina, and our two boys Oskar and William.

Fredrik Harrysson

Lund, May 2012

List of Acronyms and Abbreviations

3GPP 3rd Generation Partnership Project

ASD angular spectral domain

BS base station

CENELEC European Committee for Electrotechnical Standardization

COST European Cooperation in Science and Technology

D2D direction-to-direction

DCM directional channel model

DDPC double-directional propagation channel

DFT discrete Fourier transform

DGBE diethylene glycol butyl ether

DOA direction-of-arrival

DOD direction-of-departure

DRA dielectric resonator antenna

EMCAD electromagnetic computer aided design

FCC Federal Communications Commission

FDTD finite difference time domain

FFT fast Fourier transform

GO geometrical optics

GSCM geometry-based stochastic channel model

GTD geometrical theory of diffraction

I2I indoor to indoor

ICNIRP International Commission on Non-Ionizing Radiation Protection

IEEE Institute of Electrical and Electronics Engineers

IF intermediate frequency

IMT International Mobile Telecommunications

ISC ideal selection combining

ITU International Telecommunication Union

LNA low-noise amplifier

LOS line-of-sight

LTE Long Term Evolution

MEG mean effective gain

MIMO multiple-input multiple-output

ML maximum likelihood

MPC multi-path component

MRC maximum ratio combining

MS mobile station

MUX multiplexer

O2I outdoor to indoor

OFDM orthogonal frequency division multiplexing

P2D point-to-direction

P2P point-to-point

PDA personal digital assistant

PIFA planar inverted-F antenna

RF radio frequency

RMS root mean square

RX receiver

RxPUCA Rx patch uniform cylindrical array

SAGE Space Alternating Generalized Expectation Maximization

SAM Specific Anthropomorphic Mannequin

SAR Specific Absorption Rate

SCM spatial channel model

SISO single-input single-output

SM spatial multiplexing

SNR signal-to-noise ratio

SVD singular value decomposition

SVM spherical vector modes

TX transmitter

TxPURA Tx patch uniform rectangular array

UE user equipment

ULA uniform linear array

UTD uniform theory of diffraction

V2I vehicle to infrastructure

V2V vehicle to vehicle

VNA vector network analyzer

WINNER Wireless World Initiative New Radio

WLAN wireless local area network

Contents

Part I

Overview of Research Field and Problem Approach

Chapter 1

Introduction

Electromagnetic wave propagation is, of course, the most essential property of most radio and microwave systems for, e.g., wireless communication, radar, radio astronomy etc. Thanks to the 19th century physicists and experimentalists like James Clerk Maxwell, Heinrich Rudolf Hertz, Nikola Tesla, Guiglielmo Marconi and Stepanovich Popov *et al.*, we know in principle how radio waves propagate, how they are generated, how to transmit and receive them, and how to utilize them to communicate information. Later, in the 20th century, thanks to information, communication and signal processing scientists like Claude Shannon *et al.*, we learned how to communicate more efficiently using improved modulation, digital communication and coding techniques, also over a channel with large receiver noise and/or interference.

However, radio waves would be completely useless for transferring information without the antennas to radiate and receive the energy they carry. In some situations we need only one antenna, e.g., in a microwave oven we only need one radiating unit to heat the food by absorbed radio waves, and in radio astronomy we only need one receiving unit to identify the emitted radio waves from distant astronomical objects. However, in a wireless communication system we always need at least two antennas that are separated in space, one at the transmitter and one at the receiver side.

An antenna may be used for both transmitting and receiving signals, e.g., as in most radar and cellular applications. It is often assumed that the antenna is a linear passive component that contains isotropic materials, making it by default *reciprocal*. This means that the characteristics of the antenna are independent of whether it is transmitting or receiving. Thus, for simplicity, it is common practice for antenna engineers to always refer to an antenna as a transmitting unit. If nothing else is stated, this is also the practice in this thesis.

The main property of the antenna is to provide efficient transition of radio waves from a transmission line into open-space propagation or vice versa. This quality is quantified by the *radiation efficiency*[1]. The second but equally important property of the antenna, and perhaps the property that to most radio engineers actually define the antenna, is that it radiates or receives radio waves with some distribution in direction and polarization. The latter is referred to as the *antenna pattern* or *radiation pattern*[2] and is often considered in the *far-field region*[3].

Between the two antennas we have the (wireless) *propagation channel*, referring to the propagating radio waves, generated at the transmitter (TX) side antenna and impinging towards the receiver (RX) antenna. The simplest form of a wireless propagation channel is the line-of-sight (LOS) channel where a radio wave propagate in free space (often assumed to be identical to vacuum), expanding spherically, from the TX to the RX antenna. A more complicated situation occurs if the radio waves are obstructed by an object causing *shadow fading* or find several paths through a complex environment with a variety of several scattering obstacles. The latter case is called a *multi-path* channel and the components of the channel that constitutes the multiply propagated wave-fronts are referred to as the multi-path components (MPCs). Temporal constructive and destructive addition of such complex MPCs (the phase depend on the path length) give rise to *small-scale fading* while the much slower shadow fading is termed *large-scale fading.*

The TX and RX antennas together with the propagation channel form the *radio channel.* By incorporating up/down-converting of frequency to baseband, modulation/demodulation, coding and detection, etc., we get the *information-theoretic channel.* However, in this thesis we mainly deal with the radio channel and use information theoretic entities like the *channel capacity* only for evaluation of potential system performances. The channel is considered by time-harmonic field propagation (i.e., we neglect time transient effects) and is thus characterized by the analog complex vector properties amplitude, phase and polarization. We also refer to a few different types of channels depending on if there is movement in the channel or not. In a *static radio channel* the antennas and all obstacles in the propagation channel are completely still relative to each other, while in a *dynamic radio channel* one of or both the antennas are moving relative the environment, or the environment is changing with time.

---

[1] "The ratio of the total power radiated by an antenna to the net power accepted by the antenna from the connected transmitter." [42]

[2] "The spatial distribution of a quantity that characterizes the electromagnetic field generated by an antenna." [42]

[3] "That region of the field of an antenna where the angular field distribution is essentially independent of the distance from a specified point in the antenna region." [42]

There are a variety of methods to model the radio channel for wireless communications, and the appropriate choice depends on the situation. Simple statistical fading models like the Rayleigh and Rice distributions for single antenna or single-input single-output (SISO) channels and the correlation-based models like the Kronecker model for multiple antenna or multiple-input multiple-output (MIMO) systems, are very popular due to the simplicity and speed when it comes to system simulations. Nevertheless, for evaluation of specific antenna arrangements we need physical channel models that describe the directional domain, e.g., the COST 259 directional channel model (DCM) [10,66] and the 3GPP SCM [1] that combine a plane-wave multi-path cluster model for the propagation channel with the possibility to insert antenna patterns for test antennas of interest. These models use the classical assumption that a far-field antenna pattern can readily be combined with a directional multi-path propagation channel characterized by its plane-wave spectrum. Such an assumption rely on that all obstacles in the propagation channel can be considered to be in the far-field region of the antennas. But what if this is not true? A mobile phone in the hand of a user that sits at the office desk indoor with the base station (BS) at the roof-top of a house a few blocks away in a dense urban environment should be a quite common scenario in todays cellular networks.

When people talk about "antennas" in mobile devices, such as mobile phones or lap-top computers, they often refer to the little piece of dielectric material in combination with some bent metal piece, a PIFA (planar inverted F-antenna) or a DRA (dielectric resonator antenna) etc., positioned at the edge of a ground plane inside the device, e.g., as in [105]. In fact, this little piece is only part of the antenna, serving as a feed and matching unit. The antenna, as characterized by its far-field, is really the whole structure since currents may flow all over the ground plane of the phone[4].

In the case of a mobile phone in cellular communication systems, the user hand and body absorbs radiated energy and the fingers induce impedance mismatch as they may touch very close to the antenna elements. In fact, we can just as well call the whole body an antenna – a *super-antenna*. And what about other obstacles in the environment very close to the mobile phone antenna, like when the user enters a car or another vehicle like a buss or a train, or in indoor scenarios with furniture and other objects very close to the mobile?

The questions are: "What is the antenna part and what is the propagation part of the channel?", "Is it possible and/or necessary to separate the channel into parts in channel modeling?", "How do we deal with the interfaces between the components?". These questions are exactly the questions we would like to answer or at least stress in this thesis and to some extent discuss based on

---

[4]Which, to be precise, is not really a ground plane since it is not necessarily connected to a ground. Instead this is sometimes referred to as a *counterpoise*.

some prior results and some recent research. Especially, we concentrate on the MIMO case where we study multiple antenna terminals in, what we consider, *realistic scenarios.*

We also test and evaluate a simple practical approach to channel modeling in, particularly, mobile communication systems by an assumption that the channel can be divided into separate parts or regions that can be treated and modeled individually. In short the idea is that the antenna part can be the part considered in design of the user equipment (UE) and can be characterized by single measurements, while the propagation channel can be characterized by, e.g., measurements with open areas around the BS and mobile station (MS) positions. The intermediate regions would encounter the *scattering environments* to the BS and MS, e.g., obstructing building structures, the office desk or a vehicle. Such a model approach is here termed a *composite channel approach.*

The subsequent chapters of Part I are organized as follows; Chapter 2 contains an overview of multiple antenna techniques, Chapter 3 give the background to physical channel modeling and the multi-path propagation channel, Chapter 5 presents a composite channel approach to channel modeling, and Chapter 6 wraps up Part I with brief presentations of the included papers and some general conclusions. Part II of the thesis contains the included papers.

Chapter 2

Multiple Antenna Techniques

Multiple element antennas, or antenna arrays, were originally used in, e.g., mobile communication systems at the base station side, providing mainly an efficient and flexible design process where the antennas can be configured with respect to gain, beam-width, and electrical beam tilt. However, in this sense an array antenna is still a single antenna function with only one feed/receive port.

With the use of multiple antennas with a multiple amount of individually accessible feed/receive ports, system capacity can be improved in fading multipath channels by the use of spatial *diversity* techniques, adaptive *beam-forming*, and *spatial multiplexing* [7]. The latter is often the beneficial characteristic that is referred to by using the term MIMO but is more specific since the term MIMO could account for any system or channel with multiple ports at both ends of the link. In fact all these techniques can be considered as beam-forming if one may accept a generalization of the term *beam* to represent an arbitrary (but specific) array antenna radiation pattern related to a complex antenna array element weight vector (or steering vector). Spatial, directional and/or polarization diversity is equivalent to single-sided TX or RX beam-forming, with selection combining by binary weights, equal gain combining by phase-only weights, and maximum ratio combining (MRC) by complex weights. In the same manner, certain forms of spatial multiplexing (SM) can be considered as superimposed multiple layers joint TX and RX beam-forming, e.g., by using the complex MIMO channel singular vectors, found from singular value decomposition of the channel matrix, as steering or *precoding* vectors. This

physical point-of-view on MIMO and particularly on SM are very appealing to radio frequency (RF) antenna and propagation engineers with experience in array antenna technology.

2.1   Diversity

In a multi-path radio channel the signal at the RX is composed of individually attenuated and phase-shifted replicas of the transmitted signal, arriving from different directions. The replicas may add up in a constructive or a destructive manner as a function of time, giving rise to fluctuations in the received signal. These fluctuations, or rather when we observe the dips in the fluctuations, is what we refer to as signal *fading*. Fading may cause severe instantaneous dips (fades) in the signal level at the receiver that reduce the information throughput of the system. However, due to the statistical nature of a mobile channel, we can utilize the fact that the probability that the signal level is low at more than one signal port at the same time is very low. This technique to combat fading is termed *diversity*.

Diversity can be applied in a number of domains; e.g., the frequency domain as in frequency-hopping and coded orthogonal frequency division multiplexing (OFDM), the time domain as in repetitive coding, or the spatial (space) domain by using multiple antennas. In this context we focus on multiple antenna techniques that utilize the spatial and polarization domains of the radio channel. Several identical antennas can be spread out in space so that the fading at each antenna location is independent, or the antennas may have orthogonal radiation patterns or polarization providing diversity [26, 58]. For antennas in a limited volume such as the casing of a mobile phone these properties get indistinguishable [17].

A spatial diversity system can consist of a sensor system that; with some interval detect and switch to the antenna with the highest signal level (selection diversity), or at a drop below a certain threshold switch antenna port by some predefined pattern (switch diversity). An even more sophisticated spatial diversity system combines the antenna signals with appropriate phase weights (equal gain combining) or, optimally, with amplitude and phase weights (maximum ratio combining) to maximize the signal strength. An early overview and analysis of space diversity methods can be found in [16].

With channel state information at the TX, all these diversity techniques can be utilized in the same way also at the transmitter side providing dual-side diversity.

2.2 Adaptive Beam-forming

With *adaptive beam-forming* we address the case of accessible multiple antenna array feed or receive port signals that can be individually weighted with respect to amplitude and phase. The benefit of such arrays is often quantified by the *array gain* which is the amplification of the signal arriving or departing from/in a certain direction due to coherent (in-phase) combination over the array element signals which increase the channel signal-to-noise ratio (SNR) [8]. In a general sense, considering a beam as just any spatial filter or radiation pattern corresponding to the element signal weights of an array antenna, the diversity technique "maximal ratio combining" is a beam-forming technique where the beam is chosen to compensate for the phase-shifts (and magnitude differences) in the arriving waves. Also the other previously mentioned diversity techniques are in a general sense beam-forming, e.g., selection diversity that correspond to a weight vector with a single one and all other zero, and equal gain combining that is the same as phase-only beam-forming. Beam-forming at the transmitter and receiver is in principle the same thing, but with the important distinction that at the transmitter it determines the directions of the radiated power.

2.3 Spatial Multiplexing

The capacity of a SISO channel (wired or flat fading wireless) with limited frequency bandwidth (W) and in the presence of white Gaussian noise is determined by the logarithm of the receiver SNR (γ) as [21, (9.62)]

$$C = W \log_2 (1 + \gamma) \tag{2.1}$$

This is the channel capacity that defines the theoretical upper limit of the information rate in a communication channel. Now, if the available power at the TX can be allocated to several parallel channels, i.e., a MIMO system, the capacity on each sub-channel will decrease logarithmically as the signal power is divided onto several transmitters. At the same time the total capacity will increase linearly as the sum over the number of sub-channels. If the power allocation is chosen carefully in relation to the quality of the channel branches, the MIMO system will always beat (or equal) the SISO system capacity. The optimum power allocation technique is done by *water filling* [21, pp. 274–277].

In a wireless communication system the MIMO technique is explored by using multiple antennas at both the TX and the RX side of the link. In this case the transmitted radio signals are not in general separated by transmission lines or by a large distance in space, but may be subject to multi-path propagation

through complex environments. Nevertheless, by using the spatial filtering property of antenna arrays together with the concept of super-position, it is possible to find multiple channel branches in such an environment, and the MIMO capacity can be explored. This technique to utilize the available signal power in an optimum way by utilizing the multiple parallel channels available in a multi-path environment is called spatial multiplexing (SM) and the great benefits regarding channel capacity was originally shown for Gaussian channels in [31, 91, 100].

Chapter 3

Wireless Channel Modeling

A channel model is a function that maps the signal from the TX to the RX in a sufficiently accurate way. This function may be a stochastic process, a deterministic function or even a set of empirical or directly recorded data.

The two main applications of a channel model in mobile communication are wireless system simulations and optimization of a specific wireless network. In system simulations location independent stochastic or semi-stochastic models are often preferred since the simulations aim at optimizing systems performance in general, while location dependent, site-specific, or empirical models, are required for network planning and deployments. Channel models is also divided into narrowband or wideband models, stationary or non-stationary models, directional models (or not), single or multipath models, and single or multiple antenna (MIMO) models [65]. Comprehensive overviews of MIMO channel models can be found in [5, 99].

3.1 Physical Channel Modeling

Depending on the complexity of the channel model, a certain amount of details in the channel phenomena are considered, such as time and space clustering, Doppler frequency shift, etc. Models that encounter such physical properties are called physical channel models since they may capture the specific propagation phenomena of a certain site-specific or typical environment.

Furthermore, for evaluation of antenna properties in general and for antenna arrays in particular, directional propagation models are essential since the great benefit of multiple antennas is the ability to exploit the spatial domain.

3.1.1 Deterministic Propagation Models

The most detailed class of physical channel models are the electro-magnetic full-wave models with comprehensive geometrical and material descriptions of the antennas, and the scattering and propagation environments. Such a model is a deterministic model for site-specific evaluations that uses a specific geometrical description of the environment. The propagation part may be handled by, e.g., high-frequency approximation methods such as ray-tracing [96] and ray-launching [54] techniques utilizing the laws of geometrical optics (GO) and diffraction techniques such as the geometrical theory of diffraction (GTD) [45] and the uniform theory of diffraction (UTD) [47, 56]. The UTD method for dielectric wedges has been shown to be able to accurately model real building corner diffraction [9], rough edges [25], and combined with GO it is found in [39] to be able to also quite accurately predict the path-loss in an urban environment nearby the BS.

A problem with the UTD model is its inability to model multiple diffractions which is important when the distance between the BS and the MS increases and there are many obstructing buildings in between. There are extensions to the UTD method that tries to solve this problem [6, 95]. Others methods use simplified heuristic knife-edge models that are computer efficient and well suited for path loss calculations in network planning when the distance between base station are large and the channel include many obstructing buildings between the BS and the MS, e.g., [12, 13]. An overview of various models can be find in, e.g., [97].

3.1.2 Empirical Propagation Models

Another type of physical channel models are the models based on measurement records. These models are truly site-specific, but an ensemble of such measurements may be used to extract typical channel parameters that can be used in cell-planning tools (e.g., the popular Okumura-Hata model [41]) or in the geometry-based stochastic models COST 273 DCM and the semi-stochastic 3GPP SCM.

In contrast to the full-wave models that include all the interaction of a propagating wave traveling from the TX to the RX, the directional empirical model only account for what is seen from the TX and the RX antennas, respectively. To capture the directional properties the propagation measurements has to be; i) measured with rotating highly directional probe antennas, or ii) measured with array antennas in an omni-directional fashion or, if the channel is static, with a (wide-beam) antenna and positioning robots. In the latter case the directional properties of the channel is extracted by signal post-processing.
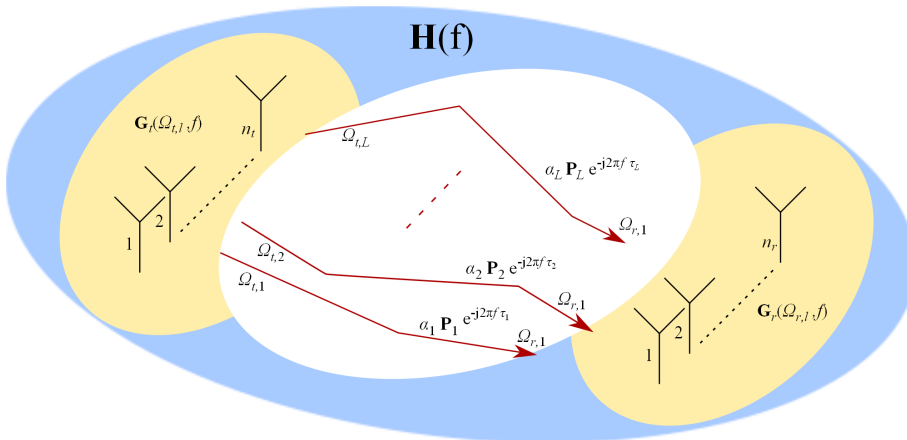
Figure 3.1: Illustration of MIMO and the double-directional propagation channel with transmit and receive antenna arrays.

3.2 The Double-Directional Propagation Channel

For multiple-antenna performance evaluations, the full double-directional propagation channel (DDPC) model [88] is a preferable tool to produce realistic channel statistics [5] and to evaluate channel capacity, even if alternative simplified models utilizing the correlation-based Kronecker model has been proposed [46, 59, 84, 87], and also questioned for their inability model the joint correlation between BS and MS elements in a MIMO channels [72, 98]. The DDPC model describes the channel by a finite number of MPCs, originating at the TX and terminating at the RX, see Figure 3.1. Even though the MPCs represent the radio waves propagating through the environment, subject to reflection, scattering, and diffraction; the DDPC does not (and need not) include the information about these interactions. Only the direction-of-departure (DOD) and the corresponding direction-of-arrival (DOA), the delay, the complex amplitude and the polarization of each MPC are considered.

3.3 The MIMO Channel

With multiple antennas at both ends of a wireless communication link, the channel representation becomes a matrix that includes properties like the (intra

and inter) correlation between the TX and RX antenna elements, and the possibility to resolve parallel sub-channels for spatial multiplexing by singular value decomposition (SVD). With a directional channel representation, like a full-wave ray tracing solution or the DDPC model, the antenna independent propagation channel is completely characterized as seen from the antennas. Thus, the full channel transfer matrix for arbitrary TX and RX antenna arrays (once characterized by their radiation patterns) can be found. Since many full wave propagation solutions as well as many measured MIMO channels, can approximately be represented by the DDPC model, we can in general write the frequency-domain multi-path MIMO channel transfer matrix as

$$\mathbf{H}(f) = \sum_{l=1}^{L} \alpha_l \mathbf{G}_r^T(\Omega_{r,l}, f) \mathbf{P}_l \mathbf{G}_t(\Omega_{t,l}, f) e^{-j2\pi f \tau_l}, \tag{3.1}$$

whose elements $H_{ij}(f)$ describe the transfer function from the j-th transmit to the i-th receive antenna element. The expression (3.1) includes a sum over the L MPCs, with the TX and RX antenna far-field matrices in $\mathbf{G}_t$ and $\mathbf{G}_r$ and the polarimetric transfer matrix $\mathbf{P}_l$. Here $\mathbf{G}_t$ and $\mathbf{G}_r$ have to contain the array location vector phase term for each element in the columns, and for the polarization component (θ, ϕ) in the rows, i.e., $2 \times n_{r,t}$.

The MPCs in (3.1) are independent of the Tx and Rx antennas, and the l-th one has the following DDPC parameters:

α_l amplitude and phase

$\Omega_{t,l}$ direction of departure (DOD)

$\Omega_{r,l}$ direction of arrival (DOA)

τ_l path delay.

The polarimetric transfer matrix of the l-th MPC can be written as

$$\mathbf{P}_l = \left[\begin{array}{cc} P_{\theta,\theta} & P_{\theta,\phi} \\ P_{\phi,\theta} & P_{\phi,\phi} \end{array} \right]$$

which is normalized in relation to the complex amplitude α_l, e.g., to have unit Frobenius norm. In the DDPC model the frequency dependency is taken into account only in the phase factors representing the plane-wave path distances $e^{-j2\pi f \tau_l}$.

The expression in (3.1) seems general since it combines any antenna array with a directional channel model. However, the model in (3.1) assumes that the

arriving signal[1] can be represented by a finite spectrum of plane waves. This
is only true if we consider interacting obstacles (scatterers) at large enough
distance from the RX antennas, i.e., if the obstacles are in the far-field of the
antennas array.

3.4   MIMO Channel Measurements

Channel models usually depend on measurements in some way, or "any chan-
nel model is based on channel measurement data" [65]. Even the most simple
statistic channel model with only a few model parameters needs input or ver-
ification from measured scenarios to be valid. Different measurement setups
(disregarding the vast amount of possible measurements scenarios) are used de-
pending on the parameters to be investigated, from the simplest non-coherent
narrowband setups for path loss and fading statistics measurements, to complex
wideband systems with multiple array antennas for delay and direction esti-
mation, or even with multiple radio chains for direct fast time-variant MIMO
channel measurements.

In the work presented in the included papers, we have used three differ-
ent setups: a coherent narrowband vector network analyzer (VNA) setup for
direct 2×2-MIMO channel measurements (Paper I), a wideband VNA setup
with virtual arrays for DDPC parameter estimation and 8×4-MIMO channel
measurements (Paper II and Paper III), and the RUSK Lund MIMO channel
sounder from Medav (Paper IV and Paper V). The three different setups are
described below.

3.4.1   Narrowband 2-Port Vector Network Analyzer Mea-
surements with Frequency Offset

A VNA is commonly used in different channel measurement setups, mainly
since it is available in many radio labs and, hence, easily accessible. The
VNA is a versatile equipment with many possibilities and features that may be
utilized depending on the scenario and channel characteristics of interest. In the
measurements described in Paper I the VNA is set up for coherent detection of
two simultaneous narrowband signals generated by two signal generators with
a frequency separation of 500 Hz with no phase reference between TX and RX,
Figure 3.2. The frequency is swept very fast compared to the movements in
the channel and registered over time by a computer.

---

[1]The same apply at the transmitter side.
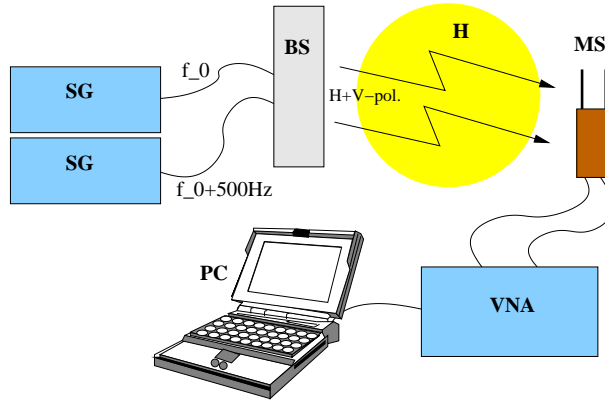
Figure 3.2: 2×2 channel measurement setup using two narrowband signal generators with a frequency offset and a 2-port VNA for coherent detection of the RX signal at the dual-antenna terminal.

3.4.2   Vector Network Analyzer and Virtual Array Positioners

In the channel measurements referred to in Paper II and Paper III the VNA is used together with one linear, see Figure 3.3, and one three-dimensional positioning and rotation robot, see Figure 3.4, at the BS and the MS sides of the channel, respectively, to form virtual array antennas for truly coherent wideband measurements. Appealing features of this measurement system are that it is, (i) accurate, (ii) easily adjustable with respect to frequency, output power, IF bandwidth etc., and (iii) simple to use. However, especially for wideband measurements with virtual array antennas for direction estimation, the disadvantages are (i) low measurement speed due to the positioning system that require static channels, (ii) phase reference between TX and RX limit the measurement distance due to the synchronization requirement via a long cable or a separate steady radio link. The measurement system described in Paper II and Paper III utilize a long optical fiber in combination with RF-opto converters.

Figure 3.3: Linear positioning robot with TX probe antenna.

Figure 3.4: 3-D positioning robot with rotational RX probe antenna.

Figure 3.5: RUSK Lund MIMO channel sounder RX unit with cylindrical probe array antenna.

3.4.3   RUSK Lund MIMO Channel Sounder and Switching Antenna Arrays

For dynamic time-variant MIMO channel measurements where the channel changes rapidly compared to the sweep time of a VNA, a fast wideband measurement system is needed. Such a system is the RUSK Lund channel sounder that uses multi-tone frequency domain correlation processing [92] similar to OFDM, Figure 3.5. This system provides a very fast measurement system that, when combined with fast RF switches and large antenna arrays, can be used to record up to 32×128 MIMO channel matrices with a bandwidth of 240 MHz (in for example the 2.2–2.7 GHz band), a sampling rate of 640 MHz, and an impulse response sample interval of $T_s = 1.6$ ns. Thus, a full MIMO snapshot with n_T transmit antennas and n_R receive antennas, and with an extra T_s cycle to avoid switching transients, takes $2\,T_s\,n_T\,n_R \approx 13.2\,\mu$s in which the channel must be essentially invariant. It is then possible to do DDPC estimation for each snapshot. This system is primarily designed for tests with a moving Rx unit in cellular or vehicle to infrastructure (V2I) channels, and possibly also with a moving Tx unit for vehicular-to-vehicular channels vehicle to vehicle (V2V).

In the measurements presented in the papers included in this thesis we have used only stationary TX and RX units. The fast measurement system is, however, still very important for outdoor channel measurements were windswept trees and other moving object in the surrounding neighborhood, induced non-stationarity in the channel that reduces the performance of channel esti-

mation. This was experienced in the first outdoor-to-indoor measurement campaign where we used the VNA system with positioning robots as is described in Paper II and in [40].

Chapter 4

Antenna Environments in Mobile Communication

In many practical wireless communication scenarios the antenna is surrounded by more or less close objects that interact with the antenna in different ways. Not only the shape, size and material of the interacting objects affect the antenna performance; also the distance to the antenna is of great importance. A very close object may affect the antenna radiation impedance match, while objects at a somewhat larger distance mainly distort the radiation pattern by absorption and scattering of radiated energy.

4.1 Field Regions of the Antenna

It is common to divide the space surrounding the antenna into three different regions; the *reactive near-field*, the *radiating near-field*, and the *far-field* regions, see Figure 4.1.

In IEEE Standard Definition of Terms for Antennas [42] the reactive near-field region is defined as "that portion of the near-field region immediately surrounding the antenna, wherein the reactive field predominates", and the radiating near-field region is defined as "that portion of the near-field region, wherein the angular field distribution is dependent upon the distance from the antenna", while the far-field region of an antenna is defined as "that region of the field of an antenna where the angular field distribution is essentially independent of the distance from a specified point in the antenna region".

The boundaries of these regions are not distinct, but from a practical point-of-view the outer boundary (as seen from the center of the antenna) of the reac-
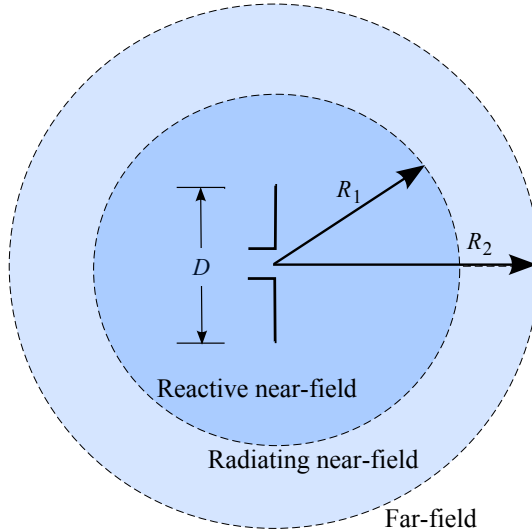
Figure 4.1: Field regions of an antenna [11].

tive near-field region is the region surrounding the antenna wherein interfering obstacles affect the radiation impedance of the antenna, and the far-field region is the region where the antenna can be regarded as a (directive) point source. The boundaries of the regions are commonly assumed to be $R_1 = 0.62\sqrt{D^3/\lambda}$ and $R_2 = 2D^2/\lambda$, respectively, where D is the largest dimension of the antenna and λ is the wavelength, with the requirement that D is large compared to λ [11, 42]. For small antennas where $D \ll \lambda$ the radiation near-field region decreases and the outer boundary of the reactive near-field region "is commonly taken to exist at a distance $\lambda/2\pi$ from the antenna surface" [42].

4.2   Installed Base Station Antenna

In the case of a BS antenna, the placement is in general chosen so that interaction with scattering objects is avoided. However, there are situations in dense urban environments or indoor deployments where it is impossible, unpractical or non-affordable to avoid interference from high-rise buildings or obstacles on the roof-tops, influence from wall-mounting or other indoor obstacles.

For simple geometric objects and buildings found in the far-field of the antennas where a geometric model is available, methods like UTD is accurate and effective for prediction as is shown in [39]. In the case of large array an-

tennas common in BS implementations and having objects within the nearfield of these antennas, the method can be utilized by coherent superposition of solutions for each array element. In more complicated situations we may need electromagnetic computer aided design (EMCAD) such as finite difference time domain (FDTD) tools, at the price of extensive computing power and time.

If the aim is to evaluate performance of installed single or multiple element antenna arrays in typical realistic BS environments, e.g., with respect to antenna separation for MIMO performance as in [101] but with obstructive structures in the close vicinity of the antenna, a statistical approach is needed. The statistical basis for such an approach can be hard to find by measurements since it may require extensive measurement campaigns to get statistical confidence. In this thesis we mainly focus on the MS side of a wireless communication link and leave the BS side to future research.

4.3   Human Interaction

The human operator of a hand-held mobile device is a typical unavoidable near-field interaction problem of MS antennas. Different parts of the body interact with the antennas in different ways; the hand and the fingers are usually placed very close above the antenna feed structure and even the head when the device is operated in talk position. The presence of the hand may cause severe degradation of the radiation performance due to both impedance mismatch (reflection) and absorption, while the body in general mainly causes shadowing. These effects has been investigated by many [4,34,55,70,73,75,93]. Within this thesis the impact on multiple antenna system performance measures such as correlation and diversity is investigated in Paper I, Paper II, and Paper III. The indoor diversity measurements with human interaction in Paper I is similar to the investigation by Bolin *et al.* [14].

When modeling the user influence in a cellular system, different approaches are possible. Simplified geometrical models of the user body, e.g., by an absorbing infinitely long vertical plane or cylinder as in [60], can mimic directional effects when the body can be considered being in the far-field of the antenna. However, in cases including the user hand or when the antenna is very close to the user body, the problem becomes more difficult to simplify and must possibly be treated in a statistical manner, where the expected value, the distribution and the correlation of the radiation efficiency is estimated [86]. These statistics can be gathered by the use of antenna measurements with a real human hand or with a realistic hand phantom [27] or, alternatively, by EMCAD simulations as in [15,43], and can also be extended into statistical human hand grip studies as in [74].

4.3.1   User Phantom

To perform measurements of the impact of a human body in a mobile radio
channel, regardless of whether we target the impact of the operator (user) or
by-passing interfering people, either we need live test persons or we can use a
phantom. A large and representative amount of live human operators naturally
give the most trustworthy results in an evaluation of equipment or a system. For
evaluation of a method where we need high accuracy regarding repeatability,
however, a model of some kind, a *user phantom*, is a better choice.

The body phantom has historically been basically anything that resem-
bles a human operator with reasonably similar electro-magnetic characteristics
(permittivity and conductivity) [33], e.g., simple dielectric cylinder or sphere
(massive or liquid filled with a sugar-salt-water mixture) [4], etc.

However, nowadays in the case of SAR (Specific Absorption Ratio) mea-
surements where the field strength and radiated power absorption inside the
user body is tested thoroughly and consumer products are certified with re-
spect to human exposure, the quality of the phantom is very important. Both
the phantom properties and the test procedures are restricted by standards
from the IEEE, FCC, CENELEC, ICNIRP etc. Manufacturers are, e.g., re-
quired to use the SAM (Specific Anthropomorphic Mannequin) body phan-
tom for conformance tests, e.g., as in [49]. SAM is based on the 90th per-
centile of a survey of American male military service personnel and represents
a large male body. Standard phantoms are being developed also to encounter
the hand, and quite recent publications presents very sophisticated and de-
tailed EMCAD hand models [53] and sophisticated user phantoms including
head and hand has been used in channel measurements by Nielsen and Ya-
mamoto *et al.* [69,102]. Also multiple antenna terminal performance and chan-
nel simulations with simplified yet full upper body phantom EMCAD models
have been reported by Ogawa *et al.* [71]. Furthermore, in-channel performance
evaluations by measurements of a generic versus a realistic phantom in browse
mode, Yamamoto *et al.* [103] shows that a realistic phantom actually are im-
portant for accurate channel performance investigations.

In our investigations of user influence described in [40] and in Paper II, we
used an upper body full scale user phantom including the head, the upper torso,
the right arm and hand, see Figure 4.2. The body part of the phantom are
made up by a 60 cm high glass-fiber shell filled with tissue simulant liquid made
by a mixture of 45% diethylene glycol butyl ether (DGBE) and 55% distilled
water to be in compliance with the recommendations of the IEEE Std. 1528
for 2.6 GHz, with a relative permittivity $\epsilon_r = 39.7$ and conductivity $\sigma = 2.14$.
The hand/arm part is a massive full-scale right hand model from IndexSAR
with the arm extension tailor-made. The body and arm parts are mounted
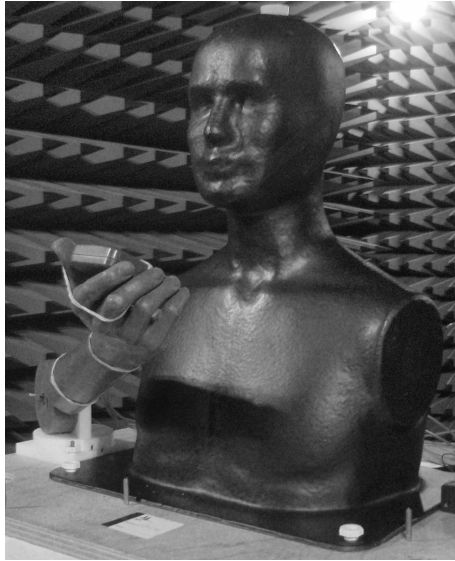
Figure 4.2: User phantom in browse mode.

on a plywood board; the arm via a plastic joint providing the possibility to orient the hand and handset to different operation positions. This joint was in our investigations fixed to two positions, one talk mode and one browse mode position.

4.4 Confined Scattering Environments

If the human body from a modeling perspective is considered as a scatterer that obstruct a fraction of the directional space as seen from the antenna, a *confined* scattering environment, on the other hand, is the situation where the radiation as seen from the antenna is mainly obstructed in the directional domain. A confined scattering environment is, e.g., a vehicle or an office room where the user equipment with the antenna(s) is placed inside.

Such an environment may change the channel properties from the outside to the inside severely, depending on the openings (amount and sizes), the reflectivity and penetration loss of the walls and windows, and the scattering and absorbing objects inside. Questions like; "Where does the radio waves enter the confined volume?", "Is the scattering due to inside multiple reflections and diffractions increased compared to outside giving rise to Rayleigh fading inside

even if we have LOS outside?", "Or, on the contrary, does the openings, i.e., the windows, in combination with heavy absorption inside, e.g., due to passengers in a car, decrease the richness of the channel?", "Do we get a keyhole effect still providing diversity performance but no spatial multiplexing gain?", etc.

Many of these questions are still to be investigated and answered. However, a first measurement of the directional attenuation of a car is found in [38]. In addition, a simplified high-frequency diffraction model is proposed for path loss modeling. The investigation mainly supports this simple model and proposes a directional approach to outdoor-to-in-car path loss modeling, in the case when the car is not loaded with passengers. In this case, since the investigation is made for only two static single antenna positions inside the car, we can not draw any general conclusions about how the statistical distribution of the fading changes when the antenna is moved from the outside to the inside of the car. This is investigated for a test car in Paper IV and with directional estimation in Paper V.

Chapter 5

A Composite Channel Approach

For an idealized wireless communication link with antenna arrays in free space at both the TX and RX, connected by a finite number of plane waves, the double-directional MIMO channel model in (3.1) is completely adequate. However, in a mobile communication scenario we may have, e.g., a user interfering with the antennas at the MS side. In this case, is the user body a part of the antenna or of the channel? And what if the user is sitting in a car? These questions lead us into an idea of separating the channel into several layers. Such a layered channel model is here referred to as a *composite channel model*.

5.1 Separation of Channel Regions

In a composite channel a key issue is how and where to divide the channel model. A full-wave propagation calculation tool in combination with a full geometric data base could give all information needed for calculating the channel behavior in any scenario. This is the full channel representation where all the channel parts, i.e., every interacting physical object from TX to RX, are characterized. However, even very detailed geometry data may not include enough scattering details to be realistic. Instead, we often in link simulations rely on measured channels from scenarios we find typical enough, or from empirical, sometimes geometry-based, stochastic or semi-stochastic channel models.

Thus, in the case where different configurations or realizations of TX or RX antennas are to be tested and the performance in a realistic channel is to be evaluated, we rely on the channel model in (3.1). With the DDPC parame-

ters extracted from measurements or simulations in "typical" scenarios, several test antennas can be evaluated in *identical* environments by their measured or simulated far-field antenna patterns inserted, and therefore avoiding extensive measurement campaigns for each test antenna. Thus, the composite channel separation is simply the separation of the antenna and the multi-path propagation channel at both the TX and RX under the assumption that the scatterers of the channel are in the far-field of the antennas. This approach was pioneered by Suvikunnas *et al.* in [89, 90].

Considering, e.g., a cellular system where the mobile phone (MS) is in the vicinity of a user, the channel can be separated either between the phone and the user, i.e., the user is a part of the channel, or the channel can be separated between the user and the propagation channel, i.e., the user is a part of the MS. The first alternative is hardly practical since it would require channel measurements for each configuration of the user body, and the far-field requirement with the MS in a user hand is not fulfilled. The second alternative, with the user being a part of the MS antenna forming a new *super-antenna* is, however, useful and has been shown to produce good statistical agreement in an outdoor-to-indoor and an indoor-to-indoor scenario as shown in [40] and Paper II. The far-field antenna pattern for the test mobile in combination with a user phantom or a human user can readily be measured in an antenna range.

The technique in the example above does unavoidably require an increased amount of test patterns to be evaluated due to several possible user operation positions or modes (talk mode, browse mode, position of arm, mobile in hand etc.). To avoid this we need a third composite channel interface between the mobile antennas and the user body. Since the hand is very close to the mobile it seems impossible to put the interface there where the far-field assumption definitely does not hold. Furthermore, since the hand connects continuously with the body, there seems to be no natural choice. From experiments it is seen that the hand does indeed induce absorption, loss of radiated or received energy, and may cause antenna mismatch for the handset antennas [73, 76] and introduces decorrelation of the antenna signals [77, 86]. However, it does not seem to influence the radiation pattern in a predictable way like the body does, as is shown in Paper II Section 4 Figure 2. Thus, a possible approach would be to model the directional properties of the body as a separate forward scattering layer or a directional filter. This idea will be explained below.

The same approach as is described for the user body example above may be applicable to other similar possible scattering environments as well. In the case of an antenna inside a car, a simplified directional forward scattering model is proposed in [38] with the option of at least one additional mirror source to handle first order reflection. The same model could be applicable also for other scenarios with antennas inside vehicles, such as buses, trains or aircrafts, since

they are built up by similar confined metal structures with windows. This idea may also apply for other similar urban scenarios like the outdoor-to-indoor case, etc.

With such an approach to channel modeling, it is possible to evaluate e.g., different test mobile phones in different user scenarios, in a car etc., with the use of only a few "typical" propagation channel scenarios that again are *identical* for all test devices and therefore completely fair.

If the similar approach also apply for non-confined scattering environments, e.g., unavoidable scattering object in the vicinity of a BS antenna array (in a MIMO scenario), the composite channel approach can be extended also to the BS side in a cellular system or to the access point in a wireless local area network (WLAN) system. Thus, the composite channel model may have 5-6 separate layers.

5.2   Representative Models and Interfaces

With a composite channel model with several physical regions, there is a need for defining the interfaces and choosing the appropriate channel representation in each region. A model that describes the signal transition from one position in space to another one can be referred to as a point-to-point (P2P) model. However, within the channel regions the signal transition will be represented by point-to-direction (P2D) and direction-to-direction (D2D) models.

5.2.1   Antenna Region

In general there are many ways to define and characterize an antenna. In channel modeling we normally put the interface between the antenna region and the propagation region at some radius from the center of the antenna excitation port, i.e., the point where the transition between transmission line and open-space propagation occur. The corresponding region that is circumventing all the structures that is fixed to the antenna (or to the excitation port) is inserted into the channel as one unit, which may be referred to as the actual antenna itself, or alternatively as a *super-antenna*. This means that the antenna region may include, e.g., the mobile phone with casing in a cellular system, or a laptop computer in a WLAN system. If it can be assumed that all surrounding structures outside the antenna region is in the far-field, the antenna can be represented by the polarized complex electric far-field found by measurements or electromagnetic theory, i.e., by a P2D model. The far-field of a certain antenna is a deterministic property, but could be turned into a statistical representation that include small-scale uncertainties by adding a stochastic component

as proposed in [85].

An antenna far-field may also be stored and handled in different ways. There are different pros and cons for the choice of method:

Closed-form expression is of course the most convenient model for simulations of antennas but are only available in practice for simple structures like idealized dipoles, etc.

Sampled field data is normally what would come out of antenna range measurements or EMCAD tools. A disadvantage is the discrete frequency and angular samples which require interpolation to fit with a directional propagation channel.

Basis function representation is an alternative mathematical representation of full sphere field data often derived from either a closed-form representation, or sampled full sphere field data with sufficient sampling density. The field is represented by a linear combination of a set of basis functions (preferably orthonormal) with different properties depending on application.

The basis function representation is commonly used in the included papers of this thesis. The far-field data originates in most cases from measured full sphere data and once the transform or modal expansion is made in combination with the measurements, the file size becomes compact since only the complex basis function weights are stored. Furthermore, with the closed-form basis functions we avoid numerical complex interpolation in the angular domain. Another useful feature of basis function representation is the physical interpretation of the basis functions where higher order modes mainly represent radiating parts of objects with a larger size or at a larger distance from the actual antenna (if centered at the origin of the coordinate system of the measurement range). This means that it is possible to identify error sources in measured data that originate from objects outside of the actual antenna, e.g., from the anechoic chamber positioning system, etc.

One set of basis functions that is commonly used is the *vector spherical harmonics* or spherical vector modes (SVM) as described in [3]. This representation gives compact data storage and nice physical truncation properties. Another very useful representation of especially far field data is the angular spectral domain (ASD) or 2-D Fourier decomposition [20]. To do this we need to use the trick of extending the spherical vector coordinate system to map a torus geometry such that the field (over-)representation gets periodic in both θ and ϕ over $(-\pi : \pi)$. Now a 2-D discrete Fourier transform (DFT) give the angular spectral domain decomposition (referred to as the EADF in [20, 51]).

With periodic (equidistant) field data samples in (θ, ϕ) we may utilize the efficient fast Fourier transform (FFT) algorithm. The transition between ASD and SVM is easily derived making it possible to switch very fast between the representations [37, (A1.35a)]. Thus, we can utilize the advantages of minimal storage and physical truncation methods of the SVM but switch to ASD to perform fast field calculations.

For an antenna region radius of a few wavelengths the SVM expansion is a very efficient antenna representation since the number of required modes will be moderate. There is a rule-of-thumb that the maximum longitudinal and azimuthal mode numbers (l, m) has to be larger than approximately 2π times the electrical antenna radius r/λ plus 10 [37, (2.31)], i.e., if $n = l_{max} = m_{max}$ then

$$n \gtrsim kr + 10 = 2\pi \frac{r}{\lambda} + 10 \tag{5.1}$$

Since the mode numbers are defined so that $l = 1, 2, \ldots n$ and $m = -m_{max}, -m_{max} + 1, \ldots, m_{max} - 1, m_{max}$ the total number of modes n_{modes} required becomes

$$n_{modes} = 2(l_{max}^2 + 2 * l_{max}) \tag{5.2}$$

where the first 2 account for the TE plus the TM modes, and $m_{max} = l_{max}$. Thus, for a large antenna radius of many wavelengths the number of modes may become too large to be an efficient representation, compared to direct sampled field data. This may also be the case if the antenna radius expands into the scattering region.

Another very important issue when modeling multiple antenna systems is to keep a common phase reference point of all the antenna elements comprising the array. This is referred to as the steering vector or antenna location vector (3.1). It is possible to use the SVM method to find the effective radiation center of each individual antenna (pattern) by an iterative procedure that minimizes the maximum number of modes required for a certain level of field accuracy and has been found to produce reliable results [32]. This method has been used to verify the phase reference of antenna representations after being decomposed, transformed and truncated from original measured field data. Applied, e.g., on the four-antenna test terminal that was used in the experiments described in Paper II-V, see Paper II Section 3.1, gives a strong indication that the main radiating parts of the antenna manifold are located at the positions of the planar inverted-F antenna (PIFA) elements as seen in Figure 5.1. The figure shows a model of the handset with the four PIFA elements marked by blue boxes. The origins of the sub-axes of each antenna element in the graph mark the effective radiation centers found by the previously described method. Thus, it is clear that the radiation indeed stems primarily from the locations of the PIFAs and not from induced currents on the connecting cables, which is a
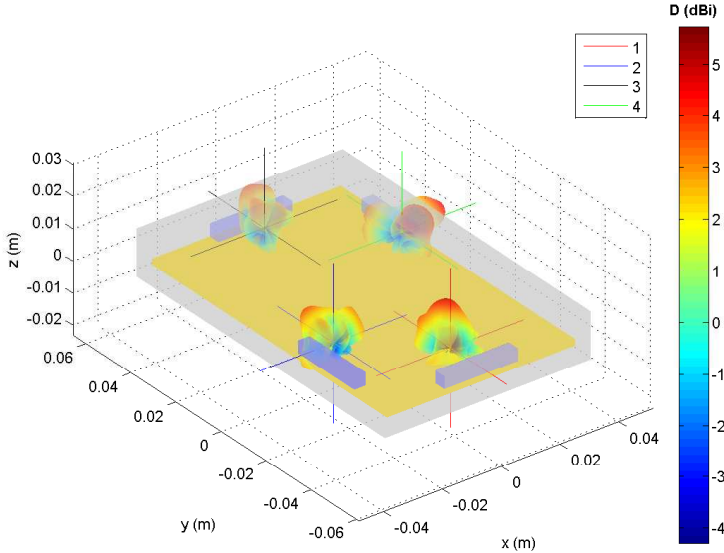
Figure 5.1: Geometry of a four-antenna handset (PDA) with superimposed 3-D measured antenna patterns with the origins at the effective radiation centers.

potential problem especially for small terminal antenna evaluations. A way to avoid this potential problem would be to use the technique with optical feed cables and RF-opto converters [67, 104].

5.2.2　Scattering Regions

The scattering regions, at either the TX and RX side of the channel, may be defined as the regions outside of the antenna region that include all scattering objects, preferably in the far-field of the antenna. These objects shall still be distinguishable from the large-scale propagating environment, i.e., the user body at the MS or obstacles on a building roof in the vicinity of a roof-mounted BS antenna in a cellular scenario, the office desk environment in an indoor WLAN scenario, or a vehicle in an outdoor scenario, etc.

To model the scattering region in a composite channel model, such as the user body or a vehicle, is a delicate matter and may be treated in different ways. A fully detailed user model requires measurements or EMCAD calculations with 3-D geometry data and realistic material parameters, see e.g., [34, 75]. In physical channel modeling we generally consider simplified models of the

electromagnetic wave propagation that in a statistical sense take into account the basic properties of the channel. An example is the so called geometry-based stochastic channel model (GSCM) [65, Sect. 7.4.5] were the contributions of the main interacting objects in the directional and the delay domains are surrounded by clusters to account for non-predictable MPCs. Thus, antenna-plus-user far-field measurements or EMCAD calculations may be used to form a predefined "super-antenna" pattern to be used in a reference channel model, i.e., with the user included in the previously defined *antenna region*. This approach is tested and verified for measured super-antenna patterns in Paper II.

An alternative method is to find a simplified generic model of the impact of a user that can be added "on the fly" as a component of the (composite) channel model on top of an arbitrary antenna far-field pattern. This model may be extracted from statistics of empirical or simulated data, or may be developed by simplified theoretical means.

In [60] a moving person is modeled by a infinitely tall cylinder. Here the channel interaction is modeled by two components, one that account for the shadowing of the cylinder shaped person, and a second that also take into account also the reflection and scattering[1] of the person. The shadowed and the scattered components are combined coherently to reflect the influence of Doppler spread. In this paper, the model uses an heuristic approximation to cylinder scattering that give a smooth scalar function for the shadow and edge diffractions without the ripple caused by coherent addition of the incident and the diffracted field components as in GO and UTD models. A rigorous calculation of the electro-magnetic scattering of a cylinder can be found in [28], but since the cylinder is only a rough model of the body of a person in movement, such advanced mathematical treatment is pointless. Instead, this smooth shadowing function is assumed to approximate a local averaging of the shadow with respect to the angle of incidence. This is often preferred in path loss modeling [12] and provides a good shadow loss model for the body. In Figure 5.2 this model is compared to the measured average user body loss from the browse mode case in Paper II, Figure 2. Here the average radiated power normalized with respect to directivity of the four handset antenna elements, is plotted in the horizontal plane (azimuth) with and without the phantom present. The shadow of the phantom body is obvious in the graph towards the azimuth angle −90 degrees, and is well caught by the model.

Thus, it seems feasible to model the shadow effect of a user by simple means in a realistic way. In this example, the two contributions of diffraction from each side of the cylinder (i.e., the user body) combined by non-coherent addition of powers. Thus, the model only account for the path loss of the user,

---

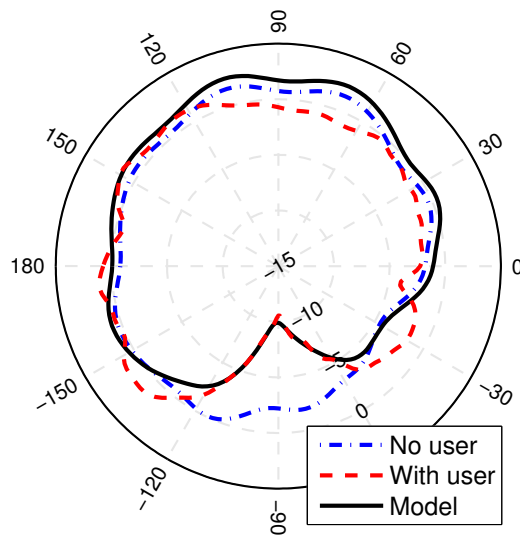[1] were the term "scattering" differ from the definition of the scattered field in, e.g., [18]

Figure 5.2: The average measured antenna azimuth patterns for the a test handset with and without the user phantom present (in browse mode) compared with the proposed simple user shadow model.

ignoring phase and polarization. By true physical coherent combination of the diffraction components we would observe deep frequency dependent fading in the shadow region which, in turn, could decrease the correlation between the signals received by multiple antennas on a handset. In our investigations of user influence in realistic indoor and outdoor channels presented in Paper II and V we find, however, that the presence of the user in the channel increases the correlation between antenna branches. This is assumed to be a consequence of shadowing since it has a potential to reduce the channel spatial richness. Thus, it seems as the user hand and body may affect antenna correlation in both ways depending on the channel. In a highly correlated channel such as a line-of-sight channel the correlation may decrease due to the user body, while in a rich scattering environment it is likely to increase. From the investigations in Paper II and V we also find that the change in correlation has little impact on important multiple antenna channel properties like diversity gain and MIMO capacity. Thus, we may assume that a directional (body) path loss model such as the one proposed above is an interesting candidate for composite channel modeling. This proposal is, however, yet to be verified in a statistical sense and may be a topic for further research.

A similar simplified modeling approach has been proposed in [38] for an antenna inside a car. Here, the proposed simple directional path loss model is compared to directional path loss measurements and a more detailed ray-tracing model, the latter using first and second order ray-tracing (based on GO and UTD) for a geometric model of the car. This analysis shows the importance of multiple reflections inside the car, an observation that can be made also from the directional estimations in Paper V, Figure 2. Therefore extra care must be taken when considering a scattering model for a car suitable for a composite channel model regarding multiple interactions inside. These effects may be handled as in [38] by image theory or, alternatively, by a semi-statistical approach similar to the GSCM.

Furthermore, we find in Paper IV that the inner scattering of a car have the potential to alter the fading statistics which means that also the statistical properties of the channel is affected. However, as was found also in the case of user interaction, this change in statistical distribution seems to have very little effect on properties like diversity gain and MIMO capacity as is shown in Paper V. Thus, we may assume that the important impact of the outdoor-to-in-car part of the channel in channel modeling is caught mainly by a directional path loss model.

Again, this is an observation that still needs to be established statistically by further investigations and is not verified by the work in this thesis. The modeling of the scattering region, together with the composite combination of several models in multiple antenna and scattering regions, is a very interesting

topic that is proposed for future research.

5.2.3   Propagation Region

Finally, the region that is left between the TX and RX is termed the propagation region. This is what would be simulated by ray-tracing and/or ray-launching techniques [23, 24, 54, 82] or measured by a channel sounder with array antennas at both ends, deliberately chosen to be well separated from scatterers, i.e., on the roof of a measurement van, on a trolley in a office or corridor etc., and that can be represented by the DDPC. It is also the D2D representation of geometry-based stochastic reference channel models like the COST 259, 273, 2100 models [10, 19, 22, 66, 78], the 3GPP SCM [1], and the WINNER II model [50], for the rural and urban macro/micro-cell scenarios with the antenna patterns extracted. A good overview of propagation models can be found in [5].

The propagation channel is in general characterized by the DDPC model, i.e., by a limited set of MPCs that represents plane waves or rays. This is a double-sided spectral domain representation that fits an electrically large environment well and can be found experimentally for a certain environment from MIMO channel sounder measurements and high-resolution parameter estimation as described below.

Plane-Wave Spectrum Parameter Estimation

The propagation region as represented by the double-directional (plane-wave spectrum) propagation channel (DDPC model) constitutes the antenna independent radio channel, and can be modeled by theoretical means (models) or from parameter estimates extracted from channel sounder measurements with dedicated probe antenna arrays. The latter method is the one that we mainly address in this thesis and also the one utilized in the included papers. Full DDPC parameter estimation [79, 80, 88] combines previously developed methods of DOA and delay estimation [48, 57] and is a research field of its own in signal processing. There are many algorithms proposed for high-resolution multi-dimensional parameter estimation of channel parameters where the most popular relies on maximum likelihood (ML) estimation, like the well known SAGE algorithm and its proposed extensions [29, 30, 94] that perform the maximization of the likelihood for one parameter at a time, or the gradient-based multi-dimensional methods like RIMAX [52, Section 5.2] or the similar method by Medbo *et al.* [62–64] that increases the convergence rate for coherent propagation paths.

Common for these methods is the estimation of the DDPC channel parameters from the channel model in (3.1). The parameters $\boldsymbol{\theta} = \{\Omega_{t,l}, \Omega_{r,l}, \tau_l, \alpha_l, \mathbf{P}_l\}$, representing the measured channel of interest, are found as a solution to the maximization problem

$$\hat{\boldsymbol{\theta}} \triangleq \arg \max_{\boldsymbol{\theta}} p(\mathbf{x}, \boldsymbol{\theta}) \tag{5.3}$$

of the likelihood function $p(\mathbf{x}, \boldsymbol{\theta})$, where $\mathbf{x}$ is a realization of the stochastic channel matrix data $\mathbf{x} = vec(\mathbf{H})$.

It can be shown that the log-likelihood function $\log p(\mathrm{x}, \boldsymbol{\theta})$ in (5.3) can be written as (e.g., [81, Section 5])

$$-\log p(\mathrm{x}, \boldsymbol{\theta}) = N_r N_t N_f \log(\pi \sigma^2) + \frac{1}{\sigma^2} \sum_{k=1}^{N_f} ||\mathbf{H}_k - \tilde{\mathbf{H}}_k||_F^2 \tag{5.4}$$

were k is the sample frequency index, $\mathbf{H}$ is the channel model from (3.1), and $\tilde{\mathbf{H}}$ is a measurement realization. Here we assume stationary white Gaussian noise ($\sigma^2 \mathbf{I}$), non-moving TX and RX (zero Doppler), and that the channel can be represented by specular plane waves[2].

Enhanced Super Resolved Channel Estimation

The channel parameter estimates utilized for the analysis in [40] and in the included Papers II–V of this thesis, are just briefly described in the papers. A more comprehensive description is outlined in [63]. This ML estimation method utilizes a novel approach to improve the efficiency and the accuracy of ML based super resolution channel estimation. ML estimation methods may suffer from considerable computational complexity as hundreds of coupled discrete waves may have to be estimated simultaneously. Standard methods are either very slow in convergence when parameters are correlated (e.g., SAGE [81]) or suffer from estimation errors as waves are not sufficiently decoupled. The problem can be solved by a modification of the original likelihood function by introducing windowing of both measurement data and the corresponding channel model [63]. In this way, waves are effectively decoupled for fairly small separations in parameter space, making local maximization of corresponding modified likelihood possible. Moreover, as the waves are decoupled a corresponding reduction of complexity is possible by clipping (gating in delay domain) of data which is outside the coupling distance of the waves subject to parameter estimation. These new approaches have shown to substantially improve both the accuracy and the efficiency of the estimation process.

---

[2]In [81] additional non-specular components referred to as dense multipath components (DMC) is considered as separate possibly correlated components of the channel.

Estimation Process

The typical estimation process is illustrated in Figure 5.3. First the maximum in the windowed power delay/angle profile is found. In this step the data is averaged over the non-windowed degrees of freedom. The data in the vicinity of the maximum is kept while the rest is removed. In order to keep high computational efficiency, a good estimate of the initial parameter values is desirable. For this purpose beamforming, which corresponds to a DFT from the antenna element locations of the array to the angular domain, is performed providing a power function of delay/direction. Each local maximum of this function, which is above the noise level, corresponds to an initial wave. In this step the measured channel is windowed also for the domains (space and/or frequency) which are not clipped in order to avoid fake initial waves. However, this windowing is not applied in any other step. The initial values are then used in the maximization of the modified likelihood step (block 1 in Figure 5.3). When the maximum is found, rays having too large parameter errors are removed. Maximization and removal of rays with large errors are repeated until the parameter errors are acceptable.

In the next step the modeled channel which corresponds to the estimated rays is subtracted from the measurement data. If the residual is above the noise threshold, additional maxima are identified and added to the already identified ones. Then the maximization is repeated keeping the window around the already identified power maximum. If the residual measurement data is close to the noise level and/or no new rays have been added, a search for new peaks in delay is performed. For any new peaks, the previous procedure is repeated. When there are no remaining new peaks, the estimation process is finished.

Nearfield and Non-Spherical Model Errors

The validity of the model in (3.1) assume plane wave fronts emanating from the TX and impinging on the RX, a model that may not be valid when scattering objects are close to the antennas. In Paper II this assumption is challenged by the indoor measurements with many obstructive and scattering objects not in the far-field (Rayleigh distance) of neither the RX synthetic antenna probe array, nor the user-phantom-plus-handset location. In this case no problems with the estimation process were found and the channel model data showed very good results utilizing the estimated parameters and comparing to direct measured data.

In Paper V, however, the plane wave estimation is further challenged by a courageous attempt to perform parameter estimation inside a car at 2.6 GHz
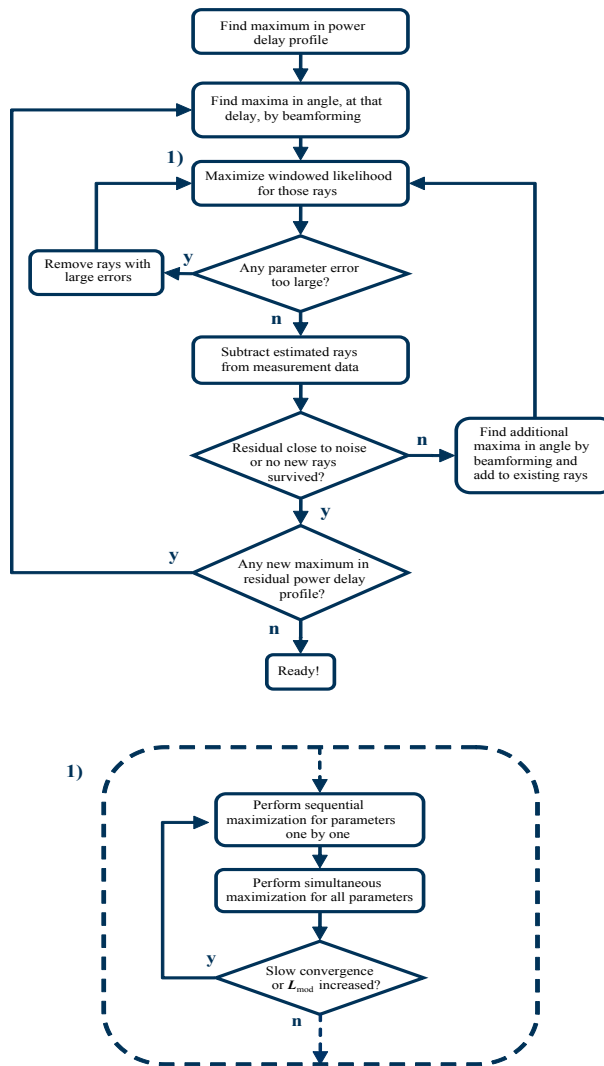
Figure 5.3: Flow chart of estimation process [63]. The lower dashed box (1) is a magnification of the third box in the top flow chart.

which is a very close environment well within the Rayleigh distance of the antenna at this frequency. As expected, the estimation process now shows much less accuracy with possible artifact scatterers as a result of close obstacles. Nevertheless, the average channel behavior still showed reasonable accuracy when comparing channel model data based on the estimated parameters, to direct measured data. This shows that channel estimation based on channel sounder measurements with properly calibrated array antennas, even in complicated close scenarios can serve as a practical tool for statistical multiple antenna system evaluations.

The errors due to non-planar wave fronts and the relation to antenna calibration distance are examined in [52]. A possible solution to the problem of non-planar wave fronts would, of course, be to introduce also the curvature radius or scattering source distance in the estimation process, extending the parameter space $\boldsymbol{\theta}$ [35, 36]. This method has been considered as a candidate solution to the in-car channel estimation problem but was never implemented. This is, however, an interesting topic for future work.

Channel Sounder Probe Antenna Calibration

The quality of the calibration of probe antennas for channel sounder measurements ultimately sets the accuracy of the channel parameter estimates. Here we only consider fully characterized antennas, i.e., the measured full sphere far-field antenna patterns with amplitude and phase for two orthogonal polarization components[3]. In Section 3.4.2 and Section 3.4.3, the two channel sounder setups used in the scope of this thesis are described.

With the first setup, using a VNA with positioning robots, the probe antenna is a two-port dual polarized single patch antenna element that is translated and rotated at the measurement location (using a SP2T switch to toggle between antenna ports). This antenna was measured in a SATIMO SG 64 compact measurement range at Sony Ericsson Mobile Communications AB, Lund, Sweden, with high measurement accuracy except in a sector in the backplane of the antenna downwards towards the mast of the measurement range.

The positioning accuracy of the channel measurement robots is better than a millimeter ($< 0.01\lambda$), while the pointing error of the patch is within a few degrees which is negligible in this case since the half-power beamwidth of the patch is about 90 degrees. Thus, this measurement system provides very high accuracy of the antenna array models which results in high quality channel parameter estimations subject to plane-wave propagation [61, 64]. The disadvantage with this method is the possible phase instability due to unavoidable

---

[3]A comprehensive overview of incomplete array antenna models and their consequences can be found in [52, Section 7.2]
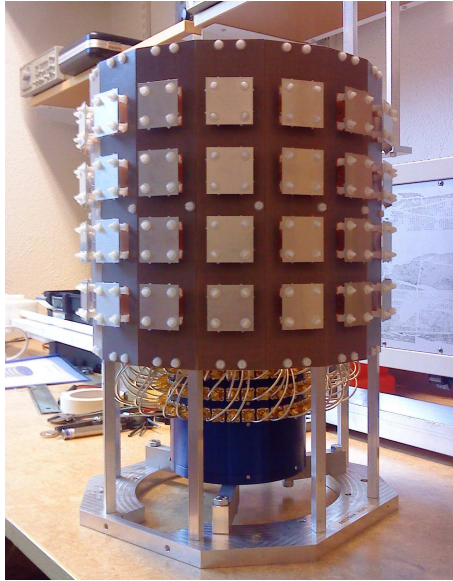
Figure 5.4: The RxPUCA antenna.

movements and bending of cables during robot movements which results in measurement errors. It is advisory to minimize this by carefully tied cable attachment, or, preferably, by fix cables and rotary joints.

The cable problem is to some extent avoided by using the channel sounder setup in Section 3.4.3 with fix probe array antennas combined with large switches, besides the obvious advantage of much faster possible measurement speed. This setup, however, put even higher demands on the quality of the antenna calibration measurements. The array antennas used in this work (Paper IV and V) is a planar patch array at the TX side, Tx patch uniform rectangular array (TxPURA), and a cylindrical patch array at the RX side, Rx patch uniform cylindrical array (RxPUCA), both with $\lambda/2$ element separation. The TxPURA has 4 rows and 8 columns of dual polarized square patch antenna elements where only the two middle rows are used (the others are terminated). The 32 ports in the two middle rows are connected to a 1-to-32 switch multiplexer (MUX) and an amplifier. The calibration of this antenna was never used in the work presented here since only RX side directional estimation was performed.

The RxPUCA has 4 rows and 16 columns of dual polarized square patch antenna elements, see Figure 5.4. In this case all 128 ports are connected to

a 1-to-128 switch MUX and an low-noise amplifier (LNA). This antenna was fully characterized including the MUX, and the LNA, at a 6 meter high quality indoor anechoic chamber with a rotation-over-azimuth turntable unit[4].

A very important issue with the antenna array characterization to be used for directional estimation, is a correct phase reference of the array elements so that the phase in the antenna pattern data model as a function of angle with high accuracy reflects the individual antenna array element location. This was discussed in Section 5.2.1 for the test terminal characterization and here we can use the same method to find estimates of the effective phase centers to test that the measurements are correct. This is shown in Figure 5.5 where the estimated effective phase centers for vertically and horizontally polarized patch antenna ports are marked on the true patch array geometry. The maximum deviation between true values and estimated effective phase centers are found to be 26.2 mm and the rms deviation is 8.4 mm, which would put a limit to the estimation accuracy of the array. However, since we do not yet know the accuracy of the method used it is hard to quantify this error but we get an indication that the antenna model is good.

Ray Tracing and Other Propagation Modeling Tools

There are of course many other ways to model directional radio propagation besides channel parameter estimation from array antenna channel measurements. Purely theoretical deterministic models as was mentioned in Section 3.1.1 that is based on ray tracing or ray launching (shooting and bouncing rays) have been used to produce reliable multipath directional propagation models in many publications [2,24,39,44,82,83,96,99,106]. The problems with these types of models is often a lack of quality or sufficient detail in building data bases together with the enormous computer resources that these details require. However, building databases seem to become more and more available both with respect to coverage and cost, and computer power is still increasing while computers get cheaper.

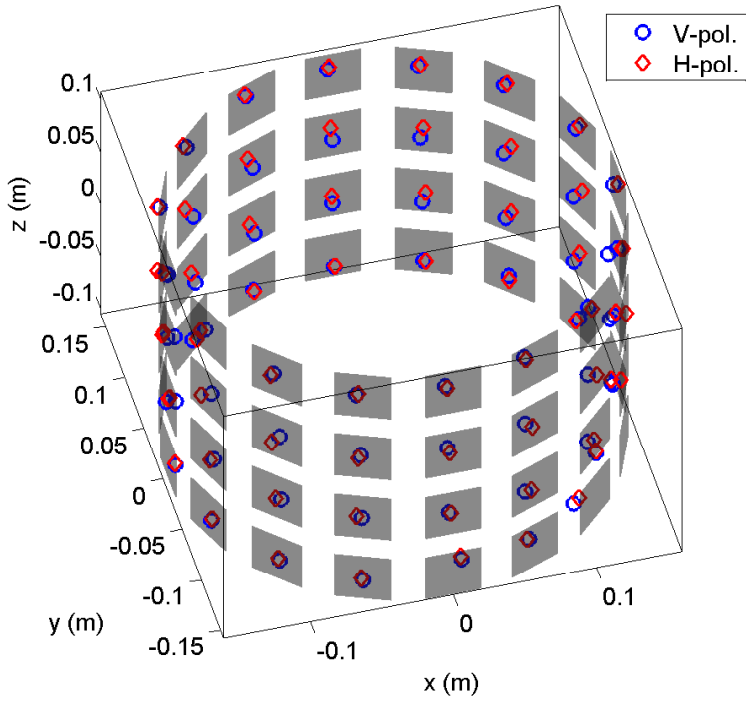[4]At RUAG Space AB, Mölndal, Sweden

Figure 5.5: The RxPUCA geometry with marked phase centers estimated from measured patterns.

Chapter 6

Contributions and Conclusions

This chapter summarizes the main research contributions of the included papers. Some general conclusions regarding the research area are also provided as a separate section.

6.1 Research Contributions

The work was supervised by Dr. Fredrik Tufvesson, in an initial phase together with Prof. Andreas F. Molisch. Co-supervisors were Dr. Anders J. Johansson, Prof. Ove Edfors, and Prof. Anders Derneryd. I am the main contributor to the scientific work presented in the included papers, and the contributions of my co-authors are mentioned below for each paper.

6.1.1 Paper I: "Dual Antenna Terminals in an Indoor Scenario"

This conference paper investigates the performance of dual-antenna test terminals in an indoor scenario including user influence. The paper specifically targets the diversity and MIMO performance impact of (i) the channel correlation and (ii) the user influence, with two different user operation modes. At the time of the writing of the paper, publications that addressed these effects were rare in the literature. Later it has been well established that even high antenna branch correlation (complex correlation magnitude above 0.7) in a channel may still provide significant diversity gain, a result that is supported by our results.

Regarding the operation modes of a user, the data mode or browsing mode where the user holds the mobile phone (or a laptop) in a position as to watch the screen, is perhaps the most interesting scenario nowadays for investigation of user effects on MIMO performance, since it is in this position we expect the highest data transfer rates.

As a feature, the paper also investigated the possibility to explore the singular *vectors* of the MIMO channel matrix as a tool to find the antenna signal weights and, thus, the individual importance or performance of the antennas. This technique was not known to the authors to have been published prior to the writing of this paper.

The work was done in cooperation with Sony Ericsson Mobile Communications AB, who provided the test terminals. I did the analysis and wrote the manuscript. The measurements were done together with Henrik Asplund and Mathias Riback. The work was supervised by Prof. Anders Derneryd.

6.1.2　Paper II: "Efficient Experimental Evaluation of a MIMO Handset with User Influence"

This paper extends and improves the evaluation of the composite channel method that was first published in a conference paper [40]. Here, the method is verified for both an outdoor-to-indoor and an indoor-to-indoor scenario, and very good agreement is found between the statistics of the synthetically found channel matrix and direct measurements. The results support the validity of this useful concept for channel modeling with the specific focus to target the important user effects in evaluating realistic MIMO performance of hand-held mobile devices and provide a tool to improve multiple-antenna design on terminals.

Novel contributions of this paper are the final validation of the composite channel method with a full phantom user model including *hand, arm, upper torso and head*. We also reevaluated the impact of different hand positions and usage positions of the handset, i.e., holding it in the browsing position vs. the standard talk position. Furthermore, we reanalyzed the MIMO capacity as well as the eigenvalue distributions and diversity performance for a realistic four antenna handset mock-up in the presence of a user phantom.

I wrote the manuscript together with Prof. Andreas F. Molisch, and I did the analysis and modeling, except for the double-directional channel estimation, to which Dr. Jonas Medbo has contributed. I and Dr. Medbo did the measurements and Dr. Anders J. Johansson contributed to the preparations of the user phantom. Prof. Molisch and Dr. Fredrik Tufvesson supervised the work. The antenna range measurements were done in cooperation with Sony Ericsson Mobile Communications AB.

6.1.3 Paper III: Evaluation of User Hand and Body Impact on Multiple Antenna Handset Performance

This conference paper evaluates the performance of a multiple antenna handset in realistic radio channels. Specifically, we utilize the previously established approach where the radiation pattern of the user-plus-antenna, is considered as one radiating unit (a super-antenna), and evaluates the performance impact of the user body and hand on properties like the antenna efficiency, performance of different diversity combining approaches, and potential MIMO channel performance. It is found that apart from efficiency loss due to the user hand, the mutual efficiency impact on the antenna elements and the directional impact of the user body shadowing, have small influence on the diversity and capacity performance. We also find that the top and bottom placements of antennas are the most efficient to be used with up to two antenna elements, and that significant diversity and capacity gain can be explored by using up to four distributed antennas, also with only two radio chains by the use of hybrid selection and combining schemes.

I wrote the manuscript and I did the analysis and modeling with valuable support by Prof. Anders Derneryd. Dr. Jonas Medbo has contributed to both measurements and channel estimations, and Dr. Anders J. Johansson has contributed to the preparations of the user phantom. Dr. Fredrik Tufvesson supervised the work. The antenna range measurements were done in cooperation with Sony Ericsson Mobile Communications AB.

6.1.4 Paper IV: Evaluation of an Outdoor-to-In-Car Radio Channel with a Four-Antenna Handset and a User Phantom

This conference paper evaluates the influence of a car on the MIMO radio channel, from a base station antenna array, to a multiple antenna handset in the hand of a user placed inside. A measurement campaigns is performed that mimic a 2.6 GHz micro-cell urban or rural scenario with two different locations and orientations of the car. The analysis includes important observables like the car penetration loss, impact on fading statistics, terminal antenna branch correlation, eigenvalue distributions, as well as the performance of various hybrid diversity combining and spatial multiplexing schemes, with and without the vehicle present in the channel. It is found that the car, in general, makes the channel statistics become closer to Rayleigh-distributed by increased inner scattering, increases multipath channel richness, improving the potential of diversity gain and, to some extent, spatial multiplexing. The overall impact of these effects is found to depend substantially on the orientation of the car and

the outer channel scenario.

I wrote the manuscript and I did the analysis and modeling. The measurements were done together with Dr. Tommy Hult. Dr. Jonas Medbo has contributed to both measurements and channel estimations, and Dr. Anders J. Johansson has contributed to the preparations of the user phantom. Dr. Fredrik Tufvesson supervised the work.

6.1.5   Paper V: Experimental Investigation of the Directional Outdoor-to-In-Car Propagation Channel

This submitted journal paper evaluates the possibility to accurately enough perform channel estimation inside a car in an outdoor-to-in-car environment, despite the violation of the required "rule-of-thumb" Rayleigh distance to the surrounding channel scatterers. The investigation is based on 32×128 and MIMO channel measurements with probe array antennas for channel characterization, and 32×4 MIMO reference channel measurements with an upper body phantom and a four-antenna handset mock-up located outside and inside of a standard family car. It investigates whether the combination of a plane-wave spectrum propagation representation combined with arbitrary but realistic multiple antenna representations, in the presence of a difficult confined scattering environment, can appropriately account for and model important statistics of the channel. In both cases the results of this investigation show that this is possible with high accuracy. The main specular components of the channel seem to account for the important statistical properties.

The novel contributions of the paper are the test of the composite channel model with a body phantom that includes hand and upper body placed inside and outside a car, the impact of a car environment (outdoor-to-in-car), and the investigation of the possibility to perform directional channel estimation inside the car. Furthermore, we test the accuracy of the synthetic channel based on the estimated channel in the presence of a user inside and outside the car, regarding MIMO channel statistics, diversity and capacity gain.

I wrote the manuscript and I did the analysis and most of the modeling. The measurements were done together with Dr. Tommy Hult. Dr. Jonas Medbo has assisted with the channel estimations, and Dr. Anders J. Johansson has contributed to the preparations of the user phantom. Dr. Fredrik Tufvesson supervised the work.

6.2   Conclusions and Future Work

Proper physical channel modeling including all parts of realistic yet typical wireless channel is, indeed, a tricky task. Realistic channel properties such as scattering around and close to base stations, and near-by interactions with close environments at the mobile user side, such as the hand and body, vehicles, etc., tend to make channel modeling very complex.

The trade off between complexity and simplicity of a channel model is crucial. Simply, if the channel model is too complicated it will not be implemented and used by link or system simulators. Still, for evaluation of a specific single or multiple antenna arrangement, the model has to catch realistic channel characteristics that may strongly affect the benefits of such an arrangement. For example, it is well established that MIMO may provide extensive capacity gain in rich propagation environments, a property that is precious in mobile communication systems. However, it is also extremely expensive for manufacturers of mobile phones and other terminals to extend existing single antenna mobile platforms into devices with multiple antennas and multiple radio chains, e.g., to support at least two layers MIMO in LTE and possibly up to 8 layers in future cellular standard evolutions. Therefore, the possibility to evaluate the performance in an efficient and simple manner of such specific multiple antenna arrangements in truly reliable *realistic* scenarios, including the human hand and body at the mobile side, together with scattering environments like vehicles, etc., is something that save tremendous efforts and money. These considerations also apply for future macro, pico and femto base stations, relays, or WLAN access points where very dense outdoor and indoor deployments may introduce similar obstructive and/or scattering problems at the BS side of the radio access link.

A first step in the direction of realistic channel modeling is to verify the validity of link simulations were the immediate surrounding environment to mobile phone antennas, here a mobile phone user, can be handled as a *super-antenna* with its aggregate far-field pattern to be combined with a directional channel model in a standard procedure. This is presented in Paper II and the method is in its extensible form referred to as the Composite Channel Method. It is found that this method, as we expected, work well for statistical performance evaluation of such multiple antenna techniques as diversity and MIMO spatial multiplexing. In addition we may conclude, based on our observations, that the main influence of the user body, apart from the possibly critical impact of the hand and fingers touching nearby the antenna conductive parts [68], is the shadowing in the multipath channel that statistically increases antenna correlation and, thus, impacts negatively on potential diversity and spatial multiplexing gains.

In the next step of this research we extend the investigation of realistic user environments into vehicles, specifically a standard family car. This environment has previously been investigated with respect to directional penetration loss [38] and is in Paper V extended to also include statistical properties, as well as an attempt to estimate the directional propagation channel in order to further challenge and possibly verify the composite channel modeling principle. Our observations show an increase in inner scattering inside the car (with only a driver present) that provide additional multipath richness. This increased multipath richness however, together with observed penetration loss, strongly depends on the outer scenario, i.e., the outer propagation circumstances and the orientation of the car. We also find that despite the close confined environment inside the car, where we deliberately violate the rule-of-thumb Rayleigh distance requirement when estimating channel parameters using a plane-wave channel model, we get reasonable results both regarding the directional properties of the car and the channel calculations using the composite channel method.

Furthermore, in this thesis we present an overview of a composite channel modeling concept with definitions of the separate channel parts, divided into; antennas, scattering and propagation regions. We address these definitions from our view point and discuss some basic principles without claiming to be comprehensive. Simple and accurate models of realistic environments that map on these definitions are necessary for composite channel modeling in the way we propose here. Some effort has been done on this matter, e.g., the proposed user body shadowing model, or the simple directional car model presented and discussed, but there is much more research left for the future. A proper design and evaluation of such models with the extension to other terminals, the confined or open scattering environments, as well as propagation models, e.g., based on different ray tracing methods, enhanced channel measurements and channel parameter estimations perhaps with non-planar wave fronts, semi-statistical physical propagation models, etc., is research to be continued.

References

[1] 3GPP, "Spatial channel model for MIMO simulations," 3GPP, Tech. Rep. TR 25.996, december 2008. [Online]. Available: http://www.3gpp.org

[2] F. A. Agelet, A. Formella, J. M. H. Rábanos, F. I. de Vicente, and F. P. Fontán, "Efficient ray-tracing acceleration techniques for radio propagation modeling," *IEEE Trans. Veh. Technol.*, vol. 49, no. 6, pp. 2089–2104, Nov 2000.

[3] A. Alayon Glazunov, "On the antenna-channel interactions: A spherical vector wave expansion approach," Ph.D. dissertation, Dept. Electrical and Information Technology, Lund University, Sweden, Feb. 2009.

[4] A. Alexiou, P. S. Kostarakis, V. N. Christofilakis, T. Zervos, A. A. Alexandridis, K. Dangakis, C. Soras, V. V. Petrovic, B. M. Kolundzija, and A. R. Dordevic, "Interaction between GSM handset helical antenna and user's head: Theoretical analysis and experimental results," *Environmentalist*, vol. 25, no. 2, pp. 215–221, 2005.

[5] P. S. Almers, E. Bonek, A. Burr, N. Czink, M. Debbah, V. Degli-Esposti, H. Hofstetter, P. S. Kyösti, D. Laurenson, G. Matz, A. F. Molisch, C. Oestges, and H. Özcelik, "Survey of channel and radio propagation models for wireless MIMO systems," *EURASIP Journal on Wireless Communications and Networking*, 2007.

[6] J. B. Andersen, "UTD multiple-edge transition zone diffraction," *IEEE Trans. Antennas Propagat.*, vol. 45, pp. 1093–1097, July 1997.

[7] ——, "Antenna arrays in mobile communications: Gain, diversity, and channel capacity," *IEEE Antennas Propagat. Mag.*, vol. 42, no. 2, pp. 12–16, April 2000.

[8] ——, "Array gain and capacity for known random channels with multiple elements at both ends," *IEEE J. Select. Areas Commun.*, vol. 18, no. 11, pp. 2172–2178, Nov 2000.

[9] H. R. Anderson, "Building corner diffraction measurements and predictions using UTD," *IEEE Trans. Antennas Propagat.*, vol. 46, no. 2, pp. 292–293, Feb 1998.

[10] H. Asplund, A. A. Glazunov, A. F. Molisch, K. I. Pedersen, and M. Steinbauer, "The COST 259 directional channel model-Part II: Macrocells," *IEEE Trans. Wireless Commun.*, vol. 5, no. 12, pp. 3434–3450, 2006.

[11] C. A. Balanis, *Antenna Theory: Analysis and Design*, 2nd ed. John Wiley & Sons, Inc., 1997.

[12] J.-E. Berg, "A macrocell model based on the parabolic diffusion differential equation," in *Proc. Wireless Personal Comm.*, Virginia Tech, Blacksburg, VA, USA, June 1994, pp. 131–140.

[13] ——, "A recursive method for street microcell path loss calculations," in *PIMRC'95*, vol. 1. IEEE, New York, NY, USA, 1995.

[14] T. Bolin, A. Derneryd, G. Kristensson, V. Plicanic, and Z. Ying, "Two-antenna receive diversity performance in indoor environment," *IEE Electronics Letters*, vol. 41, no. 22, pp. 1205–6, Oct 2005.

[15] K. R. Boyle, Y. Yuan, and L. P. S. Ligthart, "Analysis of mobile phone antenna impedance variations with user proximity," *IEEE Trans. Antennas Propagat.*, vol. 55, no. 2, pp. 364–72, Feb 2007.

[16] D. G. Brennan, "Linear diversity combining techniques," *Proceedings of the IRE*, vol. 47, no. 6, pp. 1075–1102, 1959.

[17] T. W. C. Brown, S. R. Saunders, S. Stavrou, and M. Fiacco, "Characterization of polarization diversity at the mobile," *IEEE Trans. Veh. Technol.*, vol. 56, no. 5, pp. 2440 –2447, Sept. 2007.

[18] S. K. Cho, *Electromagnetic scattering (with 24 illustrations)*, 1st ed. Springer - Verlag, 1990.

[19] L. M. Correia, *Mobile Broadband Multimedia Networks - Techniques, Models and Tools for 4G*, L. M. Correia, Ed. Elsevier, Oxford, UK, 2006.

[20] M. Costa, A. Richter, and V. Koivunen, "Unified array manifold decomposition based on spherical harmonics and 2-D fourier basis," *IEEE Trans. Signal Processing*, vol. 58, no. 9, pp. 4634 –4645, sept. 2010.

[21] T. M. Cover and J. A. Thomas, *Elements of information theory (2. ed.)*. Wiley, 2006.

[22] N. Czink and C. Oestges, "The COST 273 MIMO channel model: Three kinds of clusters," in *IEEE 10th International Symposium on Spread Spectrum Techniques and Applications (ISSSTA '08).*, Aug. 2008, pp. 282–286.

[23] K. R. Dandekar and R. W. Heath, Jr., "Modeling realistic electromagnetic effects on MIMO system capacity," *IEE Electronics Letters*, vol. 38, no. 25, pp. 1624–1625, Dec. 2002.

[24] K. R. Dandekar, G. Xu, and H. Ling, "Computational electromagnetic simulation of smart antenna systems in urban microcellular environments," *IEEE Trans. Veh. Technol.*, vol. 52, no. 4, pp. 733–742, 2003.

[25] B. A. Davis and G. S. Brown, "Diffraction by a randomly rough knife edge," *IEEE Trans. Antennas Propagat.*, vol. 50, no. 12, pp. 1769–1778, Dec 2002.

[26] C. B. Dietrich Jr., K. Dietze, J. R. Nealy, and W. L. Stutzman, "Spatial, polarization, and pattern diversity for wireless handheld terminals," *IEEE Trans. Antennas Propagat.*, vol. 49, no. 9, pp. 1271–1281, Sept 2001.

[27] P. S. Erätuuli and E. Bonek, "Diversity arrangements for internal handset antennas," in *IEEE International Symposium on Personal, Indoor and Mobile Radio Communications, PIMRC '97*, vol. 2, Helsinki, Finland, Sept. 1997, pp. 589–593.

[28] L. B. Felsen and N. Marcuvitz, *Radiation and scattering of waves*, ser. electromagnetic waves.   IEEE Press, 1994.

[29] J. A. Fessler and A. O. Hero, "Space-alternating generalized expectation-maximization algorithm," *IEEE Trans. Signal Processing*, vol. 42, no. 10, pp. 2664–2677, Oct. 1994.

[30] B. H. Fleury, M. Tschudin, R. Heddergott, D. Dahlhaus, and K. I. Pedersen, "Channel parameter estimation in mobile radio environments using the SAGE algorithm," *IEEE J. Select. Areas Commun.*, vol. 17, no. 3, pp. 434–450, 1999.

[31] G. J. Foschini and M. J. Gans, "On limits of wireless communications in a fading environment when using multiple antennas," *Wireless Personal Communications*, vol. 6, no. 3, pp. 311–335, 1998.

[32] J. Fridén, "Calculation of antenna radiation center using angular momentum," April 2012, personal communication (to be published).

[33] C. Gabriel, S. Gabriel, and E. Corthout, "The dielectric properties of biological tissues. I. Literature survey," *Physics in Medicine and Biology*, vol. 41(11), pp. 2231–49, 1996.

[34] J. Guterman, A. Moreira, C. Peixeiro, and Y. Rahmat-Samii, "Wrapped microstrip antennas for laptop computers," *IEEE Antennas Propagat. Mag.*, vol. 51, no. 4, pp. 12 –39, Aug. 2009.

[35] K. Haneda, J.-I. Takada, and T. Kobayashi, "Experimental evaluation of a SAGE algorithm for ultra wideband channel sounding in an anechoic chamber," in *International Workshop on Ultra Wideband Systems, Joint UWBST IWUWBS*, Kyoto, Japan, May 2004, pp. 66–70.

[36] ——, "A parametric UWB propagation channel estimation and its performance validation in an anechoic chamber," *IEEE Trans. Microwave Theory Tech.*, vol. 54, no. 4, pp. 1802 – 1811, June 2006.

[37] J. Hansen, Ed., *Spherical Near-Field Antenna Measurements*, ser. IEE electromagnetic waves series.   Peter Peregrinus Ltd., 1998, vol. 26.

[38] F. Harrysson, "A simple directional path loss model for a terminal inside a car," in *IEEE Veh. Technol. Conf. VTC 2003-Fall*, vol. 1, Boston, MA, Oct. 2003, pp. 119–122.

[39] F. Harrysson and J.-E. Berg, "Propagation prediction at 2.5 GHz close to a roof mounted antenna in an urban environment," in *IEEE Veh. Technol. Conf. VTC 2001-Fall*, vol. 3, Atlantic City, NJ, Oct. 2001, pp. 1261–1263.

[40] F. Harrysson, J. Medbo, A. F. Molisch, A. J. Johansson, and F. Tufvesson, "The composite channel method: Efficient experimental evaluation of a realistic MIMO terminal in the presence of a human body," in *IEEE Veh. Technol. Conf. VTC 2008-Spring*, Singapore, May 2008, pp. 473–477.

[41] M. Hata, "Empirical formula for propagation loss in land mobile radio services," *IEEE Trans. Veh. Technol.*, vol. 29, no. 3, pp. 317–325, 1980.

[42] IEEE Std 145-1993, "IEEE standard definition of terms for antennas," Antenna Standards Committee of the IEEE Antennas and Propagation Society, IEEE, March 1993.

[43] M. A. Jensen and Y. Rahmat-Samii, "EM interaction of handset antennas and a human in personal communications," *Proc. IEEE*, vol. 83, no. 1, pp. 7–17, 1995.

[44] Z. Ji, B.-H. Li, H.-X. Wang, H.-Y. Chen, and T. K. Sarkar, "Efficient ray-tracing methods for propagation prediction for indoor wireless communications," *IEEE Antennas Propagat. Mag.*, vol. 43, no. 2, pp. 41–49, April 2001.

[45] J. B. Keller, "Geometrical theory of diffraction," *J. Opt. Soc. Amer.*, vol. 52, no. 2, pp. 116–130, Feb 1962.

[46] J. P. Kermoal, L. Schumacher, K. I. Pedersen, P. E. Mogensen, and F. Frederiksen, "A stochastic MIMO radio channel model with experimental validation," *IEEE J. Select. Areas Commun.*, vol. 20, no. 6, pp. 1211–1221, Aug. 2002.

[47] R. G. Kouyoumjian and P. S. H. Pathak, "A uniform geometric theory of diffraction for an edge in a perfectly conducting surface, UTD," *Proc. IEEE*, vol. 62, no. 11, pp. 1448–1461, Nov. 1974.

[48] H. Krim and M. Viberg, "Two decades of array signal processing research: the parametric approach," *IEEE Signal Processing Mag.*, vol. 13, no. 4, pp. 67–94, 1996.

[49] J. Krogerus, C. Icheln, and P. S. Vainikainen, "Dependence of mean effective gain of mobile terminal antennas on side of head," in *2005 European Microwave Conference*, Paris, France, Oct. 2005.

[50] P. Kyösti, J. Meinilä, L. Hentilä, X. Zhao, T. Jämsä, C. Schneider, M. Narandzic, M. Milojevic, A. Hong, J. Ylitalo, V.-M. Holappa, M. Alatossava, R. Bultitude, Y. de Jong, and T. Rautiainen, "WINNER II channel models," IST-WINNER, Tech. Rep. D1.1.2 V1.1, September 2007. [Online]. Available: http://www.ist-winner.org

[51] M. Landmann, M. Käske, and R. S. Thomä, "Impact of incomplete and inaccurate data models on high resolution parameter estimation in multidimensional channel sounding," *IEEE Trans. Antennas Propagat.*, vol. 60, no. 2, pp. 557 –573, Feb. 2012.

[52] M. Landmann, "Limitations of experimental channel characterisation," Ph.D. dissertation, TU Ilmenau, Ilmenau, Germany, May 2008.

[53] C.-H. Li, E. Ofli, N. Chavannes, H. U. Cherubini, E. andGerber, and N. Kuster, "Effects of hand phantom and different use patterns on mobile phone antenna radiation performance," in *IEEE Antennas and Propagation Society International Symposium, AP-S 2008*, San Diego, CA, July 2008.

[54] G. Liang and H. L. Bertoni, "A new approach to 3-D ray tracing for propagation prediction in cities," *IEEE Trans. Antennas Propagat.*, vol. 46, no. 6, pp. 853–863, June 1998.

[55] P. Lindberg, A. Kaikkonen, and B. Kochali, "Body loss measurements of internal terminal antennas in talk position using real human operator," in *iWAT*, Chiba, Japan, 2008, pp. 358–361.

[56] Y. Liu and I. R. Ciric, "Improved formulas for the diffraction by a wedge," *Radio Science*, vol. 28, no. 5, pp. 859–863, Sep.-Oct. 1993.

[57] U. Martin, "Echo estimation-deriving simulation models for the mobile radio channel," in *Vehicular Technology Conference, 1995 IEEE 45th*, vol. 1, Chicago, IL, July 1995, pp. 231–235.

[58] P. S. Mattheijssen, M. H. A. J. Herben, G. Dolmans, and L. Leyten, "Antenna-pattern diversity versus space diversity for use at handhelds," *IEEE Trans. Veh. Technol.*, vol. 53(4), pp. 1035–42, 2004.

[59] D. McNamara, M. Beach, and P. Fletcher, "Spatial correlation in indoor MIMO channels," in *Personal, Indoor and Mobile Radio Communications, 2002. The 13th IEEE International Symposium on*, vol. 1, Sept. 2002, pp. 290–294.

[60] J. Medbo, J. E. Berg, and F. Harrysson, "Temporal radio channel variations with stationary terminal," in *IEEE Veh. Technol. Conf. VTC 2004-Fall*, vol. 1, Los Angeles, CA, Sept. 2004, pp. 91–95.

[61] J. Medbo, F. Harrysson, H. Asplund, and J. E. Berg, "Measurements and analysis of a MIMO macrocell outdoor-indoor scenario at 1947 MHz," in *IEEE Veh. Technol. Conf. VTC 2004-Spring*, vol. 1, Milan, Italy, May 2004, pp. 261–265.

[62] J. Medbo, H. Asplund, J.-E. Berg, and N. Jaldén, "Directional channel characteristics in elevation and azimuth at an urban macrocell base

station," in *Antennas and Propagation (EuCAP), Proceedings of the 6th European Conference on*, Prague, Czech Republic, March 2012.

[63] J. Medbo and F. Harrysson, "Efficiency and accuracy enhanced super resolved channel estimation," in *Antennas and Propagation (EuCAP), Proceedings of the 6th European Conference on*, Prague, Czech Republic, March 2012.

[64] J. Medbo, M. Riback, H. Asplund, and J.-E. Berg, "MIMO channel characteristics in a small macrocell measured at 5.25 GHz and 200 MHz bandwidth," in *IEEE Veh. Technol. Conf. VTC 2005-Fall*, vol. 1, Dallas, TX, Sept. 2005, pp. 372–376.

[65] A. F. Molisch, *Wireless Communications*. Chichester, U.K.: IEEE Press - Wiley, 2005.

[66] A. F. Molisch, H. Asplund, R. Heddergott, M. Steinbauer, and T. Zwick, "The COST 259 directional channel model-Part I: Overview and methodology," *IEEE Trans. Wireless Commun.*, vol. 5, no. 12, pp. 3421–3433, 2006.

[67] J. Ø. Nielsen, B. Yanakiev, I. B. Bonev, M. Christensen, and G. F. Pedersen, "User influence on MIMO channel capacity for handsets in data mode operation," *IEEE Trans. Antennas Propagat.*, vol. 60, no. 2, pp. 633–643, Feb. 2012.

[68] J. Nielsen, "Is the iPhone 4 born with antenna problems?" IDG Denmark A/S, Hørkær 18, 2730 Herlev, June 2010. [Online]. Available: http://www.comon.dk/nyheder/Er-iPhone-4-foedt-med-antenne-problemer-1.362104.html

[69] J. Ø. Nielsen and G. F. Pedersen, "In-network performance of handheld mobile terminals," *IEEE Trans. Veh. Technol.*, vol. 55, no. 3, pp. 903–916, May 2006.

[70] J. Ø. Nielsen, G. F. Pedersen, K. Olesen, and I. Z. Kovacs, "Statistics of measured body loss for mobile phones," *IEEE Trans. Antennas Propagat.*, vol. 49, no. 9, pp. 1351–1353, Sept. 2001.

[71] K. Ogawa, A. Yamamoto, and J.-I. Takada, "Multipath performance of handset adaptive array antennas in the vicinity of a human operator," *IEEE Trans. Antennas Propagat.*, vol. 53, no. 8, pp. 2422–2436, 2005.

[72] H. Özcelik, M. Herdin, W. Weichselberger, J. Wallace, and E. Bonek, "Deficiencies of 'Kronecker' MIMO radio channel model," *Electronics Letters*, vol. 39, no. 16, pp. 1209 – 1210, Aug. 2003.

[73] G. F. Pedersen, K. Olesen, and S. L. Larsen, "Bodyloss for handheld phones," in *IEEE Veh. Technol. Conf. VTC 1999-Spring*, Houston, TX, May 1999, pp. 1580–1584.

[74] M. Pelosi, O. Franek, M. B. Knudsen, M. Christensen, and G. F. Pedersen, "A grip study for talk and data modes in mobile phones," *IEEE Trans. Antennas Propagat.*, vol. 57, no. 4, pp. 856–865, April 2009.

[75] M. Pelosi, O. Franek, M. B. Knudsen, G. F. Pedersen, and J. B. Andersen, "Antenna proximity effects for talk and data modes in mobile phones," *IEEE Antennas Propagat. Mag.*, vol. 52, no. 3, pp. 15–27, June 2010.

[76] M. Pelosi, G. F. Pedersen, and M. B. Knudsen, "Influence of human hand on mobile phone radiation," COST 2100, Lisbon, Portugal, Tech. Rep. TD (07)036, Feb. 2007.

[77] V. Plicanic, B. K. Lau, A. Derneryd, and Z. Ying, "Actual diversity performance of a multiband diversity antenna with hand and head effects," *IEEE Trans. Antennas Propagat.*, vol. 57, no. 5, pp. 1547–1556, May 2009.

[78] J. Poutanen, K. Haneda, L. Liu, C. Oestges, F. Tufvesson, and P. Vainikainen, "Parameterization of the COST 2100 MIMO channel model in indoor scenarios," in *Antennas and Propagation (EUCAP), Proceedings of the 5th European Conference on*, April 2011, pp. 3606–3610.

[79] A. Richter, D. Hampicke, G. Sommerkorn, and R. S. Thomä, "Joint estimation of DoD, time-delay, and DoA for high-resolution channel sounding," in *IEEE Veh. Technol. Conf. VTC 2000-Spring*, vol. 2, Tokyo, Japan, May 2000, pp. 1045–1049.

[80] ——, "MIMO measurement and joint M-D parameter estimation of mobile radio channels," in *IEEE Veh. Technol. Conf. VTC 2001-Spring*, vol. 1, Rhodes, Greece, May 2001, pp. 214–218.

[81] A. Richter, "Estimation of radio channel parameters: Models and algorithms," Ph.D. dissertation, TU Ilmenau, Ilmenau, Germany, May 2005.

[82] J.-P. Rossi and Y. Gabillet, "A mixed ray launching/tracing method for full 3-D UHF propagation modeling and comparison with wide-band

measurements," *IEEE Trans. Antennas Propagat.*, vol. 50, no. 4, pp. 517–523, April 2002.

[83] T. M. Schäfer and W. Wiesbeck, "Simulation of radiowave propagation in hospitals based on FDTD and ray-optical methods," *IEEE Trans. Antennas Propagat.*, vol. 53, no. 8, pp. 2381–2388, Aug. 2005.

[84] M. Shafi, M. Zhang, A. L. Moustakas, P. J. Smith, A. F. Molisch, F. Tufvesson, and S. H. Simon, "Polarized MIMO channels in 3-D: models, measurements and mutual information," *IEEE J. Select. Areas Commun.*, vol. 24, no. 3, pp. 514 – 527, March 2006.

[85] A. Sibille, "A small signal analysis of statistical antenna modelling," in *Proceedings of the 3rd European Conference on Antennas and Propagation (EuCAP), 2009*, March 2009, pp. 2102–2106.

[86] A. Sibille and M. A. Mellah, "A statistical model of handsets effective gain accounting for user influence and local propagation," in *Proceedings of the Fourth European Conference on Antennas and Propagation (EuCAP), 2010*, April 2010, pp. 1 –4.

[87] K. Sivasondhivat, J.-I. Takada, I. Ida, and Y. Oishi, "Polarimetric Kronecker separability of site-specific double-directional channel in an urban macrocellular environment," *EURASIP Journal on Wireless Communications and Networking*, 2009.

[88] M. Steinbauer, A. F. Molisch, and E. Bonek, "The double-directional radio channel," *IEEE Antennas Propagat. Mag.*, vol. 43, no. 4, pp. 51–63, Aug. 2001.

[89] P. S. Suvikunnas, K. Sulonen, J. Villanen, C. Icheln, J. Ollikainen, and P. S. Vainikainen, "Evaluation of performance of multi-antenna terminals using two approaches," in *IEEE Instrumentation and Measurement Technology Conference, IMTC 2004*, vol. 2, Lake Como, Italy, May 2004, pp. 1091–1096.

[90] P. S. Suvikunnas, J. Villanen, K. Sulonen, C. Icheln, J. Ollikainen, and P. S. Vainikainen, "Evaluation of the performance of multi-antenna terminals using a new approach," *IEEE Trans. Instrum. Meas.*, vol. 55, no. 5, pp. 1804–1813, Oct. 2006.

[91] I. E. Telatar, "Capacity of multi-antenna gaussian channels," *European Transactions on Telecommunications*, vol. 10, no. 6, pp. 585–595, Nov/Dec 1999.

[92] R. S. Thomä, D. Hampicke, A. Richter, G. Sommerkorn, A. Schneider, U. Trautwein, and W. Wirnitzer, "Identification of time-variant directional mobile radio channels," *IEEE Trans. Instrum. Meas.*, vol. 49, no. 2, pp. 357–364, 2000.

[93] J. Toftgård, S. N. Hornsleth, and J. B. Andersen, "Effects on portable antennas of the presence of a person," *IEEE Trans. Antennas Propagat.*, vol. 41, no. 6, pp. 739–746, 1993.

[94] N. Tyler, B. Allen, and A. H. Aghvami, "Robust DoA estimation by extension of the SAGE algorithm: algorithm description and trails results," *Microwaves, Antennas and Propagation, IEE Proceedings*, vol. 153, no. 6, pp. 568–572, Dec. 2006.

[95] C. Tzaras and S. R. Saunders, "An improved heuristic UTD solution for multiple-edge transition zone diffraction," *IEEE Trans. Antennas Propagat.*, vol. 49, no. 12, pp. 1678–1682, Dec 2001.

[96] R. Valenzuela, "A ray tracing approach to predicting indoor wireless transmission," in *Proceedings of 1993 IEEE Vehicular Technology Conference (VTC)*, Secaucus, NJ, May 1993, pp. 214–218.

[97] R. Vaughan and J. B. Andersen, *Channels, Propagation and Antennas for Mobile Communications*, IEE Electromagnetic Waves Series, no. 50, London, UK, 2003.

[98] W. Weichselberger, M. Herdin, H. Ozcelik, and E. Bonek, "A stochastic MIMO channel model with joint correlation of both link ends," *IEEE Trans. Wireless Commun.*, vol. 5, no. 1, pp. 90–100, Jan. 2006.

[99] W. Wiesbeck, T. Fügen, M. Porebska, and W. Sörgel, "Channel characterization and modeling for MIMO and other recent wireless technologies," in *Proceedings of the European Conference on Antennas and Propagation: EuCAP 2006*, Nice, France, Nov. 2006.

[100] J. H. Winters, "On the capacity of radio communication systems with diversity in a rayleigh fading environment," *IEEE J. Select. Areas Commun.*, vol. 5, no. 5, pp. 871–878, June 1987.

[101] A. Yamamoto, T. Hayashi, K. Ogawa, K. Olesen, J. Ø. Nielsen, and G. F. Pedersen, "Cellular MIMO system performance versus base station element spacing," in *2008 IEEE Antennas and Propagation Society International Symposium*, Chicago, IL, July 2008, pp. 1–4.

[102] A. Yamamoto, T. Hayashi, K. Ogawa, K. Olesen, J. Ø. Nielsen, N. Zheng, and G. F. Pedersen, "Outdoor urban propagation experiment of a handset MIMO antenna with a human phantom located in a browsing stance," in *IEEE Veh. Technol. Conf. VTC 2007-Fall*, Baltimore, MD, Sept. 2007, pp. 849–853.

[103] A. Yamamoto, H. Toshiteru, O. Koichi, K. Olesen, J. Ø. Nielsen, N. Zheng, and G. F. Pedersen, "Comparison of phantoms for browsing position by a NLOS outdoor MIMO propagation test," in *Proceedings of ISAP2007*, Niigata, Japan, Aug. 2007, pp. 1342–1345.

[104] B. Yanakiev, J. O. Nielsen, M. Christensen, and G. Frolund Pedersen, "Small device for short-range antenna measurements using optics," *IEEE Antennas Propagat. Mag.*, vol. 53, no. 6, pp. 148 –152, Dec. 2011.

[105] S. B. Yeap, X. Chen, J. A. Dupuy, C. C. Chiau, and C. G. Parini, "Integrated diversity antenna for laptop and PDA terminal in a MIMO system," *IEE Proc. Microw. Antennas and Propagat.*, vol. 152, no. 6, pp. 495–504, 2005.

[106] Z. Zhang, Z. Yun, and M. F. Iskander, "Ray tracing method for propagation models in wireless communication systems," *IEE Electronics Letters*, vol. 49, no. 6, pp. 2350–2358, Nov. 2000.

Part II

Included Research Papers

Paper I

Dual Antenna Terminals in an Indoor Scenario

Abstract

The performance of two different dual antenna hand-held test mobile terminals has been investigated in a realistic indoor office environment and scenario, with respect to antenna performance, diversity combining and Shannon MIMO channel capacity. Measurements of a 2×2 MIMO channel at 1877.5 MHz (narrowband) were performed using a dual-polarized base station antenna. Analyses show that diversity gains, using ideal selection combining and maximum ratio combining, between 0.7 and 4.6 dB was achieved at the 10% outage probability level. Ideal dual-side beamforming (single branch) gives up to 3.3 dB capacity gain compared to single antenna systems at SNR less than 10 dB, however, decreases with rising SNR. Dual branch MIMO capacity gain is only significant at higher SNR above 10 dB. In addition, horizontal polarization at the base station was found to outperform vertical polarization in this scenario.

1   Introduction

Multiple antenna systems at the base station and in the mobile terminal are already being developed to improve system capacity in mobile communication systems. The system gain may either be reached by tackling multipath fading, using antenna diversity (diversity gain), improve link gain using antenna beam-forming (directivity gain) or by taking full advantage of the multipath channel and increase throughput by spatial multiplexing using parallel propagation channels (MIMO). Several investigations have been published dealing with spatial and/or the polarization properties of multiple antennas in various indoor scenarios, using dipole antenna arrays or similar at the terminal side, e.g., [1] [2]. Colburn *et al.* [3] evaluated diversity for a set of realistic dual antenna terminal implementations at 900 MHz, but without the influence of users. Recently a strategic approach to combine measured channels with antenna simulations is proposed [4]. However, it is still an important and interesting issue, how to accomplish good multiple antenna performance in practice in a hand-held mobile terminal, taking into account the restrictions on size, the antenna element design and the influence of the hand and the head of a user.

Addressing this issue, a simple experimental investigation is presented here where the performance with respect to diversity and Shannon MIMO capacity (i.e., maximum mutual information) of a couple of test dual-antenna terminals is evaluated in a realistic propagation environment and user scenario. The environment is a single floor office corridor with rooms at both sides. A dual polarized (horizontal and vertical) base station sector antenna was placed at the end of the corridor, and a test person was carrying the test terminal, walking along the corridor and taking turns into the neighboring office rooms. The measurements were set-up for 2x2 forward link MIMO channel measurements at 1877.5 MHz (narrowband). The experimental results are presented here together with analyses of diversity and potential capacity.

2   Test Antennas

At the mobile station (MS) two dual antenna test terminals with the same ground plane size were used. One solution with spatially separated orthogonal $\lambda/4$ slot antennas (DSA), and one with two co-located antennas, a bent PIFA together with a slot antenna (PSA), see Figure 1. A summary of antenna characteristics gathered from laboratory measurement of antenna loss and antenna farfield patterns, together with calculated dual-antenna pattern correlations (over the full sphere), can be found in Table 1. The test antennas were poorly matched yielding significant reflection losses. This is because the measurement
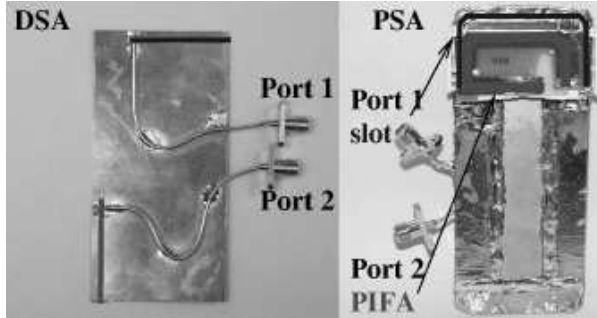
Figure 1: The dual antenna test terminals.

Table 1: Reflection loss and antenna pattern correlation at the frequency 1877.5 MHz for the test antennas.

Terminal	Loss (dB) Port 1	Loss (dB) Port 2	Loss Diff. $|\Delta_{1,2}|(dB)$	Corr. $|\rho_{12}|$
DSA	2.6	1.5	1.1	0.2
PSA	6.6	2.7	3.9	0.4

frequency was chosen somewhat outside the design frequency bands of the terminals, in particular in the PSA slot antenna case (Port 1). The DSA terminal antenna pattern cross-correlation is low (0.2), while it is higher (0.4) for the PSA.

3 Measurements

3.1 Measurement Setup

The measurement setup is shown in Figure 2. A dual-polarized ($0°/90°$), sector base station antenna (BS) with 14 dBi gain and $60°$ half-power azimuth beamwidth, was used at the Tx side. Each of the two BS antenna ports (horizontal and vertical polarization) was fed by a signal generator (SG) with a CW signal at 1877.5 GHz, separated by 500 Hz. At the receiver the antenna ports were connected to a vector network analyzer (VNA) with sample frequency set to 1600 Hz. The measurement time for each antenna test run was about 200 s. The two signals were separated by windowing in the frequency domain. During all measurements the minimum SNR was found to be 29 dB.
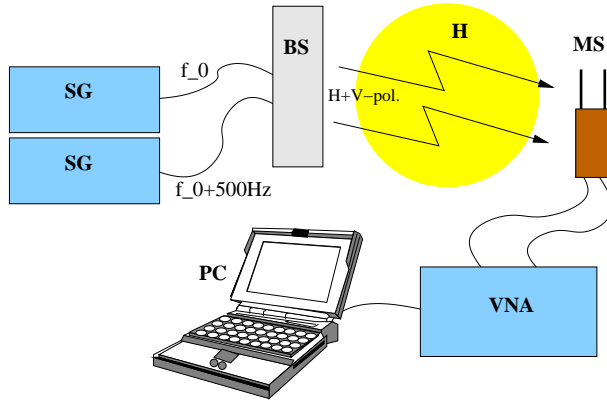
Figure 2: The measurement setup.

3.2   Measurement Scenario

The measurements took place at a single floor in an office environment, with a corridor about 40 m long and rooms at both sides, of an Ericsson building in Stockholm, Sweden. A test user was gently holding one of the test terminals at a time, with one hand in two different user modes, *data mode* and *talk mode*. With data mode means that the terminal was held in front of the user in a position typical for viewing a terminal screen, e.g., a video call or web browsing and with talk mode means that the terminal was held at the right ear a few centimeters from the head, see Figure 3. During the measurements (about 4 minutes each), the test user was walking one turn back and forth along the corridor making turns into several rooms that were passed along the way. An additional measurement operator, not entering the rooms but unavoidably influencing the channel, was following a few meters from the test user with a trolley carrying the VNA and the data recording PC.

4   Experimental Results and Analyses

4.1   Channel Matrix

From the four channel measurements of each test terminal the 2x2 channel matrix **H** was formed over measured time, as

$$H(t) = \begin{bmatrix} h_{V1}(t) & h_{H1}(t) \\ h_{V2}(t) & h_{H2}(t) \end{bmatrix} \tag{1}$$

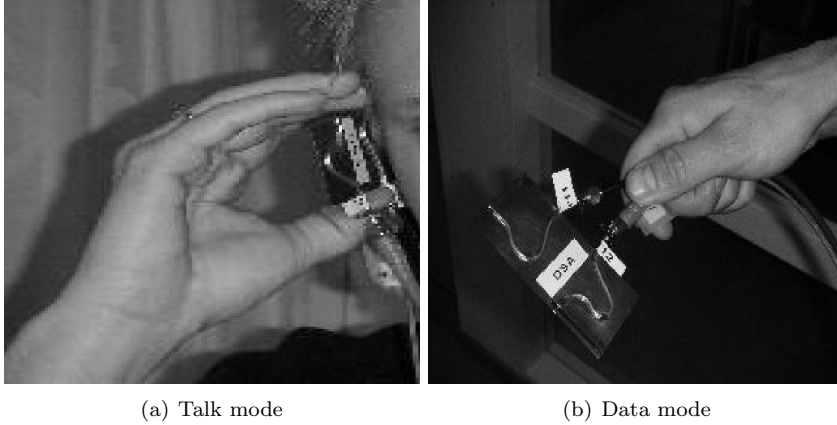(a) Talk mode   (b) Data mode

Figure 3: User modes in this investigation.

where the indices represent the horizontal (H) and vertical (V) polarization
ports of the BS antenna and the antenna ports numbered 1 and 2 of the MS.
The channel data was normalized to unit maximum gain of the BS antenna for
both polarization ports separately, and includes the antenna efficiency of the
MS test antennas.

In Figure 4 the sliding average of the measured channel components are
shown for the DSA terminal in data mode. In this case the sliding average
is taken by convolution of the complex channel data, i.e., the channel matrix
components, over time, with a Kaiser window (Matlab) of width 2 s (3200
samples). It is seen that the signal decreases roughly 20 dB as the MS is
moved away from the BS through the office corridor.

4.2   Path Loss

To show the channel behavior the path loss distance dependency is plotted for
the case of a vertical dipole test antenna measurement in Figure 5. The distance
is a rough estimate based on the length of the corridor with no consideration
taken to the turns into the rooms. The dots show the mean over 1600 samples
or 1 sec. In average the path loss follows a distance dependency ($L \sim d^n$) with
a path loss exponent of $n = 3$, which is typical for NLOS corridor propagation,
when the MS antenna is inside office rooms. The lower dips seem to have a
path loss exponent around $n = 2$ which is similar to free-space propagation, or
even less at some locations, which indicate a "wave-guide" effect of the corridor.
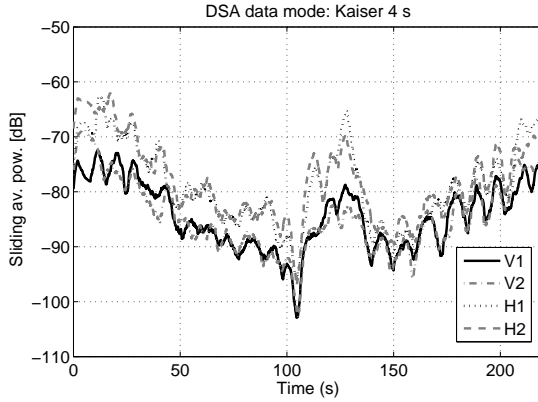
Figure 4: Sliding average of the measured channel for the DSA in data mode over 2 s (3200 samples) vs. measured time.

The results are similar to what has been previously found at the same location at 5 GHz [5].

4.3   Antenna Correlation

The observable signal correlation between adjacent antennas elements in an environment may be either the magnitude of the complex correlation coefficient calculated from the complex channel measurements or the correlation coefficient of the envelope of the channel measurements, i.e., the envelope correlation. In a Rayleigh channel these two are supposed to be equal. In this investigation we have chosen to consider only complex channel correlation since this seems to be the most robust treatment [2]. The complex correlation coefficient ρ_{xy} between two simultaneous measured signal branches x and y, provided by the dual antennas in the terminals, is calculated as

$$\rho_{xy} = \frac{\sigma_{xy}^2}{\sqrt{\sigma_x^2 \sigma_y^2}} \tag{2}$$

where σ_{xy}^2 is the covariance, i.e.,

$$\sigma_{xy}^2 = \frac{1}{N-1} \sum_n (x_n - \mu_x)(y_n - \mu_y) \tag{3}$$
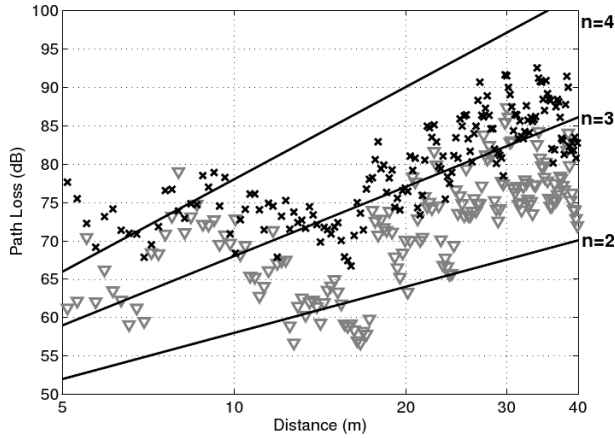
Figure 5: Local average path loss for a test measurement with a vertical $\lambda/2$-dipole at the MS, with vertical (triangles) and horizontal (crosses) polarization at the BS.

The mean of the complex correlation coefficients magnitude, $|\rho_{12}|$, is plotted in Figure 6 as a function of time bin size N. As can be seen, the mean correlation coefficient approaches about 0.3 for the DSA and 0.8 for the PSA terminal (almost independent of user modes), to be compared to the free space isotropic channel correlation in Table 1 where the correlation was 0.2 and 0.4 respectively. The difference is due to the directional and polarization properties of the channel. At time bins shorter than about 2 s the autocorrelaton of the measurement is apparent and the number of fades to average over diminish.

4.4 Diversity Combining

To investigate potential diversity performance of the two terminal solutions, two common diversity combining techniques are studied,

ISC Ideal selection combining, $r_c = max(r_1, r_2)$

MRC Maximum ratio combining, $r_c = \sqrt{(r_1^2 + r_2^2)}$

where r_1 and r_2 are the envelopes (or absolute values) of the channel matrix elements at MS ports 1 and 2, respectively, for either V or H polarization at the BS. For comparison simultaneous Tx and Rx selection combining (2x2 ISC) is also studied where the channel is assumed to be known at all time at both transmitter and receiver. The results for the DSA and the PSA in
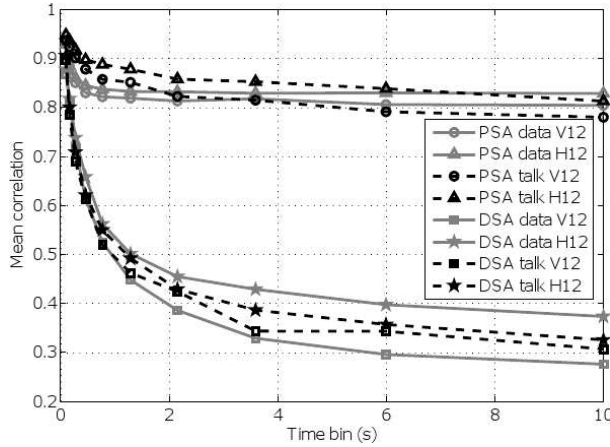
Figure 6: The mean magnitude of the complex correlation coefficients as a function of time bin.

talk and data mode, are shown in Figure 7 for vertical polarization at the BS. The graphs show the cumulative distribution of the *path gain*, i.e., the path loss times the terminal antenna gain. From the graphs the *diversity gain* and the *path gain difference* can be found at a certain system dependent outage level (typically 10%). The diversity gain is defined as the ratio between the combined solution and the strongest branch and the path gain difference is the difference between the path gain of the two branches. Both theese enteties are in this paper observed at an outage level of 10%.

4.5 Capacity

The theoretical Shannon capacity or maximum mutual information throughput of a MIMO channel is calculated as the sum of the individual capacities of each parallel channel branch i, with corresponding branch output power providing the receiver SNR's P_i, as

$$C = \sum_i \log_2(1 + \lambda_i P_i) \quad [\text{bits/s/Hz}] \tag{4}$$

where λ_i is the i:th non-zero eigenvalue of the *normalized* correlation matrix HH^H. The eigenvalues were found as the square of the singular values by singular value decomposition of the channel matrix

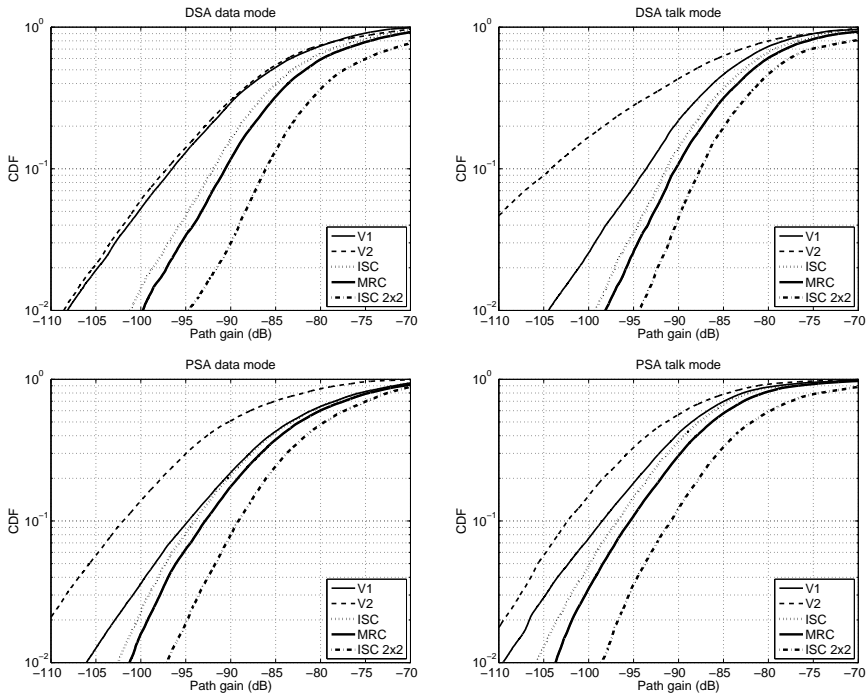$$[U, S, V] = \texttt{svd}(H). \tag{5}$$

Figure 7: Path gain distribution for single MS antennas, with MS diversity (ISC and MRC) and with double sided 2x2 ISC, for vertical BS polarization. The results for the DSA are shown in the upper graphs and for the PSA in the lower graphs with data mode to the left and talk mode to the right.

where S is a diagonal matrix with the singular values in the diagonal

$$S = \left\{ \begin{matrix} \sigma_1 & 0 \\ 0 & \sigma_2 \end{matrix} \right\} \tag{6}$$

The transformation matrices U and V contain the singular vectors which can be interpreted as the complex antenna steering vectors, i.e., the pair-wise corresponding beamforming vectors for each channel branch, for the MS and BS, respectively. The cumulative distribution of the eigenvalues is shown in Figure 8. The eigenvalues are calculated for the 2x2 (unnormalized) channel matrix H formed at each time sample from the four channel measurements. The graphs show that one branch is overall dominating with between 10-20 dB over the second branch.

For a known channel, the maximum capacity is reached by "water filling", see for example [6], page 651. Each available branch power P_i for a fix average receiver SNR, are filled up to a common level D on the parallel channel branches so that

$$\frac{1}{\lambda_1} + P_1 = \frac{1}{\lambda_2} + P_2 = \cdots = D \tag{7}$$

Thus, the best branch receives the largest amount of power. The sum of the powers P_i is constrained to the average receiver SNR P by

$$\sum_i P_i = P \tag{8}$$

which gives the common level D as

$$D = \frac{1}{N}\left(P + \sum_i^N \frac{1}{\lambda_i}\right) \tag{9}$$

For a branch where $1/\lambda_i \geq D$, the corresponding power is set to zero.

The channel matrix H was in the capacity analysis, at each time sample, normalized with the uniform sliding mean of the channel matrix elements found for each terminal as

$$\tilde{H}(n) = \frac{H(n)}{\frac{1}{W+1}\sum_{i=n-W/2}^{n+W/2}\sqrt{\frac{1}{MN}||H(i)||_f^2}} \tag{10}$$

where M, N is the number of ports at the BS and MS ($MN = 4$), $W + 1$ is the length of the averaging window and $||H_i||_f$ is the Frobenius norm of H at sample i. The measurement traces were not exactly similar between the terminal measurements so the performance could not be compared to a
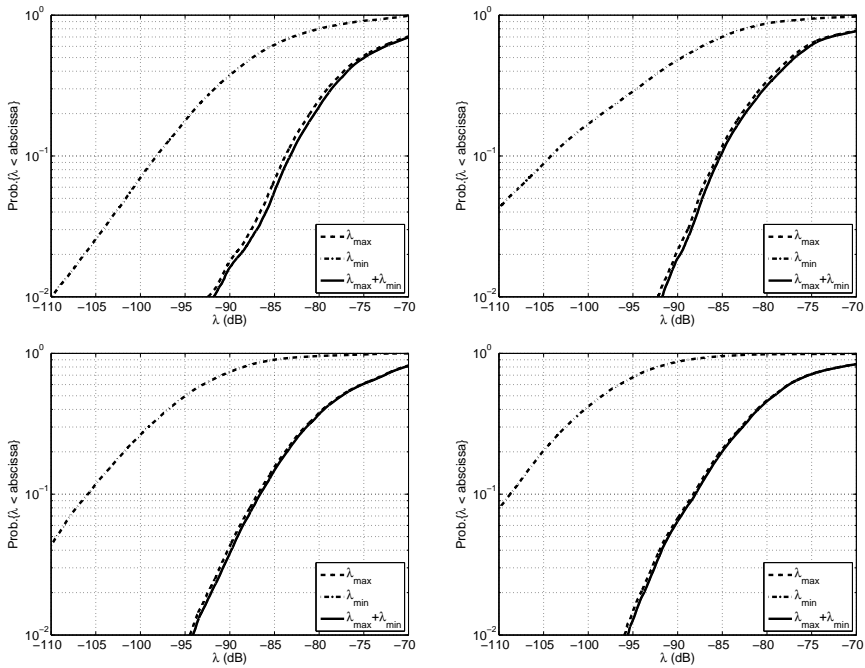
Figure 8: Cumulative probability distribution of the eigenvalues for different terminal scenarios taken over the whole measurement route. The results for the DSA are shown in the upper graphs and for the PSA in the lower graphs with data mode to the left and talk mode to the right.

common reference which is the preferred choice if true terminal performances are to be compared. Thus, the difference in mean efficiency of each terminal in the scenario is omitted in the capacity evaluation.

The mean capacity over the measurement route, for different antenna configurations is plotted in Figure 9 as a function of mean receiver SNR. Without significant lack of precision the channel matrix was resampled with 16 Hz (1600/100) to save simulation time. Thus the sampling rate was $2.4/\lambda$ (i.e., well within the Nyqvist theorem) assuming a measurement speed of 1 m/s. The sliding mean window was set to 1 s, i.e., $W = 16$.

The circles show a mean over the four possible SISO configurations, V1, V2, H1 and H2. The triangles show the mean capacity over the two 1x2 configurations H1H2, V1V2, which is the same as instantaneous MRC or beamforming at the MS. The diamonds show the mean capacity for a full 2x2 antenna configuration using only the channel branch with the strongest singular value (i.e., double-sided MRC or beamforming at the BS and MS), while the crosses show the mean capacity for full MIMO using water filling.

In Figure 10 the capacity gain over SISO is shown for the same cases as in Figure 9. Similar performance is found for all terminal solutions with a slightly better result for the DSA. From this graph it is obvious that the capacity gain using full MIMO is insignificant, compared to using MRC at both BS and MS, at an SNR level below 10 dB. However, substantial capacity gain is reached using 2x2 diversity (assuming a known channel). At high SNR (larger than 10 dB) the 2x2 capacity gain narrows down towards the MS diversity case, while full MIMO with two signal chains seems to level off at a gain of almost a factor of 2 (3 dB).

The matrices U and V from (5) contain the singular vectors, i.e., the ideal complex antenna steering vectors or beamforming vectors for each channel branch, for the MS and BS, respectively. In Figure 11 the cumulative distribution of the square magnitudes of the corresponding singular vector elements of the branch with the strongest singular value, are presented (in linear scale). In all cases the horizontal polarization port antenna was quite highly dominating at the BS side. At the MS side, the PSA Port 1 (the slot antenna) was the best choice, while in the DSA case the difference between the antenna elements in performance was small. In the DSA case, the Port 1 antenna was slightly the better one in data mode, and the Port 2 antenna was slightly the better one in talk mode. The latter could be explained by the 90° tilt of the terminal in talk mode, see Figure 3. In this case the Port 2 slot antenna pattern is mainly horizontally polarized which matches the BS polarization. In data mode, however, both antennas are almost horizontally oriented. As expected the user mode severely influences the performance of a certain antenna solution at the BS. At the BS the H-polarization seems to be the best choice for the
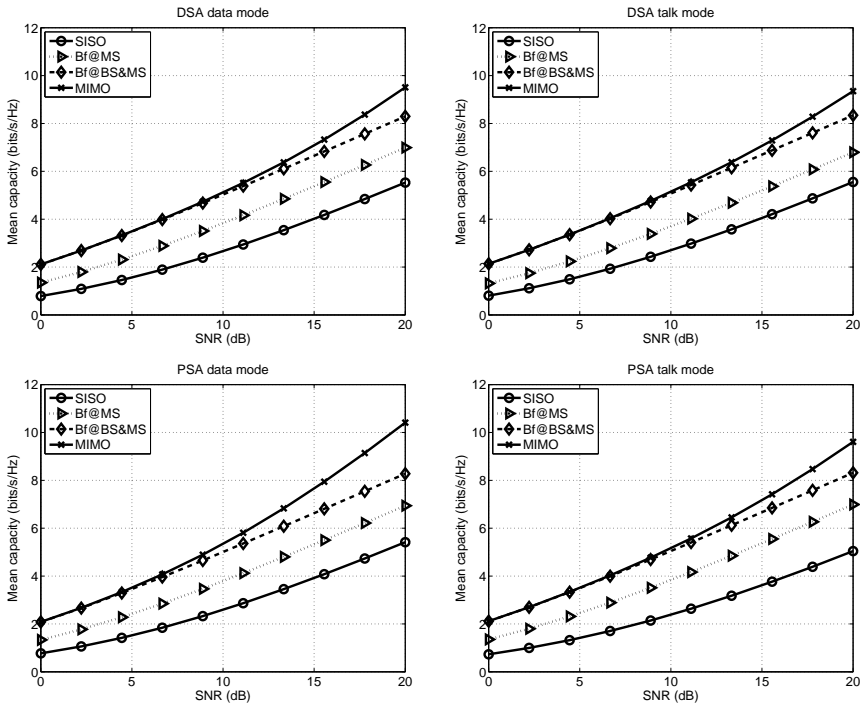
Figure 9: Mean Shannon capacity for SISO, MS MRC diversity, single branch MIMO, and full MIMO with water filling. The results for the DSA are shown in the upper graphs and for the PSA in the lower graphs with data mode to the left and talk mode to the right.
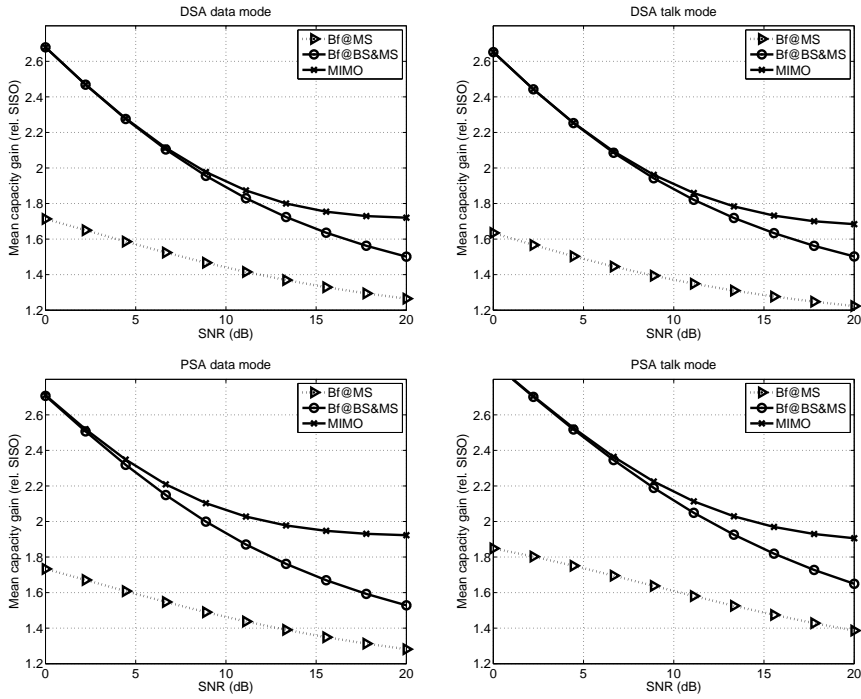
Figure 10: Capacity gain relative the mean SISO capacity. The results for the DSA are shown in the upper graphs and for the PSA in the lower graphs with data mode to the left and talk mode to the right.
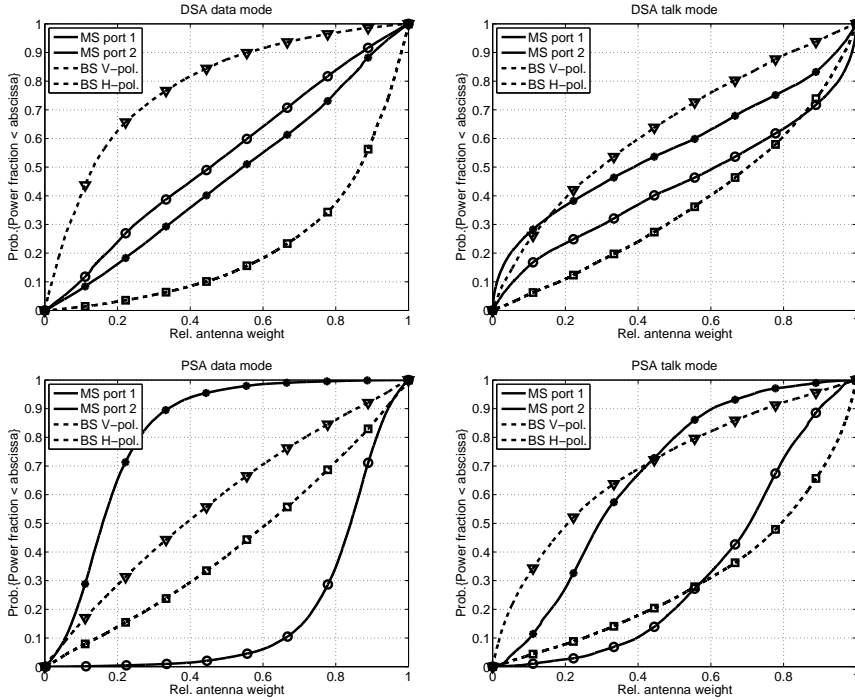
Figure 11: Antenna weight distribution for the MIMO channel branch with maximum singular value. The results for the DSA are shown in the upper graphs and for the PSA in the lower graphs with data mode to the left and talk mode to the right.

data user mode, while in talk mode, both H- and V-polarization have almost equal weight probability.

5   Summary and Discussion

Two different dual-antenna test terminals have been evaluated with respect to path gain difference, diversity gain and MIMO capacity in an indoor office scenario with influence of the hand and body of a user. The results are summarized in Tab. 2. It can be noticed that the selection diversity gain differs between 0.7 and 4.6 dB at 10% outage. With MRC (or singular vector beamforming) at the MS) the diversity gain differs between 1.9 and 5.9 dB, i.e., an

Table 2: Summary of results for path gain difference (Δ), diversity gain and potential mean capacity gain for 10 dB mean SNR . "Best in class" values are marked with bold face.

	DSA data	DSA talk	PSA data	PSA talk
Δ dB at 10%	**0.6-1.3**	8.4-10.6	5.8-7.3	3.9-4.0
ISC gain dB at 10%	**3.6-4.6**	2.3-3.1	0.7-0.8	1.4-1.7
MRC gain dB at 10%	**5.0-5.9**	3.3-4.2	1.9-2.1	2.9-3.1
Cap. gain MRC@MS	1.7	**2.1**	1.6	1.4
Cap. gain MRC@BS&MS	2.9	**3.3**	2.8	2.8
Cap. gain MIMO (wf)	3.2	**3.4**	2.9	2.8

additional 1.2-1.3 dB.

Furthermore, substantial capacity gain can be reached using antenna signal combining at either the BS or the MS, or even better using MRC at both the BS and the MS (i.e., the strongest single branch MIMO or best dual-side beamforming). However, MIMO gain using 2x2 parallel channels and waterfilling is only significant at high SNR (>15 dB). The overall "best in class" terminal solution was found to be the DSA.

Looking at the graphs of Figure 11, apparently, horizontal polarization is in overall the better choice of a single BS antenna polarization in this scenario. This, however, may depend on the configuration of the antennas on the terminal, the antenna elements radiation patterns and the influence of the users hand and head, i.e., the effective radiation pattern. For example, the result for the DSA in this case, the one terminal with two antennas that have almost equal performance with respect to the reflection loss and antenna pattern correlation (Table 1), is not clear due to the hand holding the terminal that may influence the Port 2 slot severely, i.e., the slot that would couple the most to the V-polarization of the BS. To be sure about this conclusion, the polarization characteristics of both antennas must be taken into consideration. This may be an issue for future investigations.

6   Conclusions

The results from the investigation presented here pose the following conclusions.

- Dual antennas in a mobile give a diversity gain in average from 0.7 up to 4.6 dB at the 10% outage level in an office scenario. Even though antenna signals are strongly correlated (median>0.8 for the PSA) the diversity gain at 10% outage may reach 3 dB (MRC).

- High path gain difference decreases the diversity gain. This is, in addition to the difference in inherent antenna gain, introduced depending on how the terminal is oriented and positioned (relative the user body and the channel). In general the minimum path gain difference is found to be close to the difference in previously measured antenna loss (within less than 0.5 dB). From this study, however, the relation between path gain difference and diversity gain can not be quantified.

- The investigated 2x2 MIMO channel have in average one eigenvalue 10-20 dB stronger than the second eigenvalue. Thus, 2x2 MIMO using both branches by water filling add up to 3 dB capacity gain at SNR above 10 dB, compared to SISO. At SNR below 10 dB single branch MIMO (or dual side beamforming) is the most effective solution.

- The user mode influences the performance of the terminals tested severely, due to body (hand and head) loss and terminal orientation (or effective antenna pattern polarization).

- In the chosen environment, horizontal polarization was found to be the better choice of a single BS antenna polarization for all the tested terminal antenna configurations.

Acknowledgment

References

[1] J. P. Kermoal, L. Schumacher, F. Frederiksen, and P. Mogensen, "Experimental investigation of the joint spatial and polarisation diversity for MIMO radio channel," in *Proceedings of the 4th International Symposium on Wireless Personal Multimedia Communications (WPMC)*, Aalborg, Denmark, Sept. 2001, pp. 147–152.

[2] R. M. Narayanan, K. Atanassov, V. Stoiljkovic, and G. R. Kadambi, "Polarization diversity measurements and analysis for antenna configurations at 1800 MHz," *IEEE Trans. Antennas Propagat.*, Vol. 52(7), pp. 1795–1810, 2004.

[3] J. S. Colburn, Y. Rahmat-Samii, M. A. Jensen, and G. J. Pottie, "Evaluation of personal communications dual-antenna handset diversity performance," *IEEE Trans. Veh. Technol.*, Vol. 47(3), pp. 737–746, 1998.

[4] P. Suvikunnas, J. Salo, J. Kivinen, and P. Vainikainen, "Empirical comparison of MIMO antenna configurations," *IEEE Veh. Technol. Conf. VTC 2005-Spring*, Stockholm, Sweden, May 2005.

[5] J. Medbo and J.-E. Berg, "Simple and accurate path loss modeling at 5 GHz in indoor environments with corridors," *IEEE Veh. Technol. Conf. VTC 2000-Fall*, Boston, MA, Sept. 2000.

[6] R. Vaughan and J. Bach Andersen, *Channels, Propagation and Antennas for Mobile Communications*, IEE Electromagnetic Waves Series, No. 50, pp. 650–652, 2003.

Paper II

Efficient Experimental Evaluation of a MIMO Handset with User Influence

Abstract

The immediate environment of handset antennas, including the casings and the users holding the handsets, has a strong impact on the radio channel in mobile communication. In this paper we investigate a composite channel method that synthetically combines double-directional measurements of the user-less propagation channel with measured *super-antenna* patterns, i.e., patterns of the combined antenna-casing-user arrangement. We experimentally evaluate the method by comparing results (power, capacity, and eigenvalue distribution) obtained from this composite method with direct measurements in the same environment. The measurements were done in two static 8×4 MIMO scenarios at 2.6 GHz, with the user indoors and the base station located outdoors and indoors, respectively. A realistic user phantom together with a "smart-phone" handset mock-up with four antenna elements was used, and different configurations and orientations were tested. The method gives statistical distributions of the MIMO eigenvalues, that are close to the measured. By using the composite method, we found that the user, apart from introducing hand and body loss that mainly decreases the SNR of the channel, slightly increases the correlation between the fading at the antenna elements.

1   Introduction

User body impact and the choice of antenna configurations in user equipments are essential when implementing new mobile communication systems utilizing MIMO (multiple-input multiple-output). However, channel models incorporating the user interaction in a realistic way are rare.

While there is an abundance of MIMO channel measurements (for an overview, see, e.g., [1]) especially in indoor scenarios, those seldom include (and actually often explicitly avoid) the influence of a human being near the antennas. On the other hand, measurements of antennas in the presence of human beings are usually restricted to determining quantities such as radiation efficiency, specific absorption rate, mean effective gain, etc.

In a more detailed empirical channel model, the decision has to be made whether to include the user in the antenna or in the channel characterization. If the user is considered a part of the channel, we need to perform new channel measurements for each user operation configuration. In this paper, we investigate an approach where the user together with the antenna, is considered as one radiating unit or a *super-antenna*. Thus, the number of user configurations only affects the number of superantenna measurements at the antenna test range; whereas the channel is obtained from a single channel sounder measurement (without user), with the results of the measurement represented by the *double-directional propagation channel* (DDPC), i.e., a sum of multi-path components (MPCs); each characterized by its direction-of-arrival (DoA), direction-of-departure (DoD), path delay, and complex amplitude [2].

The method of calculating the channel transfer matrix by combining the DDPC with far-field radiation patterns of both transmit (Tx) and receive (Rx) superantennas, here referred to as a *composite channel method* (CCM), is based on two assumptions; (i) the DDPC describes only the multi-path propagation itself and is thus free of any influence of the antennas, and (ii) the user (including its head, hand, and torso) together with the actual handset (antennas as well as casing) can be interpreted as a superantenna that can be characterized by its frequency dependent far-field radiation pattern that weights and adds up the MPCs. Thus, a DDPC measurement can be combined with *any* superantenna pattern measurement to describe the combined effect of channel, user, and antenna. This in particular allows a completely fair and reproducible comparison of different antenna arrangements in the chosen propagation environment. Now, the question is to what extent this composite method with the far-field assumption inherent both in the double-directional tapped delay-line model and in the large aperture superantenna radiation pattern, is valid for MIMO performance prediction, and how much it suffers from the (unavoidable) measurement inaccuracies.

Several published papers describe the principle of combining double-directional channel characterization with antenna radiation patterns. Molisch *et al.* [3] used the method with simple antenna arrangements to generate multiple channel realizations; Dandekar *et al.* [4] used ray tracing and Method-of-Moment simulations in a similar fashion, and Suvikunnas *et al.* [5,6] pioneered the combination of channel measurements with antenna patterns of realistic handset antenna configurations and compared the results to direct measurements. The use of a directional propagation channel model combined with simulated or measured radiation patterns for different mobile terminal antennas and user configurations, was found to work well for multi-antenna terminals in talk position beside a phantom head. However, to our knowledge, no work exists that investigates a composite method in the presence of user body as well as hand. A measurement campaign using a realistic upper-body phantom, including the arm and hand, has been presented by Yamamoto *et al.* [7], where it was shown that the difference in gain and potential MIMO capacity for a realistic user phantom compared to simplified models were significant. Furthermore, the user hand and the terminal position inside the hand may have a severe impact on the antenna efficiency, as, e.g., shown by simulations by Li *et al.* [8] and Pelosi *et al.* [9]. Thus, a realistic user phantom including the hand together with realistic test terminals are important when evaluating potential MIMO performance.

The goal of the present paper is to investigate to what extent the composite channel method can appropriately account for the presence of the user in realistic scenarios. The novel contributions of the paper are the following:

1. we test the composite channel model with a body phantom that includes hand and upper torso as well as head.

2. we test the impact of different hand positions on the results.

3. we investigate the influence of different usage positions of the handset (i.e., holding it in browsing mode vs. standard talk mode).

4. we analyze the MIMO capacity as well as eigenvalue distribution and diversity performance for a four antenna handset in the presence of a user.

The investigation is based on channel measurements in two static scenarios with an upper body phantom and a four-antenna handset mock-up, in the LTE band 2.5–2.7 GHz for a synthetic 8x4 MIMO arrangement. Previously, we presented some results for the first scenario in a conference paper [10].

The remainder of the paper is organized as follows: Section 2 outlines the basic principle of the composite method, Section 3 describes the details of the

equipment and the test setup, and Section 4 the measurements of the antenna patterns. Section 5 elaborates on the measurement of the propagation channel and the resulting double-directional characterization. Next, the comparison procedure between direct measurements and composite results is described in Section 6, with the comparison of eigenvalue distributions as the key experimental results of our campaign. Finally, diversity and capacity performance are investigated in Section 7, and a summary and conclusions in Section 8 wrap up the paper.

2   The Composite Channel Method

2.1   Super-Antenna Characterization

We assume, that the base station (BS) as well as the mobile station (MS) antennas, with or without a user present, can be characterized by their farfield patterns, i.e., the far-zone radiating complex vector fields, written as

$$\boldsymbol{g}(\Omega, f) = \hat{\theta} g_\theta(\Omega, f) + \hat{\phi} g_\phi(\Omega, f) \tag{1}$$

where $\Omega = \{\theta, \phi\}$ is the space angle, f is the frequency and $g_{\theta,\phi}$ are the complex field amplitudes with the unit vectors $\hat{\theta}$ and $\hat{\phi}$ defining the polarization. With the measurements performed using a common phase reference (at the MS side), the array factors or location vector phase factors $e^{-j\boldsymbol{k}(\Omega)\cdot\boldsymbol{r}_i}$ of the antenna array (with antenna element i at location $\boldsymbol{r}_i$) are incorporated in the measured radiation patterns. Now, the multiple $i = 1, 2, \cdots, n_r$ antenna field vectors for each frequency and DoA (at Rx), $\boldsymbol{g}_i(\Omega, f) = [g_{\theta,i}(\Omega, f)\, g_{\phi,i}(\Omega, f)]^T$, can be arranged into a $2 \times n_r$ matrix as

$$\mathbf{G}(\Omega, f) = \left[\begin{array}{cccc} \boldsymbol{g}_1(\Omega, f) & \boldsymbol{g}_2(\Omega, f) & \cdots & \boldsymbol{g}_{n_r}(\Omega, f) \end{array} \right] \tag{2}$$

allowing a compact matrix formulation of the channel calculations (see below). The field representation in (1) requires complex interpolation when used in combination with DoAs and DoDs that can take on arbitrary values. A nice way of avoid this interpolation is to expand the measured sample farfield onto spherical vector harmonics or modes as

$$\boldsymbol{g}(\Omega, f) = \sum_{q=1}^{Q} \psi_q(f) \boldsymbol{\Psi}_q(\Omega) \tag{3}$$

where $\psi_q(f)$ are the complex mode amplitudes, $\boldsymbol{\Psi}_q(\theta, \phi)$ are the complex spherical vector mode functions, and q is a compound index representing the TE/TM

field types, and the polar and azimuthal (l, m) indices. Hence, the farfield is represented by the complex mode amplitude vectors, independent of directions, and the directional sample resolution of the patterns is exchanged to an equivalent truncation of the set of modes Q, defining the accuracy of the field.

2.2   The Double-Directional Propagation Channel

In our case, we assume that the double-directional propagation channel is described by a finite number L of multi-path components, originating at the transmitter (Tx), subject to reflection, scattering and diffraction before terminating at the receiver (RX). Plane wave propagation is assumed implying that the nearest non specular interaction (scattering point) to either antenna is much farther away than the size of the antenna. The MPCs are independent of the Tx and Rx antennas, and the l-th one has the following parameters:

α_l amplitude and phase

$\Omega_{t,l}$ direction of departure (DoD)

$\Omega_{r,l}$ direction of arrival (DoA)

τ_l path excess delay

and the polarimetric transfer matrix

$$\mathbf{P}_l = \left[\begin{array}{cc} P_{\theta,\theta} & P_{\theta,\phi} \\ P_{\phi,\theta} & P_{\phi,\phi} \end{array} \right]$$

which is normalized to have unit Frobenius norm. In the DDPC model the frequency dependency is taken into account only in the phase factors representing the plane-wave path distances $e^{-j2\pi f \tau_l}$.

2.3   The Composite Channel Matrix

The formation of the frequency-domain channel transfer matrix function $\mathbf{H}(f)$, whose elements $H_{ij}(f)$ describe the transfer function from the j-th transmit to the i-th receive antenna element, is with the superantenna assumption found by joining the MPCs of the DDPC with the Tx and Rx antenna farfields. This can be written as a sum over the L MPCs, with each term found as a matrix product of the Tx and Rx antenna matrices $\mathbf{G}_t$ and $\mathbf{G}_r$ from (2), with the polarimetric transfer matrix as

$$\mathbf{H}(f) = \sum_{l=1}^{L} \alpha_l \mathbf{G}_r^T(\Omega_{r,l}, f) \mathbf{P}_l \mathbf{G}_t(\Omega_{t,l}, f) e^{-j2\pi f \tau_l} \qquad (4)$$

where $\mathbf{G}_t$ and $\mathbf{G}_r$ contain the complex farfield and array location vector phase term for each element in the columns, and for the polarization component (θ, ϕ) in the rows, i.e., $2 \times n_{r,t}$.

2.4   Channel Estimation and Calculation

To be able to compute (4) for a certain test antenna or AUT (antenna under test), the channel has to be characterized. Using dual polarized probe antennas at the Tx and Rx, with antenna field vectors $\mathbf{G}_{p,t}$ and $\mathbf{G}_{p,r}$, a channel sounder samples the channel matrix at discrete positions and frequencies within a frequency band. Next, a channel estimator extracts the parameters of the MPCs by, e.g., the Maximum Likelihood (ML) method described in [11]. After this step, the estimated MPC complex amplitude and polarimetric matrix (in our case) include the antenna patterns and gains of the probe antenna elements as

$$\tilde{\alpha}_l \tilde{\mathbf{P}}_l = \alpha_l \mathbf{G}_{p,r}^T(\Omega_{r,l}) \mathbf{P}_l \mathbf{G}_{p,t}(\Omega_{t,l}). \tag{5}$$

This means that when computing the channel transfer matrix for an arbitrary receive AUT pattern $\mathbf{G}_{aut}$, the influence of the probe pattern at the MS side is removed by a multiplication with the inverted probe antenna matrix. At the BS side, however, this operation is not necessary in our case since the BS antenna remained unchanged during all measurements. Solving $\alpha_l \mathbf{P}_l$ from (5), and inserting into (4) gives

$$\mathbf{H}(f) = \sum_{l=1}^{L} \tilde{\alpha}_l \left(\mathbf{G}_{p,r}^{-1}(\Omega_{r,l}, f) \mathbf{G}_{aut}(\Omega_{r,l}, f) \right)^T \tilde{\mathbf{P}}_l \mathbf{I}_t e^{-j2\pi f \tau_l}$$
$$\mathbf{I}_t = \left[e^{-j\boldsymbol{k}\cdot\boldsymbol{r}_{t,1}}, e^{-j\boldsymbol{k}\cdot\boldsymbol{r}_{t,2}}, \cdots, e^{-j\boldsymbol{k}\cdot\boldsymbol{r}_{t,n_t}} \right] \otimes \mathbf{I}_{2\times2} \tag{6}$$

where $\boldsymbol{k}$ is the directional wave number vector and $\boldsymbol{r}_t$ is the location vector at Tx.

An efficient way of performing the channel computations in (6) is to use the spherical vector mode expansion from (3). Thus, the antenna array pattern matrix (at the receiver) can be written as

$$\mathbf{G}_l(f) = \boldsymbol{\Psi}_l \mathbf{W}(f) \tag{7}$$

where the antenna array pattern matrix $\mathbf{G}_l(f)$ (for each l) is a $(2 \times n_r)$, the mode matrix $\boldsymbol{\Psi}_l$ is $(2 \times Q)$, and the array modal coefficient matrix

$$\mathbf{W}(f) = [\mathbf{w}_1(f), \mathbf{w}_2(f), \cdots, \mathbf{w}_{n_r}(f)]$$

is $(Q \times n_r)$. Here, the vectors

$$\mathbf{w}_i(f) = [\psi_1(f), \psi_2(f), \cdots, \psi_Q(f)]^T$$

represent the modal coefficient vectors for antenna i. Now, using (7) in (6) yields

$$
\begin{aligned}
\mathbf{H}(f) &= \sum_{l=1}^{L} \tilde{\alpha}_l \left(\mathbf{G}_{p,l}^{-1}(f) \mathbf{\Psi}_l \mathbf{W}(f) \right)^T \tilde{\mathbf{P}}_l \mathbf{I}_t(\boldsymbol{r}_t, f) e^{-j2\pi f \tau_l} \\
&= \mathbf{W}^T(f) \sum_{l=1}^{L} \tilde{\alpha}_l \left(\mathbf{G}_{p,l}^{-1}(f) \mathbf{\Psi}_l \right)^T \tilde{\mathbf{P}}_l \mathbf{I}_t e^{-j2\pi f \tau_l} \\
&= \mathbf{W}^T(f) \mathbf{M}(f)
\end{aligned}
\tag{8}
$$

The matrix function $\mathbf{M}(f)$ is the AUT-independent *modal channel transfer matrix function*, i.e. the channel matrix related to the spherical vector modes for a specific propagation channel realization [12]. Now, the calculation of the channel matrix for a specific AUT is done simply by the last matrix multiplication in (8) with the spherical vector mode coefficients. This is a fast and convenient operation even if the number of AUT's is large.

3   Test Equipment and Setup

3.1   Handset and User Phantom

The test handset used in the experiments is a 7x11x2 cm^3 PDA-type mock-up, (Figure 1 or [10] Fig. 1 with lid open). It is equipped with four planar inverted F-antenna (PIFA) elements, with different placements and orientations on one side of a ground plane (antenna side). During both pattern and channel measurements, a semi-conductor switch was used to select the active port, while the other antenna ports were terminated by matched loads. The user phantom consist of two separate parts, a liquid filled upper body phantom (torso and head) and a solid hand/lower arm phantom[1].

3.2   User Operation Modes

Two different user operation situations or modes were investigated, *talk mode* and *browse mode*, (Figure 1). Talk mode represents the scenario where the user holds the handset in the right hand, towards the right ear, with the antenna side opposite to the head, whereas browse mode represents the scenario where the user hold the handset in the right hand as if to watch the screen. In browse mode the handset was tested both with the antenna side turned downwards

---

[1]Head tissue simulant liquid in compliance with IEEE Std. 1528 at 2.6 GHz, with $\epsilon_r = 39.7$ and $\sigma = 2.14$. Hand and lower arm piece from IndexSAR (www.indexsar.com)
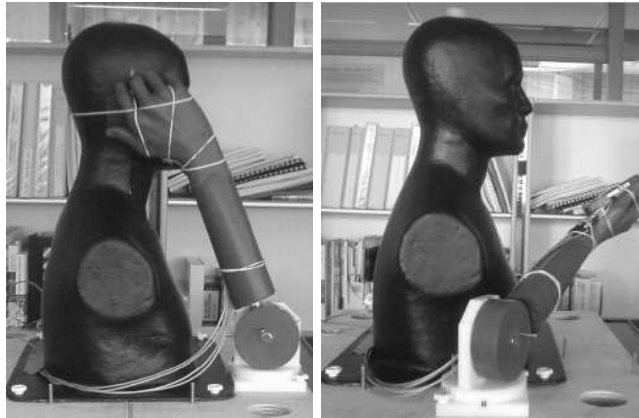
(a) Talk mode   (b) Browse mode

(c) Handset in phantom hand

Figure 1: The user phantom in talk mode and in browse mode, and the four-antenna handset mock-up at one position inside the phantom hand.

and upwards. Furthermore, since the individual performance of the antenna elements may depend strongly on the precise positioning of the handset into the hand phantom, e.g., due to the finger positions which are hard to reproduce with high accuracy, the measurements were repeated for three positions inside the hand that are offset 10 mm with respect to each other. The choice of hand phantom and the placement of the handset was made for availability and practical reasons. Recently published rigorous user grip investigations by Pelosi *et al.* [9] support the grip choice in talk mode, while in browse mode the variability was found to be very large.

4   Antenna Characterization

The radiation patterns and efficiencies of the handset with and without the phantom present in the different user modes, have been measured at two separate occasions, at a Satimo nearfield range. The first occasion was performed in connection to a first publication in [10]. For testing repeatability and to find possible measurement errors, these measurements have since then been repeated at the same measurement range, though it had been recalibrated in the meantime.

4.1   Radiation Pattern Measurements

In our case the antenna measurement range provided the *realized gain* [2] which means that the efficiency calculated from the radiation pattern as

$$\eta = \int_{4\pi} \boldsymbol{g}(\Omega, f) \cdot \hat{n} d\Omega \tag{9}$$

also includes the loss due to impedance mismatch. A separate measurement of the reflection coefficient (Γ) was done with and without the hand phantom present. In the free space case, the four antennas were very similar with $20 \log |\Gamma| < -10$ dB within 2.53–2.63 GHz, corresponding to an insertion loss ($-10 \log(1 - |\Gamma|^2)$) of less than 0.5 dB. With the hand present, however, the mismatch increased significantly with insertion loss up to 2 dB; similar results were found for live test persons by Pedersen *et al.* [13].

The total loss (including the reflection loss, as well as the conduction and dielectric losses of the connector, integrated feed cable, PIFA element, ground plane and casing) was also found to be quite similar in free space for the four antennas (2.8–3.7 dB) but increased in the presence of the phantom (3.2–10.2 dB). The talk mode case showed the highest loss figures (5.9–10.2 dB),

---

[2]IEEE Std 145-1993, "Standard Terms of Antennas"

whereas the loss in browse mode with the antennas upwards was lower (3.2–5.9 dB). Hence, the head in talk mode seems to absorb more radiated energy than the body in browse mode. The difference of the loss (mean over handset antennas and different in-hand positions) to the free space case, was found to be 4.8, 3.6 and 1.4 dB, for talk mode, and browse mode with antennas down/up, respectively. The values for talk mode are, again, close to those reported in [13] (patch antenna case).

Allowing a rough reasoning the results from above can be used to give an estimate of the actual average body, head and hand losses for this phantom. In browse mode with the antennas turned upwards the handset antennas are almost free from hand influence (Figure 1) and we can assume that the loss is mainly due to the phantom body, i.e., the body loss is 1.4 dB. With the antennas downwards towards the palm the main loss is the hand loss (with a soft hand/finger touch) estimated as the difference between antenna-up and antenna-down cases, i.e., $3.6 - 1.4 = 2.2$ dB. Now, in a similar manner the head loss may be roughly estimated as the talk case with the hand loss subtracted, i.e., $4.8 - 2.2 = 2.6$ dB.

It was also found that the efficiencies and thus the realized gains were well repeatable between separate antenna range measurements, even with the phantom present. The results from the first measurement campaign were in close agreement with those from the second. The difference in radiation efficiency, averaged over antenna ports, positions and orientations, was found to be about 1.4 dB for the phantom measurements. This is mainly due to the additional feed cables, which were different during the two measurement campaigns.

Figure 2 shows the realized gain in the horizontal plane at 2.6 GHz, averaged over the four handset antennas in each direction, with and without the phantom present. The phantom was oriented with the nose pointing towards 90° with the handset in the right hand. It is obvious how the phantom head and body shadow the handset antennas in predictable directions. In the talk mode case the attenuation is strongest in the direction of the head, i.e., to the left and somewhat backwards, whereas in the browse cases the attenuation is strongest backwards towards the body. Typically a shadow loss of up to 10 dB is found, with a -3 dB angular spread of approximately 120° in talk mode, and about 60° in browse mode. The average gain is based on the four antenna elements, separate measurement occasions, the three in-hand positions, and the frequency samples.

4.2   Pattern Correlation

A requirement for antenna diversity and MIMO capacity is that the complex farfield antenna patterns (including the phase factor due to location of the el-
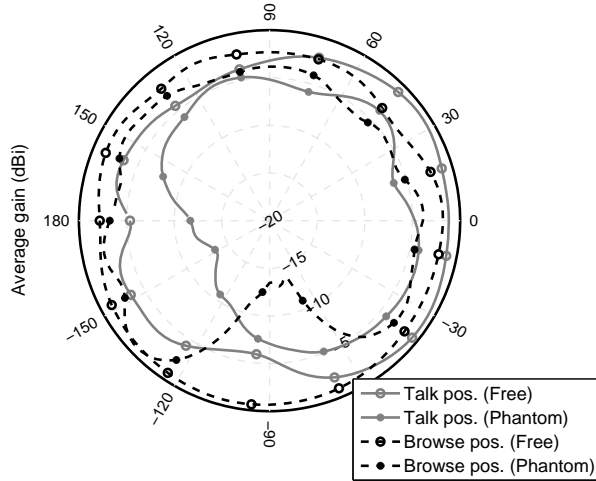
Figure 2: Average realized gain in the horizontal plane for the handset with and without (Free) the phantom present in talk mode and browse mode positions.

ements) are not identical. The normalized scalar product of pair-wise farfield patterns of the antennas, here referred to as the *pattern cross-correlation coefficient*, is calculated for antenna i and j as

$$\rho_{ij} = \frac{< \boldsymbol{g}_i, \boldsymbol{g}_j >}{\sqrt{< \boldsymbol{g}_i, \boldsymbol{g}_i >< \boldsymbol{g}_j, \boldsymbol{g}_j >}} \tag{10}$$

with

$$< \boldsymbol{g}_i, \boldsymbol{g}_j > = \int_{4\pi} \left\{ \boldsymbol{g}_{\theta,i}(\Omega)\boldsymbol{g}_{\theta,j}^*(\Omega) + \boldsymbol{g}_{\phi,i}(\Omega)\boldsymbol{g}_{\phi,j}^*(\Omega) \right\} d\Omega \tag{11}$$

or using the spherical vector mode expansions from (7) simply as

$$\rho_{ij} = \mathbf{w}_i^H \mathbf{w}_j \tag{12}$$

since the mode functions are orthonormal[3]. The pattern cross-correlation for any two antenna elements of the handset was found to be in average well below 0.2 (max 0.4) and below 0.3 (max 0.5) without and with the phantom present, respectively. Here, the user presence increased the pattern correlation (making

---

[3]For an isotropic i.i.d. channel with an infinite number of MPCs, the pattern cross-correlation coefficient is also the open circuit correlation coefficient as defined in [14].

the patterns less orthogonal). This indicate a possible increase of channel correlation and a decrease in diversity or MIMO capacity.

One of the key questions concerning the radiation pattern measurements is to what extent the results are repeatable after a disassembly and reassembly of the phantom and the handset. Thus, the pattern correlation was calculated between the *same* antenna elements as measured in the first and second pattern measurement campaigns. Ideally, those correlations should be unity, since the patterns should not change; deviation from unity indicate loss of repeatability w.r.t. the directional properties of the radiation pattern. For the case without phantom the correlation was found to be in average 0.87, and between 0.68–0.76 for the different phantom modes. The deviation in the case with no phantom present may seem a bit high since this is just a remeasurement of a simple deterministic antenna structure. The most likely explanation lies in the bending of the feed cables and perhaps to some extent recalibration of the measurement range. In the phantom cases the deviation from unity is less surprising since there are more uncertain factors, such as exact finger position in the hand phantom etc. However, at the first measurement occasion, a remeasurement of the phantom pattern before and after a disassembly-reassembly of the handset in the phantom hand, showed a correlation of 0.85 in average for the phantom modes. Thus, we cannot exclude that part of the deviations in pattern correlation between separate measurement occasions is due to the recalibration of the measurement range.

5   Channel Measurements and Characterization

The RF-cable attenuation is typically about 1 dB/m around 5 GHz, which restricts the maximum measurement distance to about 50 m. By use of a low loss optical fiber equipped with RF-to-opto converters it was possible to extend the range to more than 300 m. A laptop was used for control Two separate channel measurement campaigns were performed at an Ericsson office building in Kista, Sweden, in the frequency bands 2530–2550 and 2610–2690 MHz:

Scenario 1 A stationary outdoor-to-indoor micro-cell scenario.

Scenario 2 A stationary indoor-to-indoor scenario.

For all combinations of the transmit and receive antenna elements, the complex channel frequency response was measured with an vector network analyzer (VNA) using RF-opto converters and optical fiber cables [11], at a total of 401 equidistant discrete frequencies. In both campaigns the mobile station array (MS) was located at the same position in a lab at the 3rd floor with windows

Figure 3: Site map of channel measurements with the BS locations for Scenario 1 (BS 1) and Scenario 2 (BS 2), and the common MS location (MS), illustrated with a few (typical) MPCs.

towards the street. The base station (BS) was located in a skywalk crossing above the street at about 30 m from the MS resembling an outdoor microcell placement (Scenario 1), and in an indoor placement down the corridor at about 13 m distance from the MS (Scenario 2), Figure 3.

To enable MIMO measurements, at the BS location, a linear robot was used to move a probe antenna to 8 positions with 4 cm separation. The antenna was a vertically polarized square patch antenna, with 9 dBi gain and about 60° beamwidth, and its radiation pattern was measured in a similar fashion as the one described in Section 4. At the MS, two setups were used to enable two different types of measurements.

Firstly, a virtual array channel sounding measurement was performed to enable a double-directional characterization of the channel alone, using a 3D positioning robot and a dual-polarized square patch antenna (similar to the BS antenna) at the MS (Figure 3). The robot moved the antenna to form a vertical synthetic square 8×8-array with 4 cm element distance. This was rotated in azimuth in steps of 90° so that all directions were covered.

Secondly, direct measurements of the channel transfer functions were done with the robot and probe antenna replaced by the (static) 4-antenna terminal and the user phantom. In each setup, the phantom was rotated in azimuth in steps of 90° to four directions. The Tx power was chosen so that the SNR at the receiver was better than 50 dB, and the measurements were done late in the evening when very few people were present, to minimize time variations of the channel. However, in the outdoor-indoor campaign time-variant components

of the channel due to windswept trees were present. These components were suppressed by averaging over 10 repeated channel measurements. The resulting average ratio of the power in the static components, compared to those in the time-varying components, was estimated to be 20 dB with a worst case figure of 16 dB. In the second indoor measurement no such problems were observed, but we cannot exclude the possibility that movements from temporary visitors in neighboring rooms may have caused some interference.

5.1   Directional Channel Estimation

Based on the channel sounding measurements, the plane-wave spectrum for more than 2800 MPCs was resolved, using a successive double-directional maximum likelihood (ML) estimation method described in [11]. Some example rays for the two scenarios are illustrated in Figure 3. In the outdoor-indoor scenario (Scenario 1) the azimuth spreading at the BS is divided to two clusters, the strongest towards the MS location and the other towards the opposite building. For the indoor-indoor case (Scenario 2), the spectral model shows basically a single cluster seen from the BS in the direction of the corridor towards the MS location.

The mean delay and RMS delay spread was 127 ns and 38 ns in Scenario 1, and 74 ns and 21 ns in Scenario 2, respectively, and the related coherence bandwidth was found to be in average 9 and 14 MHz for 0.5 correlation threshold. The latter means that within the 100 MHz channel bandwidth we have at least about 10 independent channels. The azimuthal spread at the BS and MS locations where basically the same in both scenarios ($23°$ and $26°$ at the BS and $51°$ and $50°$ at the MS), whereas the elevation spread at the MS location is larger in Scenario 2 ($14°$ vs. $7°$ in Scenario 1).

5.2   Channel Measurement and Estimation Accuracy

The accuracy of the channel estimate is determined by the channel sounder SNR and other error sources like non-static components in the channel and ghost components caused by the fact that the plane wave assumption is not fulfilled. In Figure 4 the power delay profile (averaged squared magnitude of the impulse response) of the channel sounder measurements is shown, taken as the average over all channel sounder probe antenna positions of the Fourier transformed (IFFT and a Hanning filter) channel transfer function over the upper frequency band with 321 samples within 2610–2690 MHz. This is also shown for the average over the phantom/handset direct channel measurements (dashed). In both cases the channel sounder SNR is above 50 dB and is not a limiting factor in our investigation. In the channel estimation process, the ML
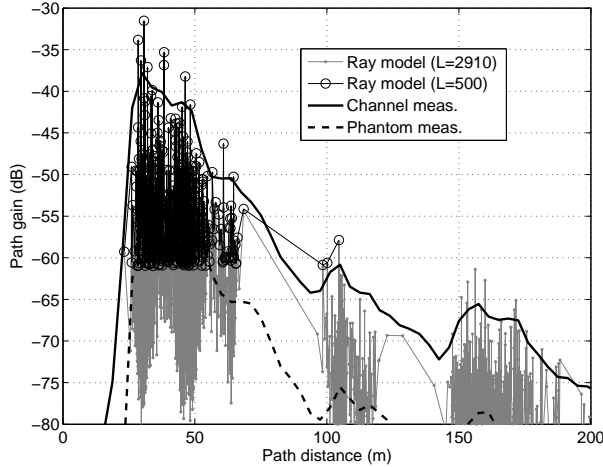
Figure 4: Average time response for the channel sounder measurements and direct measurements (Scenario 1), compared to the estimated multipath plane-wave model.

estimator was terminated for rays with a path distance of about 220 m and 180 m in Scenario 1 and Scenario 2, respectively, giving an accuracy limit of about 50 dB.

5.3   Truncation of MPCs and Test of Method for the Probe Antennas

The accuracy of the channel matrix in (4) depends among all on L, i.e., the number of MPCs used in the model. In our estimation, more than 2800 MPCs where resolved by the ML method. The sum over all the MPC powers $(\sum_{l=1}^{L} |\alpha_l|^2)$ accounts for about 96% of the average channel power. This was found from the channel sounding data using the probe antennas alone. Now, to verify our implementation of the CCM from (6) and the channel estimation process, we set up a calculation where we "positioned" the probe antenna (by the phase center) in all the positions corresponding to the channel sounder (synthetic) arrays at both the BS and MS sides. From this large channel matrix, we simulate a 4×4 MIMO system by making a selection of four elements at the BS side (vertical polarization) and four at the MS side (two vertical and two horizontal).

By looking at the sorted eigenvalue distributions (as described in Section 6.3, (16)) of these channel matrices and comparing with direct (channel sounder) measurements, we found that the model agreed almost perfectly with

the direct measured results for the full $L = 2825$ model[4]. With a truncation $L = 500$ the model accounts for about 87% and 79% of the total energy in Scenario 1 and 2, respectively, and in this case the eigenvalue distributions differed about 2 dB at the median of the weakest (fourth) eigenvalue found. This showed that taking into account a very large number of MPCs may actually improve the accuracy of the CCM.

6   Evaluation of the Composite Channel Method

6.1   Average Received Power Magnitudes

The performance of the composite channel method (CCM) is first evaluated by looking at the average received powers for individual MS antennas. This is done by comparing the squared magnitudes of the elements in the synthetic channel matrix $\mathbf{H}$ found using (6), to direct measurements of the channel. The average magnitude for each MS antenna i is taken as the mean w.r.t. BS (Tx) antennas n_t, in-hand positions n_h, and frequency samples n_f as

$$P_i^{av} = \frac{1}{n_t n_f n_h} \sum_{j=1}^{n_t} \sum_{k=1}^{n_f} \sum_{m=1}^{n_h} |H_{ij}^{(m)}(f_k)|^2 \tag{13}$$

assuming ergodicity in frequency and time (i.e., averaging over the ensemble is equivalent to averaging over time- and frequency-samples) [15]. Figure 5 shows received power levels at each terminal antenna 1–4 for the three user modes (subplot rows) and the four user rotations (subsequent in each row). The figure shows the result in Scenario 2 for CCM with $L = 500$ and with the antenna measurement files from the two separate antenna measurement, compared to the direct measurements. Error bars show the min/max interval for eight linear handset/phantom $\lambda/2$-translations in the channel at the MS location, i.e., the calculations were repeated with the AUT synthetically translated to eight locations. In the calculations the data were compensated for the loss of energy due to truncation of MPCs, as well as the measurement cable differences.

In most cases the average received power is well within ± 1 dB, which is also roughly the span of the max/min value error bars. However, there are cases where the discrepancies are up to 3 dB. Also, we notice that especially for the antenna no. 3 in talk mode, there is a large deviation of the first antenna measurement (probably due to a loose antenna connector). Table 1 shows a

---

[4]This test was done for the indoor Scenario 2 case where we did not have the problem with non-static components.
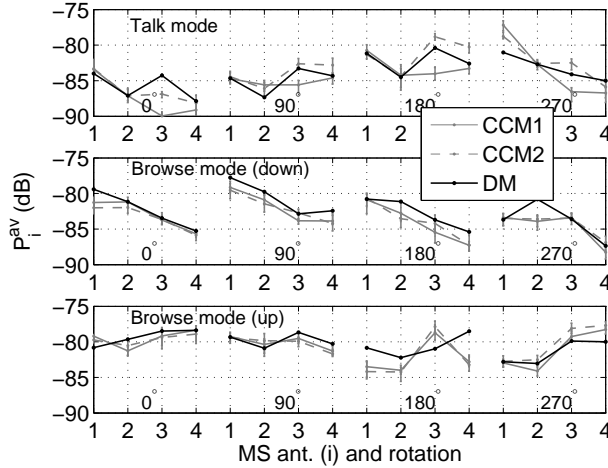
Figure 5: Average received signal powers of individual antenna elements (in Scenario 2), compared for the first and second radiation pattern calibration (CCM 1 and 2) to direct measurements (DM); at different user modes, rotations and antenna elements. The error bars show max and min of 8 $\lambda/2$ MS translations in the channel.

summary of the mean channel matrix gains for directly measured channels and CCM, the differences, and the variance of the model-to-measurement ratio, with the outlier element no. 3 omitted. The difference (error) was within 0.9 dB, and the variance was within 0.2 dB in all cases.

6.2   Antenna Correlation in Channel

The (receive) antenna correlation matrix, whose entries $R_{i,j}$ denote the correlation between signals at receive antenna ports i and j, can be estimated as the mean over frequency samples (again assuming ergodic fading) of the sample covariance matrix

$$\mathbf{R} = \frac{1}{n_f n_t} \sum_{k=1}^{n_f} \mathbf{H}(f_k)\mathbf{H}^H(f_k) \tag{14}$$

giving the estimated complex correlation coefficient with the proper normalization as

$$\rho_{i,j} = \frac{R_{i,j}}{\sqrt{R_{ii}R_{j,j}}} \tag{15}$$

Table 1: Observed average transfer power for direct measured (m) and CCM (c), respectively, the difference in mean and the variance of the model-to-measurement ratio (all in decibel). The results are shown for both Scenario 1 and Scenario 2, and using both the antenna measurement set no. 1 and 2 (separated by /).

Scenario-Mode	$\overline{|H_{i,j}^m|^2}$	$\overline{|H_{i,j}^c|^2}$	Δ_{dB}	σ_{dB}^2
Scen. 1 (Talk)	-41.7	-42.0/-41.7	-0.3/0.0	0.2/0.2
Scen. 2 (Talk)	-83.5	-83.0/-82.6	0.6/0.9	0.2/0.1
Scen. 1 (Browse)	-40.7	-40.6/-40.8	0.1/-0.1	0.2/0.1
Scen. 2 (Browse)	-80.8	-81.4/-81.3	-0.6/-0.5	0.1/0.1
Scen. 1 (All)	-40.9	-40.9/-41.1	0.0/-0.1	0.2/0.2
Scen. 2 (All)	-81.6	-81.8/-81.7	-0.2/-0.2	0.1/0.1

Figure 6 shows the cumulative distribution function of the correlation coefficients computed according to (15), where the ensemble is the slow (shadow) fading distribution, i.e., the three in-hand positions, the four phantom rotations, and the three user modes. In the figure the correlation coefficients from the CCM and from the direct measurements for the ensemble of $\rho_{i,j}$ are compared for all $i \neq j$. In general the correlation in the multipath channels is higher than the pattern correlation. Also the results for CCM with no user phantom present is shown in Figure 6, and, apparently, the phantom presence increases the antenna correlation. This is most likely due to the shadowing effect found in the average antenna-plus-phantom patterns in Section 4.1, Figure 2.

6.3 MIMO Eigenvalue Distribution

The antenna domain multiplexing capability of the channel is given by the squared singular values of the corresponding channel. The squared singular values are equal to the eigenvalues of the channel covariance matrix

$$\boldsymbol{\lambda} = \mathrm{eig}\{\mathbf{HH}^H\} \tag{16}$$

and represent signal gains of the spatial sub-channels. Taking all combinations of frequencies, hand positions and phantom user rotations as the sample space, the cumulative distributions of the ordered eigenvalues can be estimated. We thus compare ordered eigenvalue distributions for directly measured, and CCM channels with and without the presence of the phantom. This is shown for a 4x4 channel in Figure 7, for talk mode in Scenario 2. The channel matrix
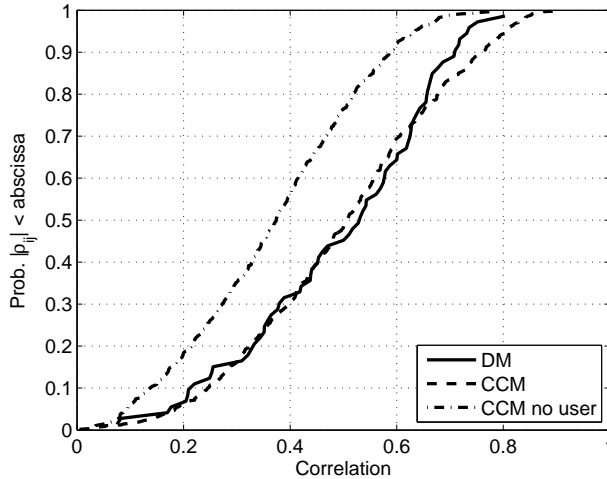
Figure 6: MS antenna correlation coefficient for model (CCM) compared to direct measurements (DM) in talk mode, and to the case with no user phantom present (CCM no user).

eigenvalues were normalized to an ergodic "sliding mean", equal to the squared Frobenius-norm ($\|\mathbf{H}\|_F^2$) averaged over frequency samples. The match between DM and CCM is very good, with a median agreement within 1 dB even for the weakest eigenvalue. In this case the number of MPCs in CCM was set to $L = 500$.

The influence of the MPC truncation L on the weakest eigenvalue for CCM compared to the direct measurements is shown in Figure 8. The figure show the difference (in dB) at the median of the weakest eigenvalue distribution between model and measurements, for talk mode and browse mode (with antennas downwards) in both scenarios. The model has been compensated for the truncated power in two different ways; a gain compensation done by normalizing the eigenvalues to their sum, and a "diffuse MPCs" compensation by additive white Gaussian noise (AWGN) as

$$\mathbf{H}' = \frac{P_L}{P_0}\mathbf{H} + \frac{P_0 - P_L}{P_0}\mathbf{H}_w \tag{17}$$

where, P_L is the average power of the channel matrix elements for L MPCs, P_0 is for all estimated MPCs, and $\mathbf{H}_w$ is a zero mean unit variance complex Gaussian matrix. In both cases the eigenvalue difference converge towards zero, but from different sides. The effect is stronger in Scenario 1 than in Scenario 2, with an increasing accuracy up to 1000 MPCs. The compensation methods
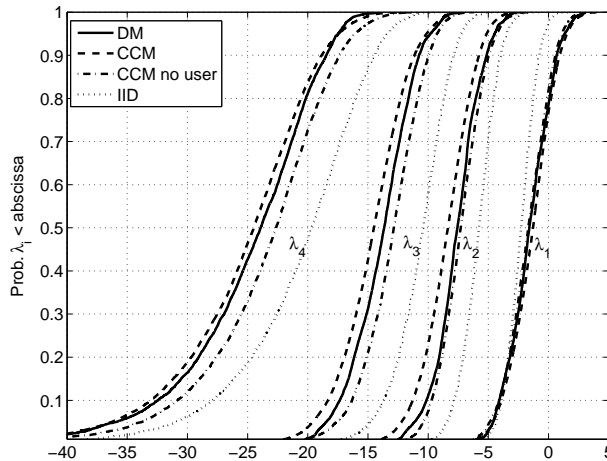
Figure 7: Ordered eigenvalue distribution of a 4×4 channel for direct measured (DM), and CCM with and without phantom in talk mode (Scenario 2). For comparison the distribution for an i.i.d. complex Gaussian channel is shown.

seem to work equally good, but still a larger amount of MPCs are required for increased accuracy. In Scenario 2 the models perform with high accuracy already with 100 estimated MPCs. Nevertheless, an increasing amount of estimated MPCs seem to improve the accuracy in both cases. This indicates that the the truncated low power MPCs can not completely be modeled as AWGN. Furthermore, the ML estimation process was found to perform very well statistically, even down to -30 dB eigenvalue levels.

7   User Impact on System Performance

Since the CCM seems to work well predicting statistical properties of the MIMO channel, we now use this tool to extract and evaluate the user impact on system performance. Here, we take a look at diversity combining and potential link capacity.

7.1   Diversity Combining

From the channel matrices the statistical distributions of the overall signal powers P_i for individual MS antenna elements and their (receive) diversity combinations can be evaluated. We investigate the cumulative distribution,
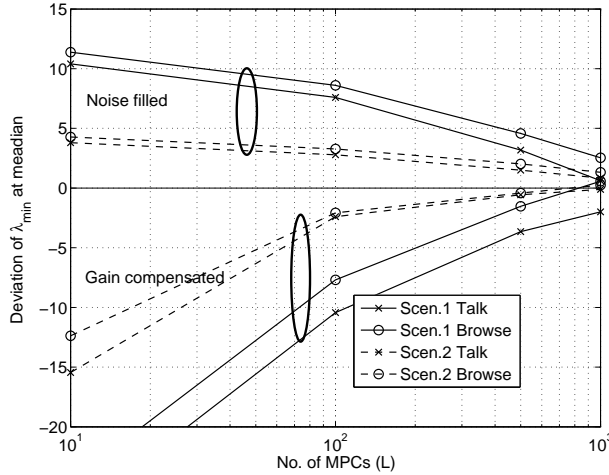
Figure 8: Difference in (weakest) eigenvalue (at the median) vs. number of MPCs for CCM compared to the direct measurements.

where the statistics are taken over BS antenna positions, phantom rotations, and in-hand positions. Figure 9 shows the impact of maximal-ratio combining (MRC) and hybrid selection/MRC (H-S/MRC) [16] as

any 2MRC Power sum of two random antennas (out of four).

best 2MRC Power sum of the two (fixed) antennas with the strongest average signal powers (out of four).

best 2/4MRC Power sum of the two antennas (of four) with the strongest signal powers at each channel sample.

4MRC Power sum of all four antennas (one receiver per antenna).

The plot shows the results for talk mode in Scenario 2 by using the CCM with $L = 500$. These results were found to be almost identical to the results found from direct measured matrices (not shown). Results for diversity combining performance were found to be almost identical for the two channels and the three user configurations. It is seen that the top antenna (Ant 1) of the handset is clearly the best one. This antenna is not obstructed by the phantom hand and quite free from the head[5]. In general (also in browse mode) the top one or

---

[5]This is also the most common antenna placement used in todays single antenna mobile phones
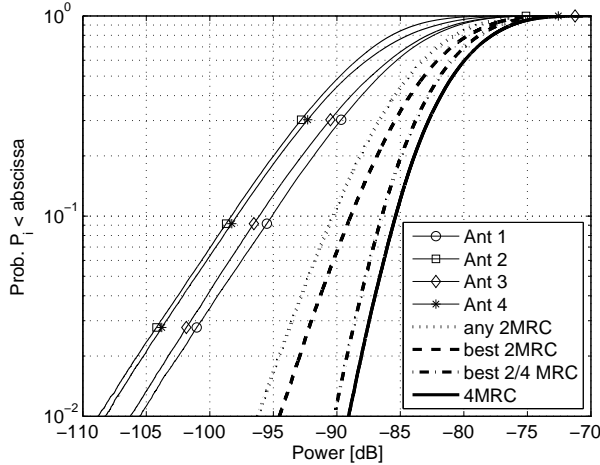
Figure 9: Rx antenna signal power distributions by CCM of separate antennas and ideal MRC diversity for the talk mode scenario (Scenario 2)

two antennas (relative the phantom), which are less obstructed by the phantom, did perform a few dB's better than the others. Looking at the diversity gain (defined as the difference between the strongest single antenna branch power and the combined power at a certain outage level), best 2/4MRC is less than 2 dB below 4MRC. This indicates that a clever selection scheme in combination with 2MRC has the potential to give high benefits out of four terminal antennas even if only two radio chains are available in the system [17, 18].

From a test of 4MRC diversity with and without the phantom present (using CCM), it was found that the diversity performance was slightly reduced due to the phantom, both due to antenna mismatch, i.e., reduced efficiency of individual elements due to the hand, and increased correlation. In talk mode the loss of diversity performance was about 0.7 dB at 1% outage and insignificant in browse mode.

7.2   Capacity

The ergodic capacity of the channel (bits/s/Hz) is the expected value over all realizations of the channel. Taking the realizations of the channel matrix **H** as the samples over frequencies (n_f), hand positions (n_h), and the four phantom

orientations; the ergodic capacity can be estimated as

$$\bar{C} = \mathcal{E} \left\{ \sum_{i=1}^{n} \log_2(1 + \gamma_i \frac{\lambda_i}{P_{ref}}) \right\} \tag{18}$$

where n is the number of sub-channels $(\max(n_t, n_r))$; each with power allocation γ_i, and corresponding normalized eigenvalue λ_i. The normalization factor P_{ref} is taken as the mean channel gain calculated as

$$P_{ref} = \mathcal{E} \left\{ \frac{1}{n_t n_r} ||\mathbf{H}(f)||_F^2 \right\} \tag{19}$$

(with expectation as in (18)) for the case with no phantom present. Hence, we refer the capacity to the user-free SNR $\bar{\gamma}$ with a common reference for all AUT's so that λ_i/P_{ref} will reflect the effect of antenna mismatch and absorption loss. Since the factor P_{ref} is a constant for all channel matrix samples, the capacity estimate will also include the user shadowing which is interpreted as "long-term fading". Figure 10 shows $\bar{C}(\bar{\gamma})$ for a 4x4 system using the two possible sets of every second of the eight BS antenna positions. The results are for the CCM matrix which was found to give almost identical results compared to direct measured matrices, but with the possibility to compare results with and without a user present. Notable is the loss in capacity due to the decrease of SNR when the user is present. At $\bar{\gamma}$=10 dB this is 3–4 bits/s/Hz for browse mode with antennas down, and 1-2 bits/s/Hz with antennas up. This shows the importance of careful placements of the antennas on a multimedia handset.

8 Conclusions

This paper has two main goals: i) to show the validity of the composite channel method to form MIMO channel models. In particular, the method can be applied for merging "user-free" double-directional channel models with farfield patterns of large objects such as handsets including a user, together forming a superantenna. ii) to investigate the user impact on mobile MIMO communication with a realistic channel and multiple-antenna handset setup. The goals have been achieved by two measurement campaigns, using a realistic upper-body user phantom (including hand and arm) and a realistic handset mock-up with four antenna elements. A number of different configurations and orientations were tested, such as user orientation, talk and browse position, and terminal position in the phantom hand. It must be noted that the super-antenna has much larger dimensions than a conventional handset, and thus
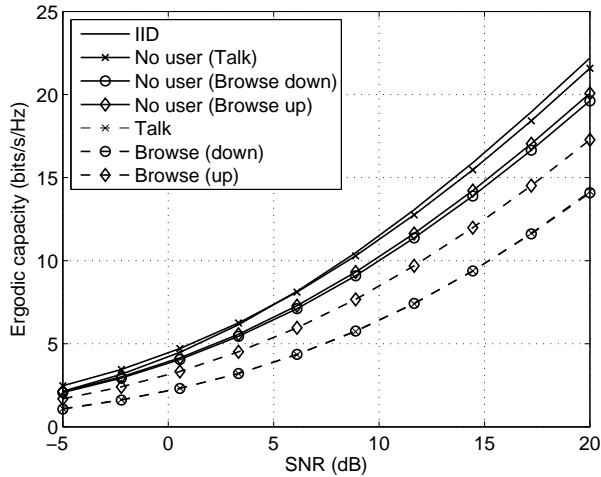
Figure 10: Ergodic capacity for a 4×4 system, with waterfilling for Scenario 2. Results with and without phantom present are shown for the three user modes.

a larger Rayleigh (or Fraunhofer) distance. As a consequence, the vital assumption that all MPCs are originating from objects in the farfield might not always be fulfilled. The differences between the model and measurements for the strongest eigenvalue is well within 1 dB, which is similar to or better than other results presented in the literature. Not surprisingly, weaker eigenvalues show a larger deviation between composite method and direct measurements; but even for the weakest eigenvalue at levels 30 dB below the strongest, the discrepancy is less than 2–3 dB, depending on the number of MPCs used. Thus, we conclude that the composite approach seems to be a highly valuable and accurate tool for the evaluation of multiple-antenna configurations, even indoors and in the presence of user head, torso, and hand.

The most important effect of the user is the efficiency loss due to the absorption of the hand and head/body, as well as the impedance mismatch loss due to the hand close to the antennas. It is found that the total average loss is between 1.4–4.8 dB depending on user operation and the antenna positions, compared to a free space handset. In an attempt to separate the effects, we found that the "hand influence" accounted for a loss in average of about 2.2 dB if the antennas were located towards the palm. Bear in mind that the hand phantom used together with the PDA-type handset only accounts for a soft touch of the device at the edges. A much larger efficiency loss is expected if the

hand would grab around the antennas or if fingers cover the antenna elements. The "head influence" is about 2.6 dB for talk mode, and the "body effect" is about 1.4 dB. All these are average figures. The worst case total loss was found to be up to 10 dB.

The second effect found is a difference between the "superantenna" pattern and the free space antenna pattern, due to shadowing. The qualitative behavior can be easily predicted from the direction of the head/body seen from the handset antennas. In this investigation we found that the shadow effect increased the antenna correlation coefficient at the handset from median 0.2–0.3 to median 0.4–0.5 with the user phantom absent and present, respectively. The increased correlation decreases the diversity gain by up to 1 dB (at 1% outage) and increases the condition number of the MIMO eigenvalues, i.e., increasing the difference between the strongest and weakest eigenvalue. However, the effect is hardly noticeable when looking at potential SNR-limited link MIMO capacity. The efficiency loss is much more important for the reduction of the capacity.

The observations of the potential diversity gain show that the 2-out-of-4 H-S/MRC gives a diversity gain that is only 2 dB less than that of 4-antenna MRC, but almost 5 dB better than 2-antenna MRC. This indicates that a handset benefits from as many as four antennas, even if only two radio chains are available by using a suitable selection diversity scheme combined with two branch MRC or MIMO. It is also found that the choice of antenna placement is crucial in a multiple-antenna handset, seen from, e.g., the improvement of almost 3 dB when putting antennas on the side away from the palm in browse mode compared to the opposite. The latter point may seem trivial, but if a handset is to be used in *both* talk mode and browse mode, it is not obvious how to place the antennas.

To conclude, we find that the CCM is a valuable and effective tool for analysis and even design of handsets with multiple antenna elements.

Acknowledgment

References

[1] A. F. Molisch and F. Tufvesson, "Multipath propagation models for broadband wireless systems," in *Digital Signal Processing for Wireless Communications Handbook*, M. Ibnkahla, Ed.   CRC Press, 2004, ch. 2, pp. 2.1–2.43.

[2] M. Steinbauer, A. F. Molisch, and E. Bonek, "The double-directional radio channel," *IEEE Antennas Propagat. Mag.*, vol. 43, no. 4, pp. 51–63, 2001.

[3] A. F. Molisch, M. Steinbauer, M. Toeltsch, E. Bonek, and R. S. Thomä, "Capacity of MIMO systems based on measured wireless channels," *IEEE J. Select. Areas Commun.*, vol. 20, no. 3, pp. 561–569, 2002.

[4] K. R. Dandekar and R. W. Heath, Jr., "Modelling realistic electromagnetic effects on MIMO system capacity," *IEE Electronics Letters*, vol. 38, no. 25, pp. 1624–1625, 2002.

[5] P. Suvikunnas, K. Sulonen, J. Villanen, C. Icheln, J. Ollikainen, and P. Vainikainen, "Evaluation of performance of multi-antenna terminals using two approaches," in *IEEE Instrumentation and Measurement Technology Conference, IMTC 2004*, vol. 2, Lake Como, Italy, May 2004, pp. 1091–1096.

[6] P. Suvikunnas, J. Villanen, K. Sulonen, C. Icheln, J. Ollikainen, and P. Vainikainen, "Evaluation of the performance of multiantenna terminals using a new approach," *IEEE Trans. Instrum. Meas.*, vol. 55, no. 5, pp. 1804–1813, 2006.

[7] A. Yamamoto, H. Toshiteru, O. Koichi, K. Olesen, J. Ø. Nielsen, N. Zheng, and G. F. Pedersen, "Comparison of phantoms for browsing position by a NLOS outdoor MIMO propagation test," in *Proceedings of ISAP2007*, Niigata, Japan, 2007, pp. 1342–1345.

[8] C.-H. Li, E. Ofli, N. Chavannes, E. Cherubini, H. Gerber, and N. Kuster, "Effects of hand phantom and different use patterns on mobile phone antenna radiation performance," in *IEEE Antennas and Propagation Society International Symposium, AP-S 2008*, San Diego, CA, July 2008.

[9] M. Pelosi, O. Franek, M. Knudsen, M. Christensen, and G. F. Pedersen, "A grip study for talk and data modes in mobile phones," *IEEE Trans. Antennas Propagat.*, vol. 57, no. 4, pp. 856–865, 2009.

[10] F. Harrysson, J. Medbo, A. F. Molisch, A. J. Johansson, and F. Tufvesson, "The composite channel method: Efficient experimental evaluation of a

realistic MIMO terminal in the presence of a human body," in *IEEE Veh. Technol. Conf. VTC 2008-Spring*, Singapore, May 2008, pp. 473–477.

[11] J. Medbo, M. Riback, H. Asplund, and J.-E. Berg, "MIMO channel characteristics in a small macrocell measured at 5.25 GHz and 200 MHz bandwidth," in *IEEE Veh. Technol. Conf. VTC 2005-Fall*, Dallas, TX, Sept. 2005, pp. 372–376.

[12] A. Alayon Glazunov, "On the antenna-channel interactions: A spherical vector wave expansion approach," Ph.D. dissertation, Dept. Electrical and Information Technology, Lund University, Sweden, 2009.

[13] G. F. Pedersen, K. Olesen, and S. L. Larsen, "Bodyloss for handheld phones," in *IEEE Veh. Technol. Conf. VTC 1999-Spring*, Houston, TX, May 1999, pp. 1580–1584.

[14] R. G. Vaughan and J. B. Andersen, "Antenna diversity in mobile communications," *IEEE Trans. Veh. Technol.*, vol. 36, no. 4, pp. 149–172, 1987.

[15] R. Kattenbach, "Characterization of time-variant indoor radio channels by means of their system and correlation functions," Ph.D. dissertation, Univ. GhK Kassel, Shaker Verlag, Aachen, Germany, 1997, (in German).

[16] M. Z. Win and J. H. Winters, "Analysis of hybrid selection/maximal-ratio combining in rayleigh fading," *IEEE Trans. Commun.*, vol. 47, no. 12, pp. 1773–1776, 1999.

[17] A. F. Molisch and M. Z. Win, "MIMO systems with antenna selection," *IEEE Microwave*, vol. 5, no. 1, pp. 46–56, 2004.

[18] P. Almers, T. Santos, F. Tufvesson, A. F. Molisch, J. Kåredal, and A. J. Johansson, "Antenna subset selection in measured indoor channels," *IET Microwaves, Antennas & Propagation*, vol. 1, no. 5, pp. 1092–1100, 2007.

Paper III

Evaluation of User Hand and Body Impact on Multiple Antenna Handset Performance

Abstract

We evaluate the user impact on antenna performance based on measurements using a realistic setup with a full (one-armed) upper body user phantom in combination with a four antenna PDA mock-up handset in realistic indoor office environment. We utilize an approach where the radiation pattern of the user together with the antenna, is considered as one radiating unit, and evaluate the performance impact of the user body and hand on such properties as the antenna efficiency, diversity combining approaches, and potential MIMO (multiple-input multiple-output) channel performance. From our investigation it is found that apart from the important efficiency loss due to the user hand, the mutual efficiency impact on the antenna elements and the directional impact of the user body shadowing have quite small influence on the diversity and capacity performance. We also find that the top and bottom placements of antennas are the most efficient to be used with up to two antenna elements. However, there are significant diversity and capacity gain that can be explored by using four distributed antennas even if only two radio chains are available through hybrid selection and combining schemes.

1   Introduction

The impact of the user in mobile communication systems may strongly affect the design and placements of antennas on terminals, as well as performance and reliability of system simulations, when utilizing multiple antenna techniques such as diversity and MIMO (multiple-input multiple-output). In this paper we evaluate the user impact on antenna performance based on measurements using a realistic setup with a full (one-armed) upper body user phantom in combination with a four antenna handset mock-up in a realistic indoor office environment at 2.5-2.7 GHz. We utilize an approach where the radiation pattern of the user together with the antenna is considered as one radiating unit, and evaluate the performance impact of the user body and hand of such properties as antenna efficiency, diversity combining approaches, and potential MIMO channel performance. In combination with radiation pattern measurements, the handset-plus-phantom radiation patterns are combined with a DDPC (double-directional propagation channel) representation of measured indoor channels by utilizing a composite channel method as described in [1, 2]. Previously the impact of the user in the mobile radio channel has been analyzed, e.g., by Yamamoto *et al.* [3] who showed by channel measurements that the impact of a realistic user phantom compared to simplified models may not be negligible in evaluation of diversity and MIMO capacity. Li *et al.* [4] and Pelosi *et al.* [5] showed that the user hand and the terminal position inside the hand may have a severe impact on the antenna efficiency.

2   Handset and User Phantom Setup

In the experiments we use a handset mock-up ($7x11x2$ cm^3) with four planar inverted F-antenna (PIFA) elements placed at the edges on one side of a ground plane. During both radiation pattern and channel measurements, a switch was used to select the active port, while the other antenna ports were terminated by matched loads. The user phantom consists of two separate parts, a liquid filled upper body phantom (torso and head) and a solid hand/lower arm phantom. Two different user operation situations or modes were investigated, *talk mode* and *browse mode*. Talk mode represents the scenario where the user holds the handset in the right hand, towards the right ear, with the antenna side opposite to the head; browse mode represents the scenario where the user holds the handset in the right hand as if to watch the screen. In browse mode the handset was tested both with the antenna side turned downwards and upwards. Furthermore, since the individual performance of the antenna elements may depend strongly on the precise positioning of the handset into
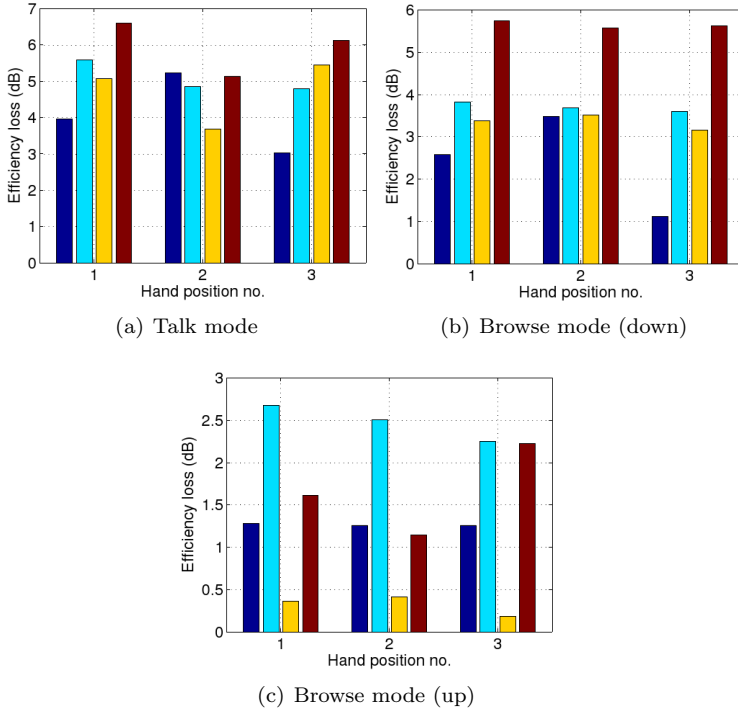
(a) Talk mode

(b) Browse mode (down)

(c) Browse mode (up)

Figure 1: The average excess efficiency loss due to the user phantom for individual antenna elements (1-4 bars) at the three positions inside the phantom hand for talk mode (a), and browse mode with antennas down (b) and up (c).

the hand phantom due to finger positions, the measurements were repeated for three positions inside the hand that are offset 10 mm with respect to each other. For further details and pictures on handset, phantom and measurements, see [1,2].

3   User Impact on Radiation Efficiency and Pattern

Radiation efficiency is undoubtly the most important feature of antennas for handheld mobile devices directly affecting the link budget and, hence, the bat-

tery power consumption. For our handset mock-up the radiation efficiency of the four individual antenna elements in free space (no user phantom present) is within $(-3.1 \pm 0.4$ dB). When placed in the hand of the phantom, however, the efficiency is reduced due to reflection (impedance mismatch) and absorption. This excess loss averaged over the frequency band 2.5-2.7 GHz is shown in Figure 1 for the three user configurations and the three hand positions. We find that both the user mode and the hand positions significantly affect the individual efficiencies of the antenna elements, so that the performance of one element compared to the other is changing. This effect is most significant when the handset is turned over in browse mode, i.e., compare graphs b and c. However, despite these differences, in our case antennas no. 1 and no. 3 seem to retain the best overall efficiency.

The individual radiation efficiency of the antennas depends on the handset placement in the hand. In Figure 2 the directional properties of the azimuthal radiation pattern is shown. The antenna gain is averaged over the used frequency band for handset antenna no. 1, in free space and in the presence of the phantom for the three hand positions. The directivity of the radiation pattern show low dependency on the hand positions and the gain difference is due to the efficiency impact. However, evidently is the shadowing effect of the phantom, showing as an absorbing sector towards about $-160°$ in talk mode and towards $-90°$ in browse mode (phantom nose points towards $90°$ with the handset at the right ear (talk) and in front of body (browse).

4   Diversity and MIMO Capacity Performance

From the channel matrices found by the combination of measured radiation patterns with the estimated DDPC based on the indoor channel sounder measurements, the statistical distributions of the individual signal powers P_i of the handset antennas and their (receive) diversity combinations are evaluated. We investigate the cumulative distribution, where the statistics are taken over frequency samples (utilizing the ergodic assumption that the small-scale fading is statistically similar over frequency and small-scale movement in the channel), simulated small-scale phantom translations, phantom rotations, base station side antenna locations, and in-hand offset positions. Figure 3 shows the impact of maximal-ratio combining (MRC) and hybrid selection/MRC [6] found as the power sum of: two random antennas (any 2MRC), two antennas with the strongest overall average signal powers (best 2MRC), two antennas of four with the strongest signal powers at each channel sample (best 2/4MRC), and all four antennas (4MRC). We note that the user presence does decrease the path gain but does not change the diversity peformance significantly, other
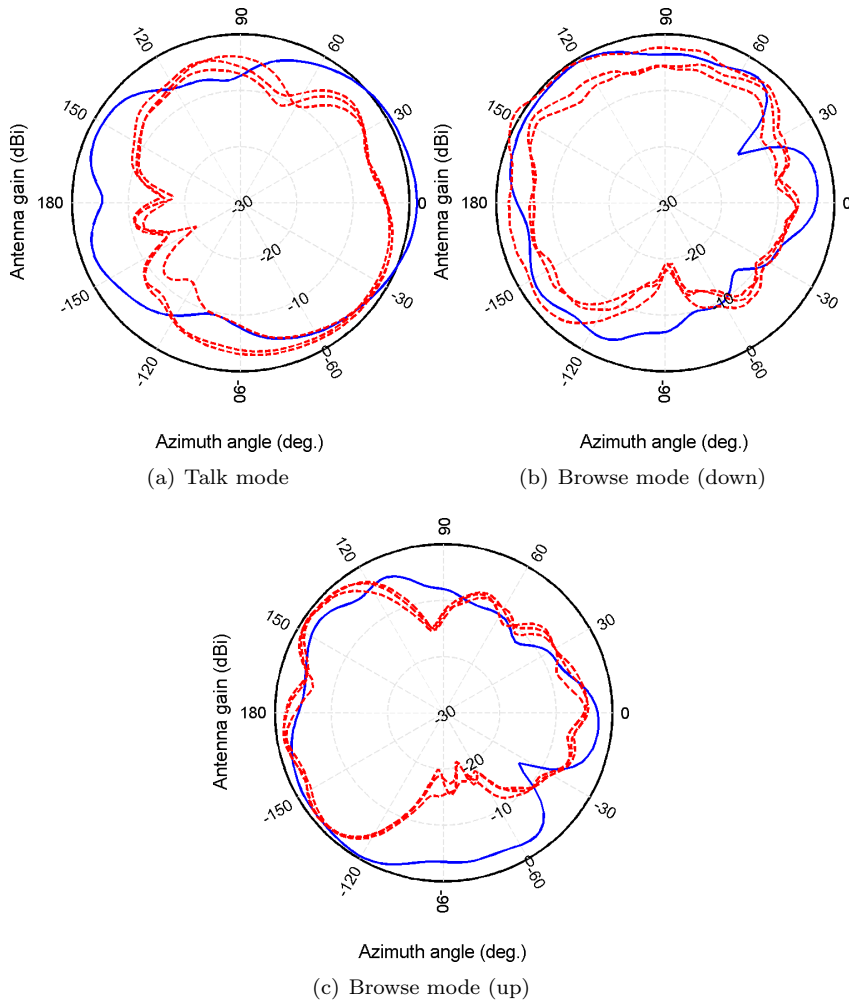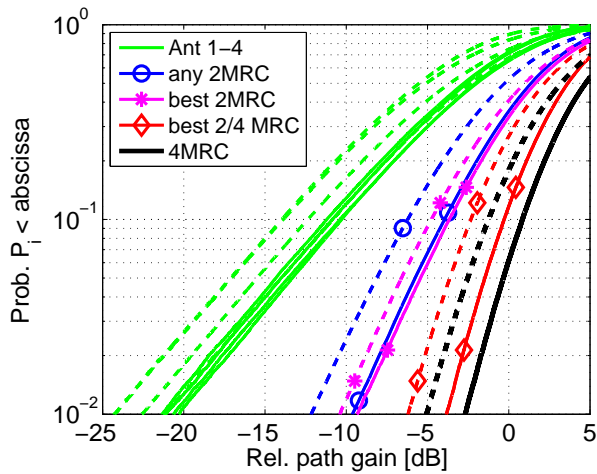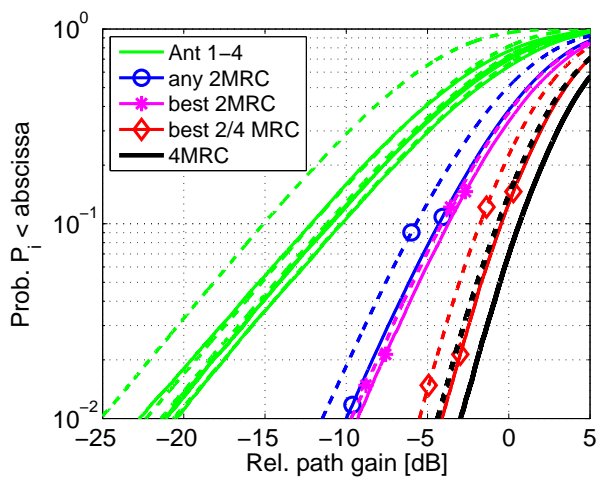
(a) Talk mode

(b) Browse mode (down)

(c) Browse mode (up)

Figure 2: Average antenna gain pattern for handset (antenna no. 1) in free space (dashed) and for the three positions inside the phantom hand (solid), in talk mode, browse mode with antennas downwards, and with antennas upwards.

(a) Talk mode

(b) Talk mode

Figure 3: Signal power distributions of antenna elements and with diversity combining with phantom user present (dashed) and without phantom user present (solid) for talk mode (a) and browse mode (b). The data is normalized w.r.t strongest antenna (phantom absent).

than in choosing the two best antennas. We also see the great benefit of four diversity antennas even if there is only two radio chains in the handset. The hybrid method (best 2/4MRC) increases diversity gain with about 6 dB (at 1% outage) compared to two antenna methods and is only about 1 dB below full 4MRC. Regarding performance with respect to MIMO capacity (spectral efficiency) as seen in Figure 4 similar conclusions about the user influence and sub-array selection methods as for diversity combining can be made. The presence of the user seems to increase path loss only, making SNR decrease. In the figure the channel matrices are normalized to the case with the phantom user absent (free space handset) so the difference in capacity is mainly due to the loss in SNR due to the user. We also find that hybrid 2x4 MIMO methods utilizing switching of 4 antennas for only 2 radio chains may significantly improve capacity compared to fix 2 antenna (2x4) systems. We find that the choice of antenna pairs based on strongest SNR (pow 2/4x4) performs very closely to the optimal choice based on capacity (best 2/4x4), which agrees with the results in [7].

5   Conclusions

From our experimental investigation of multiple-antenna performance and user impact of a realistic mobile terminal setup, we find that apart from the important loss of efficiency due to the user hand, the impact on the individual antennna elements and the directional impact of the user body shadowing have quite small influence on the diversity and capacity performance. It is found that the top and bottom placement of antennas within the handset case are the most efficient to be used with up to two antenna elements. There are, however, significant diversity and capacity gain that can be explored by using four distributed antennas even if only two radio chains are available through hybrid selection and combining schemes. It was also found that the practical method of choosing antennas based on signal power for 2 branch MIMO with 4 available handset antennas, performs well compared to the optimal solution.
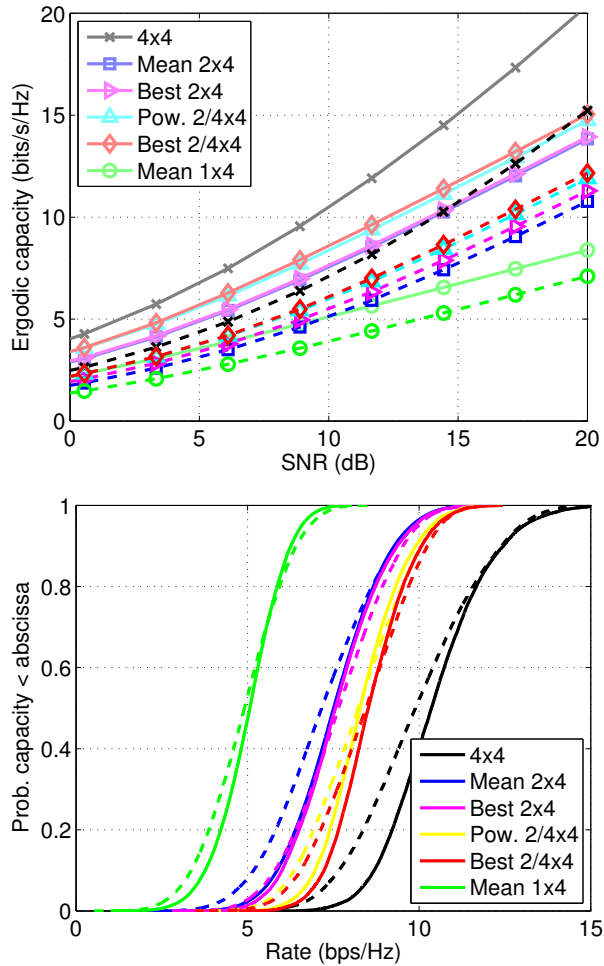
Figure 4: Ergodic capacity vs. SNR (top) and outage capacity distribution (bottom) at SNR=10dB for different MIMO systems with (dashed) and without (solid) user phantom present.

References

[1] F. Harrysson, J. Medbo, A. F. Molisch, A. J. Johansson, and F. Tufvesson, "The composite channel method: Efficient experimental evaluation of a realistic MIMO terminal in the presence of a human body," in *IEEE Veh. Technol. Conf. VTC 2008-Spring*, Singapore, May, 2008, pp. 473–477.

[2] F. Harrysson, J. Medbo, A. F. Molisch, A. J. Johansson, and F. Tufvesson, "Efficient experimental evaluation of a MIMO handset with user influence," *IEEE Trans. Wireless Commun.*, vol. 9, no. 2, pp. 853–863, May 2010.

[3] A. Yamamoto, H. Toshiteru, O. Koichi, K. Olesen, J. Ø. Nielsen, N. Zheng, and G. F. Pedersen, "Comparison of phantoms for browsing position by a NLOS outdoor MIMO propagation test," in *Proceedings of ISAP2007*, (Niigata, Japan), pp. 1342–1345, 2007.

[4] C.-H. Li, E. Ofli, N. Chavannes, E. Cherubini, H. Gerber, and N. Kuster, "Effects of hand phantom and different use patterns on mobile phone antenna radiation performance," in *IEEE Antennas and Propagation Society International Symposium, AP-S 2008*, (San Diego, CA), July 2008.

[5] M. Pelosi, O. Franek, M. Knudsen, M. Christensen, and G. F. Pedersen, "A grip study for talk and data modes in mobile phones," *IEEE Trans. Antennas Propagat.*, vol. 57, pp. 856–865, Apr. 2009.

[6] M. Z. Win and J. H. Winters, "Analysis of hybrid selection/maximal-ratio combining in Rayleigh fading," *IEEE Trans. Commun.*, vol. 47, pp. 1773–1776, Dec. 1999.

[7] A. F. Molisch, M. Z. Win, Y.-S. Choi, and J. H. Winters, "Capacity of MIMO systems with antenna selection," *IEEE Trans. Wireless Commun.*, vol. 4, no. 4, pp. 1759–1772, 2005.

Paper IV

Evaluation of an Outdoor-to-In-Car Radio Channel with a Four-Antenna Handset and a User Phantom

Abstract

Based on static outdoor channel measurements we evaluate the influence of a vehicle on the MIMO radio channel, from a base station antenna array, to a multiple antenna handset in the hand of a user placed inside a test car. The measurement scenario is chosen to mimic a 2.6 GHz (LTE) macro-cell urban or rural scenario with two locations and orientations of the car, one at an open parking lot with a strong line-of-sight component, and one between buildings with no line-of-sight. The measurements are repeated several times with the user phantom plus handset positioned at the same spot within the car and with the car absent. Figures of the penetration loss, impact on fading statistics, mean delay, delay spread, terminal antenna correlation, eigen-value distributions, as well as the performance of various hybrid diversity combining and spatial multiplexing schemes, are evaluated and compared with and without the vehicle present. It is found that the car make the channel statistics become more Rayleigh like and increases multipath channel richness, improving the potential of diversity gain and, to some extent, spatial multiplexing.

1   Introduction

In a real mobile radio channel setting the situation is seldom as simple as often assumed in channel modeling. Often, for a link budget analysis a combination of a propagation model, e.g. a path loss model, plus statistical fading outage is used, whereas for more complex multiple antenna system analysis a double directional propagation channel (DDPC) in combination with transmitting (Tx) and receiving (Rx) antenna patterns can be utilized. However, in reality the interface between the propagating radio waves (often assumed plane) and the antenna (often characterized by its farfield) is not so obvious. The effective antenna in a mobile phone includes also the casing. The hand of the user strongly affects the radiation performance of the individual antennas and the user body induces shadow fading. Furthermore, the surrounding of the users may be very complex with many close scatterers, e.g., in office environments, in crowded shopping malls, or inside vehicles. In this paper we continue our previous work on realistic terminal environments [2,3] to include the case when the user is located inside a car. The main question is the influence of the car on the multiple-input-multiple-output (MIMO) radio channel and, particularly, the performance of multiple antenna techniques, such as diversity and spatial multiplexing (SM). There is some previous work presented on penetration loss [5,6] and directional properties and in-car fading statistics [1,4], but not w.r.t. multiple antenna terminals. It is still unclear whether the presence of the car mainly provides increased scattering and, in-turn, improve the potential of multiple antenna diversity and MIMO capacity performance, or mainly cause attenuation of certain angular sections that induce shadow fading, increase antenna correlation, and thus, have a negative influence on diversity gain and MIMO capacity. These are questions we address in this investigation. Specifically, we investigate the potential performance of multiple antenna techniques at the mobile.

The novel contributions of the paper are the following:

1. we compare the radio channels with the test terminal at the same outdoor location with the car present (antenna inside), and without the vehicle present.

2. we use a realistic user setup with a four-antenna handset mock-up in browsing position, and a full scale user body phantom that includes hand, arm, upper torso and head, in combination with the test vehicle.

3. we analyze the vehicle impact on fading statistics, time delay properties, diversity performance, 4×4 MIMO eigenvalue distributions and capacity, with the test terminal in the presence of a user.

2 Measurement Setup

In the experiments we use two different Rx antenna configurations at the mobile side (MS). One was a uniform cylindrical 64 elements (4 rows, 16 columns) dual-polarized square patch antenna array (UCA) to be used for directional estimation of the channel (in this paper these measurements are only used for the time domain analysis). The second was a handset mock-up with four antennas placed at the edges. This was used in combination with an upper body user phantom. The user operation mode, *browse mode*, represents the smart-phone mobile broadband scenario where the user holds the handset as to watch the screen. Further details and pictures on handset and phantom can be found in [2].

The car was a regular middle to large size station wagon (Volvo V70) and the MS was placed in the center of the car at the location of the rear seat (the rear seats were down-folded). At the Tx base station antenna side (BS), a uniform rectangular 32 elements (4x8) dual-polarized square patch antenna array (URA) was positioned on the roof of one protruding wing of a building at the University campus at about 13 meters above the ground, resembling a microcell scenario. Two different locations were chosen for the MS, one at about 87 meters distance in an open area at a parking lot with line-of-sight (LOS) somewhat obstructed at the BS by a large tree (here denoted by "LOS" though it is not quite true!), and a second at about 37 meters distance in between two neighboring parallel protruding wings of the building, i.e., non-LOS due to the intermediate wing (denoted by "NLOS"). For the measurements we used the Medav RUSK Lund channel sounder in the frequency band 2570–2630 MHz, and the signal-to-noise ratio (SNR) was about 20 dB in both scenarios. To evaluate the impact of the car, the measurements were repeated with and without the car present at the same location for both the UCA and the phantom-plus-handset. In the latter case the measurements were repeated at nine offset ($\lambda/2$) positions to improve on statistics, and with four 90° horizontal rotations in each position.

3 Penetration Loss and Fading Statistics

The car penetration loss or the excess path loss due to the presence of the car can be found by comparing the empirical cumulative distribution of the received signal. The path loss was averaged over the 60 MHz frequency band using, as sample space, the switched Tx and Rx channels (of individual BS and MS antenna elements), the four phantom orientations, and the nine local offset positions. The resulting sample cumulative distribution function (CDF) of the
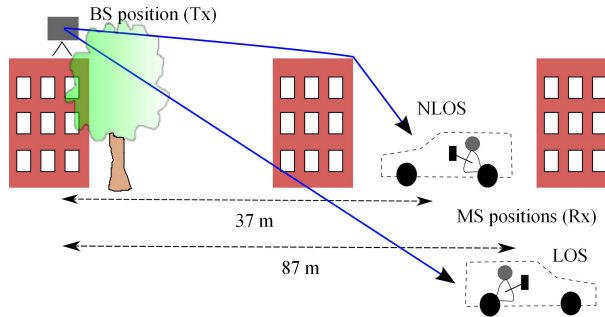
Figure 1: Illustration of the two measurements scenarios.

average signal power is shown in Figure 2.

The fading statistics in Figure 2 include statistics of both sides of the link so we do not directly see how the car influence the fading statistics around the MS. Actually, since the LOS case is rather an obstructed line-of-sight with rich scattering at the BS side and additional multi-path, even the distribution with the car absent is not completely Ricean. However, if we consider the 32×128 SISO channels with the (narrowband) statistics over MS antennas only, i.e., local MS offset positions and frequency samples; and select the channels that actually show a more Ricean-like distribution outside the car (the 7% that show $k > 1$), and compare to the corresponding case when the MS is located inside the car, the average maximum likelihood estimate (MLE) of the k-factor for the (so called) LOS case change from 1.4 to 0.3. Hence, the effect of the car on fading statistics seem to be (as expected) an increase of scattering around the MS making the channel become closer to Rayleigh distributed. One of the more notable examples of how the channel turn from Ricean outside to Rayleigh inside the car is shown in Figure 3.

4   Time Domain Properties

The impulse response of the channel is investigated by the average power delay profile (PDP) shown in Figure 4. The PDP is calculated as the squared absolute value of the inverse Fourier transform (IFFT) of the measured channel matrix using a Hann window. The average PDP is taken over the 32×128 antenna elements. From the graphs we hardly see that a significant difference between the channels with and without the car present since our 60 MHz bandwidth is to small to fully resolve multiple reflections inside the car. Calculations of
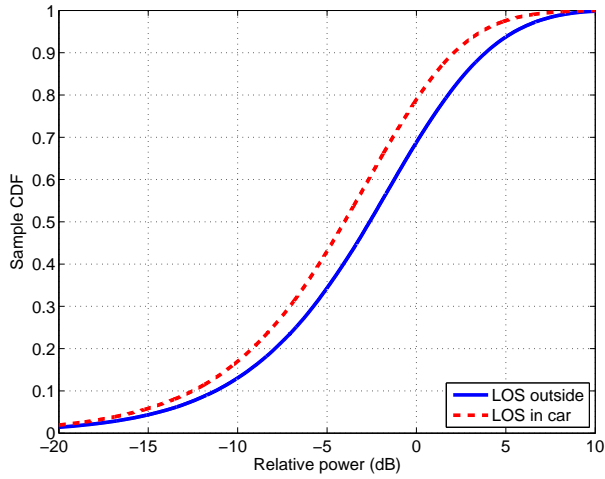
(a) LOS scenario
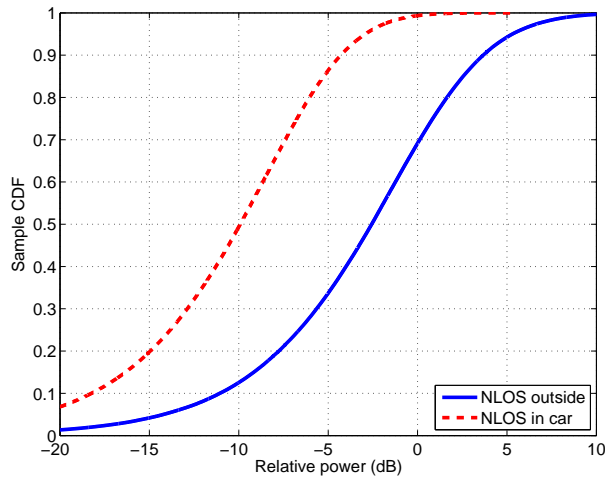
(b) NLOS scenario

Figure 2: Cumulative distribution of the average received signal power for the phantom+handset outside (solid) with the car absent, and inside (dashed) the car at same locations. The data has been normalized w.r.t the outside case.
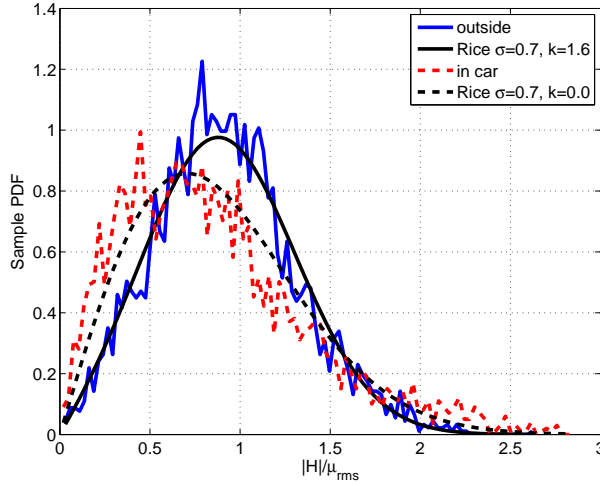
Figure 3: Example of probability density of the received signal for a case with notable change from outside to in-car. The Ricean distributions with the MLE parameters are shown for comparison.

mean delay and rms delay spread is presented in Table 1. As expected delay spread is larger in the NLOS scenario.

5   Antenna Correlation

An investigation of how the car body influence the statistical complex correlation between pair-wise MS antenna elements may give a hint on how the directional properties of the channel change when the MS is moved into the car, since the directional properties of the channel are in general connected to the channel covariance. The pair-wise MS antenna small-scale complex correlation coefficient can be estimated with respect to the n_t BS antenna elements, the n_x MS local offset positions, and by utilizing the ergodic assumption that the n_f frequency samples account for (narrowband) small-scale fading as

$$
\begin{aligned}
c_{ij} &= \frac{1}{n_t n_f n_x} \sum_{k=1}^{n_t n_f n_x} h_{ik} h_{jk}^* \\
\tilde{\rho}_{i,j} &= \frac{c_{ij}}{\sqrt{c_{ii} c_{jj}}}
\end{aligned}
\tag{1}
$$
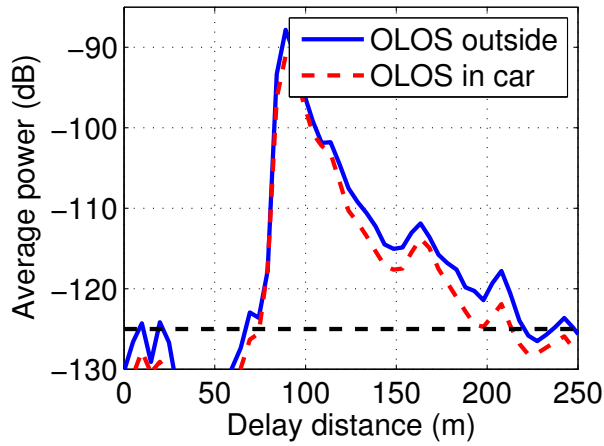
(a) LOS scenario
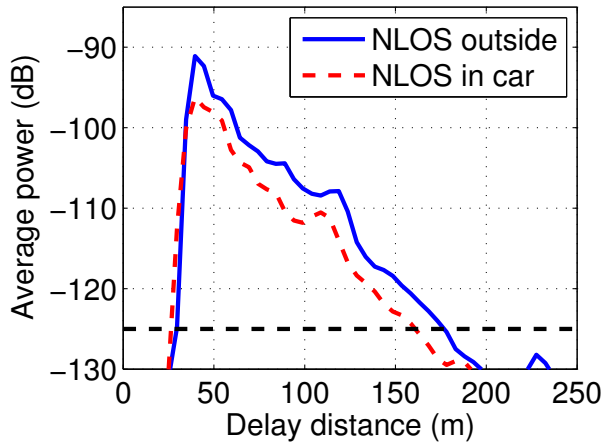
(b) NLOS scenario

Figure 4: Average PDP of the two scenarios with the UCA at the MS side with and without the car present.

Table 1: Mean delay and RMS delay spread in nanoseconds for the channel measurements with the UCA in the two scenarios with and without the car present.

	Mean delay	RMS delay spread
LOS outside	313	50
LOS in car	316	47
NLOS outside	174	78
NLOS in car	173	59

Here h_i is the measured channel response at MS antenna i. The result is shown in Figure 5. The correlation is clearly lower inside the car than outside indicating an enriched inner scattering, thus improving the possible diversity gain by using multiple MS antennas. If we compare the results from [2] were it was found that the user (phantom) body increases antenna correlation, we may assume that increased local scattering inside the car compensate for the shadowing of the user body, and thus, lowering the correlation such that diversity gain by multiple MS antennas is recovered.

6   Diversity and Spatial Multiplexing

To investigate the potential gain of diversity combining and MIMO capacity, and the influence of the car, we utilize the same method as was used in [3] for the user influence. In Section 5 we found that the car environment decreases antenna correlation at the MS, which would increase potential diversity gain. Figure 6 shows the impact of maximal-ratio combining (MRC) and hybrid selection/MRC [7] found as the power sum of; two antennas with the strongest overall average signal powers (Best 2MRC), two antennas of four with the strongest signal powers at each channel sample (2/4 HS-MRC), and all four antennas (4MRC). We notice that the car presence, apart from increasing path loss as was shown previously, improves the diversity performance in almost all cases. The increase in diversity gain due to the car is found to be about 1–1.5 dB. We also see the great benefit of four diversity antennas, providing full 4th order diversity, even with a limitation of two radio chains in the handset. The hybrid method (2/4 HS-MRC) increases diversity gain in our results about 3–4 dB (at 1% outage) compared to two-antenna methods.

The local scattering within the car that provides diversity gain does not imply MIMO spatial multiplexing (SM) gain. The car influence on SM is
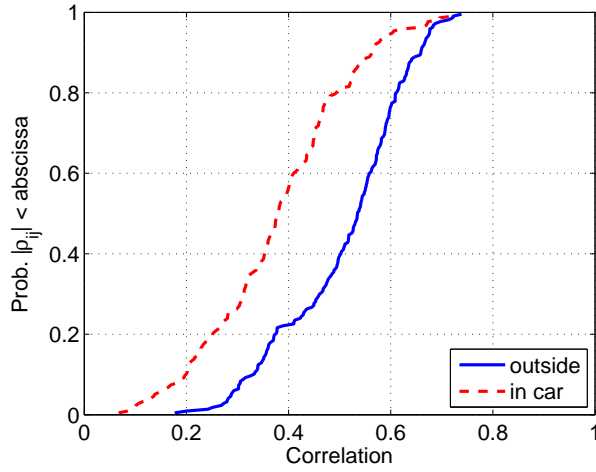
(a) LOS scenario
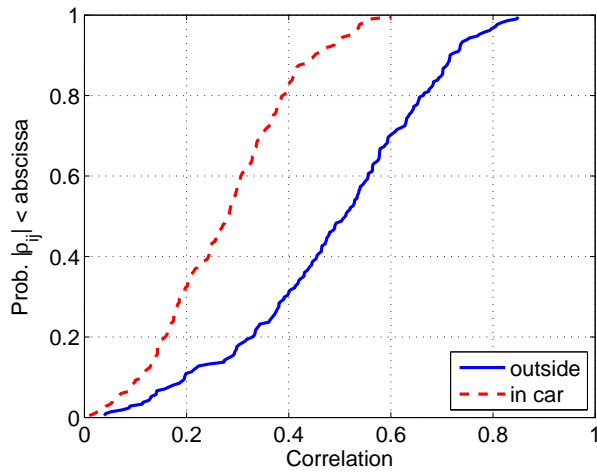
(b) NLOS scenario

Figure 5: Cumulative distribution of the estimated MS antenna correlation coefficient for the phantom+handset outside (solid) and inside (dashed) the car.

illustrated in Figure 7 by a comparison of the eigenvalue distributions for a selected set of four BS antennas (vertical polarization, separated by 1 λ), with the car present and not. The graphs show the sorted eigenvalues of $\mathbf{HH}^H$ calculated from a 4×4 sample matrix $\mathbf{H} = \mathbf{H}^{(i)}$ as

$$\lambda^{(i)} = \frac{1}{P_{av}} \text{eig} \left\{ \mathbf{H}^{(i)} \mathbf{H}^{(i)H} \right\} \tag{2}$$

where the normalization factor P_{av} is the sum of eigenvalues averaged over the sample space, i.e., the i's (here the frequency samples and MS local translations). In (2) we consider the distribution of the eigenvalues over an ensemble containing all combinations of frequency samples, MS translations and phantom user rotations. The car body surrounding the MS has the effect of decreasing the eigenvalue spread by enriched multipath and, thus, increasing the potential of SM gain. Other BS antenna configurations were tested, showing different performance, but with almost the same car dependency. was also tested However, looking at MIMO capacity with penetration loss omitted, as seen in Figure 8, we find that the car only has a small effect in some cases. Here the ergodic or mean spectral efficiency (bit/s/Hz) is plotted against the average SISO signal to noise ratio in each of the cases with and without the car present in the channel, i.e., *the car penetration loss is removed*. However, the presence of the car seems to slightly increase 4x4 MIMO capacity in the LOS case and 4x2 MIMO in the NLOS.

We also find that hybrid 4x2/4 MIMO method (HS-MIMO) with instantaneous selection of two out of four antennas at the MS and utilizing 4x2 MIMO, improve capacity compared to a fixed two antenna (4x2) handset.

7   Conclusions

The goal with this investigation was to get insight into how a regular vehicle, such as a standard station wagon, affect the radio channel from a macro-cell base station to a mobile phone operated inside. It is found in our measurements that the penetration loss, or excess path loss, due to the test vehicle was in average between 1.6–7.9 dB. These figures strongly depend on the outer channel, i.e., the scenario and orientation of the car relative the base station and can probably be even smaller and significantly larger. In our case we believe that the difference between the penetration loss in the two scenarios is mainly due to the elevation angle of the impinging radio waves which, if generalized, would indicate that the average car penetration loss could differ between urban and rural scenarios. However, much more extensive measurements are needed to provide valid statistics to, e.g., set parameters in a channel model. Furthermore, we find that the car increase inner local scattering around the mobile
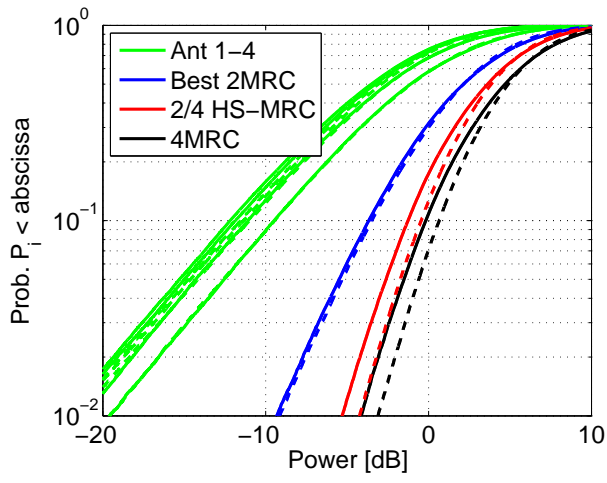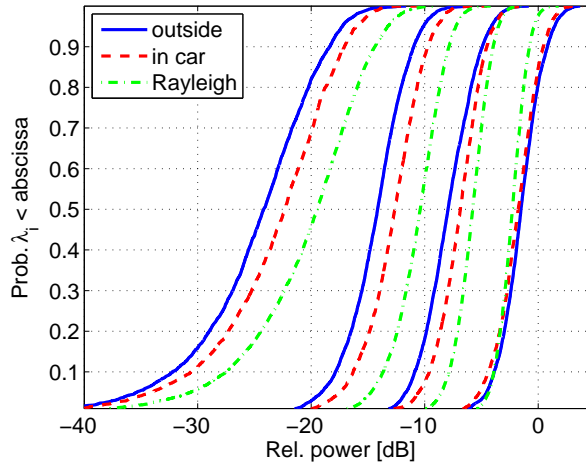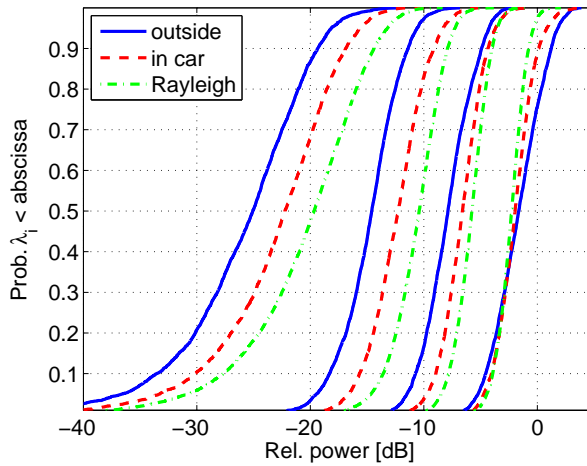
(a) LOS scenario
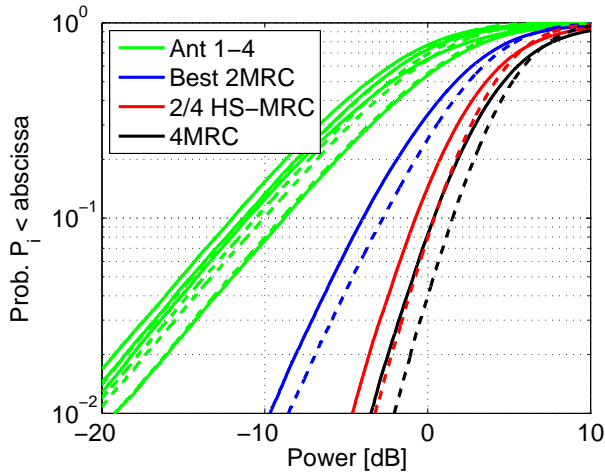
(b) NLOS scenario

Figure 6: Received signal power distributions for individual antenna elements (SISO) and with various diversity combining schemes (SIMO) for the user-plus-handset at the same location with the car absent (solid) and inside the car (dashed). The data is normalized to the average SISO channel power.
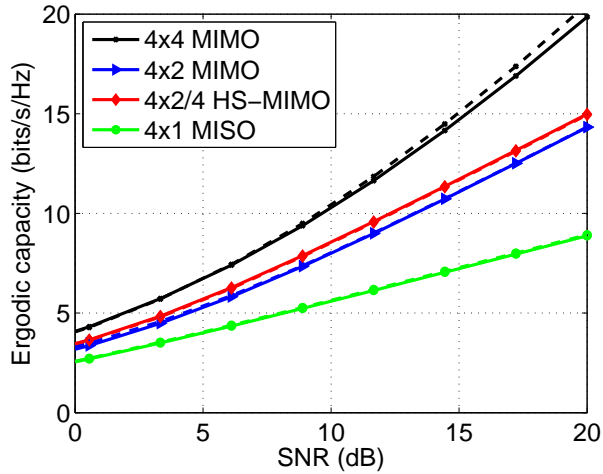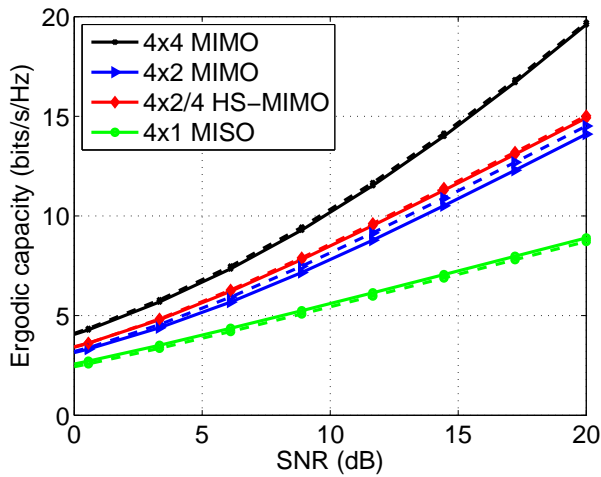
(a) LOS scenario

(b) NLOS scenario

Figure 7: Cumulative distributions of eigenvalues for a 4x4 MIMO configuration. The eigenvalues are normalized with the total power averaged over frequency points and translations.

(a) LOS scenario

(b) NLOS scenario

Figure 8: Ergodic capacity vs. SNR for different MIMO systems with the car absent (solid) and present (dashed).

user which makes the fading statistics become closer to Rayleigh distributed. Regarding terminal multiple antenna properties, our measurements show a decrease in pair-wise antenna correlation at the mobile side when placed inside the car compared to outside. An observation that explains the increase in potential diversity gain of various diversity combining schemes of about 1–1.5 dB at 1% outage level inside the car. Also when looking at eigenvalue distributions for a 4×4 MIMO system, we find that the richness increases inside the car, making the eigenvalue distribution less spread. This, in turn, provides a potential for improved spatial multiplexing gain, which we also find when we look at the theoretical capacity, even though the gain seems rather small.

Acknowledgment

References

[1] F. Harrysson, "A simple directional path loss model for a terminal inside a car," in *IEEE Veh. Technol. Conf. VTC 2003-Fall*, vol. 1, 2003, pp. 119–122.

[2] F. Harrysson, J. Medbo, A. Molisch, A. Johansson, and F. Tufvesson, "Efficient experimental evaluation of a MIMO handset with user influence," *IEEE Trans. Wireless Commun.*, vol. 9, no. 2, pp. 853–863, Feb. 2010.

[3] F. Harrysson, A. Derneryd, and F. Tufvesson, "Evaluation of user hand and body impact on multiple antenna handset performance," in *IEEE International Symposium on Antennas and Propagation, AP-S 2010*, Toronto, Canada, July 2010.

[4] C. Hill and T. Kneisel, "Portable radio antenna performance in the 150, 450, 800, and 900 MHz bands 'outside' and in-vehicle," *IEEE Trans. Veh. Technol.*, vol. 40, no. 4, pp. 750–756, 1991.

[5] I. Kostanic, C. Hall, and J. McCarthy, "Measurements of the vehicle penetration loss characteristics at 800 MHz," in *IEEE Veh. Technol. Conf. VTC'98*, vol. 1, May 1998.

[6] E. Tanghe, W. Joseph, L. Verloock, and L. Martens, "Evaluation of vehicle penetration loss at wireless communication frequencies," *IEEE Trans. Veh. Technol.*, vol. 57, no. 4, pp. 2036–2041, 2008.

[7] M. Z. Win and J. H. Winters, "Analysis of hybrid selection/maximal-ratio combining in Rayleigh fading," *IEEE Trans. Commun.*, vol. 47, no. 12, pp. 1773–1776, Dec. 1999.

Paper V

Experimental Investigation of the Directional Outdoor-to-In-Car Propagation Channel

Abstract

The demand for wireless channel models including realistic user environments is increasing. This motivates work on more detailed models that are reasonably simple and tractable but with adequate statistical performance. In this paper, we present an investigation of the spatial outdoor-to-in-car radio channel at 2.6 GHz. Specifically, we investigate the performance of a multiple antenna smartphone mock-up in the hand of a user. We evaluate and utilize a composite channel approach to combine measured antenna radiation patterns with an estimated spectral representation of the multipath channel outside and inside the car in two different scenarios. The performance of the method is investigated and comparisons with direct channel measurements are performed. Statistical and directional properties of the outdoor-to-in-car channel are presented and analyzed. It is found that the composite method, despite nearfield problems when estimating plane-wave channel parameters in a very narrow environment, constitutes a tool that provides reasonably viable statistical results. In addition, we have found that the introduction of the car in the propagation environment increases scattering and eigenvalue dispersion while it decreases pairwise antenna signal correlation. These statistical properties are found to slightly increase the possible diversity and the spatial multiplexing gains of multiple antenna terminals when located inside cars. This positive effect, however, is small compared to the negative effect of car penetration loss.

1 Introduction

Communication from vehicles have today become a prevalent scenario for hand-held mobile terminals, such as smartphones, that may be in the hands of passengers using high data rate cellular services. This scenario will affect the tuning of the cellular networks and the quality-of-service of the cellular systems serving the users, and may also affect terminal technology. In addition, a car may also serve as a relevant example of an immediate confined scattering environment, representative also for other similar surroundings like indoor parts of buildings, other vehicles, trains, sub-ways, etc, that are common surroundings in the everyday life of mobile terminal users. Thus, in ubiquitous cellular systems, like LTE (long-term evolution) and future LTE-Advanced, it is of great interest to know in detail also the impact of such environments with respect to performance (power consumption, data rate, reliability etc.) of multiple antenna terminals such as MIMO (multiple-input multiple-output) smartphones. The car environment will have impact not only on the path loss which affects power consumption and coverage, but also on the fading statistics of the radio channel. Multiple antenna techniques such as diversity and spatial multiplexing, which are essential to combat fading and to boost channel capacity are also highly affected. However, channel models that, in a realistic way, incorporate these confined environments in the immediate neighborhood of the user are rare. Such channel models are of particular importance for the development of vehicular-to-infrastructure (V2I) solutions.

In the development of an empirical channel model that includes nearby scattering objects and surroundings it is possible to include the objects either in the representation of the antenna or in the propagation channel characterization. However, if these objects, e.g. a car, are included in the channel we need to perform new channel measurements for each configuration (terminal antenna, user orientation, car type, car orientation, location, etc.). Instead, by measuring the much more rigid outer channel once (at a representative location) we can produce a model that is represented by the *double-directional propagation channel* (DDPC), i.e., a sum of multi-path components (MPCs); each characterized by its direction-of-arrival (DoA), direction-of-departure (DoD), path delay, and complex amplitude [1]. The DDPC can be estimated from good quality MIMO channel measurements by methods like SAGE [2]. With the DDPC at hand, the outer channel can easily be combined with measured or simulated radiation patterns. This composite channel modeling (CCM) methodology is verified in [3,4] wherein it is also utilized to evaluate the influence of the body of the user. In the case of, e.g., an object large as a car, the method is still possible but perhaps not feasible or practical.

In this paper, we present an investigation of the influence of a standard

family car on the spatial radio channel at 2.6 GHz, and specifically on the performance of a multiple antenna smartphone mock-up terminal in browse mode position in the hand of a user phantom. We utilize the composite channel approach where the user together with the antenna, is considered as one radiating unit or a *super-antenna* with the propagation channel represented both with the car absent and inside the car. The environment inside a normal sized car does not, however, provide enough space to reach the far-field of a several wavelengths sized array antenna necessary for directional channel characterization, of a user phantom super-antenna, at relevant frequencies around 2.6 GHz. Thus, we have to violate the far-field requirement to use the in-car composite channel approach. Hence, the question is to what extent the composite method with the far-field assumption inherent both in the DDPC and in the super-antenna radiation pattern, is valid for MIMO performance prediction inside a car, and how much it suffers from the violation of the far-field assumption and (unavoidable) measurement inaccuracies.

Several published papers describe investigations of cars and other vehicles. Several papers also describe and evaluate the principle of combining a directional propagation characterization with antenna radiation patterns (here referred to as a composite channel modeling), e.g., [4–6], but to our best knowledge no work exists that investigates and validates this composite channel modeling approach in a narrow confined scenario where, e.g. a mobile handset, in the presence of a user (phantom), is located inside a vehicle, e.g. a car.

The goal of the paper is to investigate to what extent the plane-wave spectrum composite channel method can appropriately account for a car environment with the mobile user inside. The novel contributions of the paper are the following:

1. We test the impact of a car environment (outdoor-to-in-car) with a body phantom that includes hand and upper torso as well as head.

2. We investigate the possibility of performing directional channel estimation inside a car.

3. We analyze the performance of the synthetic channel based on the estimated channel in the presence of a user inside and outside a car, w.r.t. singular value distributions and antenna signal correlation.

The investigation is based on channel measurements in two different static scenarios with an upper body phantom and a four-antenna handset mock-up located outside and inside a common type family car (station wagon), in the LTE band 2.5–2.7 GHz for a synthetic 4×4 MIMO arrangement.

The paper is organized as follows: Section 2 outlines the basic principle of the composite method, Section 3 describes the details of the equipment,

the test setup and the measurement scenarios, and Section 4 elaborates on the measured channel properties and the directional characterization of the channel from inside the car. Next, the comparison procedure between direct measurements and composite results is described in Section 5, with the comparison of eigenvalue distributions and antenna signal correlation as the key experimental results of the campaign. In Section 6 we evaluate the impact of the car on channel properties like correlation, diversity and capacity gain in different cases, and use the composite channel model to separate the user and the car influences. Finally, the paper is summed up and concluded in Section 7.

2 The Channel Matrix

2.1 Channel Model

It is assumed that the radio channel can be modeled by a finite number L of multi-path components (plane waves), originating at the transmitter (Tx) antenna propagating towards the angle $\Omega_{t,l}$ (direction of departure), subject to reflection, scattering and diffraction, before terminating at the receiver (Rx) antenna impinging from angle $\Omega_{r,l}$ (direction-of-arrival). This means that the frequency domain MIMO channel transfer function (matrix) can be written as

$$\mathbf{H}(f) = \sum_{l=1}^{L} \alpha_l \mathbf{G}_r^T(\Omega_{r,l}, f) \mathbf{P}_l \mathbf{G}_t(\Omega_{t,l}, f) e^{-j2\pi f \tau_l}, \tag{1}$$

where α_l denotes the complex MPC amplitude, τ_l the path excess delay, and $\mathbf{P}_l]$ the 2×2 normalized polarimetric transfer matrix. In (1) the assumptions is made that the antennas can be characterized by their far-field characteristics, i.e., that the closest MPC scatterer is outside the near-zone of the antenna. The antenna matrices $\mathbf{G}_t$ and $\mathbf{G}_r$ include also the complex array location vector phase term for each element in the columns, and for the polarization component (θ, ϕ) in the rows, i.e., $2 \times n_{r,t}$. Here we assume a static Rx unit which can be generalized to a dynamic case with the addition of the Doppler frequency $f = (1 + \frac{v}{c})f_0$ in (1), where $v = \hat{k}_{r,l} \cdot \boldsymbol{v}$ is the Rx velocity relative the direction of each individual MPC $\hat{k}_{r,l}$.

2.2 Channel Estimation and Calculation

With the channel model in (1) it is possible to calculate the channel matrix synthetically for any array antenna characterized by its farfield matrix $\mathbf{G}$ as long as the farfield assumption is not violated. When the channel model is used to represent an observation from a channel measurement, the channel

parameters (DDPC parameters) $\boldsymbol{\theta} = \{\Omega_{t,l}, \Omega_{r,l}, \tau_l, \alpha_l, \mathbf{P}_l\}$ can be estimated by using a maximum-likelihood (ML) estimator that performs the operation

$$\hat{\boldsymbol{\theta}} \triangleq \arg\max_{\boldsymbol{\theta}} p(\mathbf{x}; \boldsymbol{\theta}), \tag{2}$$

where $p(\mathbf{x}, \boldsymbol{\theta})$ is the probability distribution function of the observed channel $\mathbf{x} = \mathrm{vec}(\tilde{\mathbf{H}})$ and the parameter vector. It can be shown that the log-likelihood function can be written as

$$-\log p(\mathbf{x}; \boldsymbol{\theta}) = N_r N_t N_f \log(\pi\sigma^2) + \frac{1}{\sigma^2} \sum_{k=1}^{N_f} ||\tilde{\mathbf{H}}_k - \mathbf{H}_k||_F^2, \tag{3}$$

were k is the sample frequency index, σ^2 the noise variance, $\tilde{\mathbf{H}}$ is the channel model in (1), and $\mathbf{H}$ is a measurement realization.

The estimator used in this investigation is described in [7] (with reverse notation) and is here only described briefly. It starts by a search for the maximum in the power delay profile, followed by time-domain gating and dual-side beamforming to find initial parameter values ($\Omega_{t,l}$, $\Omega_{r,l}$ and τ_l) of the (multiple) MPC's within the selected delay slot. Next a binary search algorithm performs a binary tree search maximization to improve the parameter estimates one-by-one as in SAGE [2]. In a second step the estimation procedure performs an analytical gradient calculation, utilizing the multivariate quadratic Taylor expansion of the likelihood, to find the local maximum. In this step the Jacobian and the Hessian of the likelihood is calculated analytically. This step is very sensitive to model errors, e.g., due to non-planar wave fronts (while assuming planar wave fronts) when scatterers are to close to the sensor antenna array [8–10]. In Section 4.2 this problem is further discussed.

These steps in the estimation procedure are iterated and combined with a linear estimation of $\alpha_l \mathbf{P}_l$, and with possible birth of new MPC's, until an accuracy threshold is reached and until the extraction of MPC's in the delay domain reaches the noise floor of the data. The estimation method is also mentioned in [11] and was used in [4, 12].

3   Measurement Equipment and Setup

3.1   Array antenna, Handset and User Phantom

In the experiments two different antenna configurations at the mobile side (MS) were used. One was a uniform cylindrical 64 element (4 rows, 16 columns) dual polarized square patch antenna array (receiving patch uniform cylindrical array, RxPUCA) to be used for directional estimation of the channel. The second was

a handset mock-up with four (PIFA) antennas placed at the edges, connected by coaxial cables to a 1-to-4 switch. The handset is placed in the hand of a user phantom consisting of a liquid filled head-plus-torso and one solid (right) arm-plus-hand in *browse mode*. The user operation mode (browse mode) represents a smartphone mobile broadband scenario where the user watches the handset screen. Further details and pictures on handset and phantom can be found in [3, 4]. At the base station antenna side (BS), a uniform rectangular 4×8 dual polarized square patch antenna array (TxPURA) was used.

3.2   Car

The car is a 2005 model Volvo V70 station wagon with standard glazing and with the rear seats down-folded to make place for the antennas. The main investigation is made with the car empty from driver and passengers. Some additional measurements were done with a driver behind the wheel and with side windows open, but no significant effect due to the driver and the windows was found.

The orientation of the car in the two scenarios is shown in Figure 1 with the definition of the azimuth angle at the MS (Az_{MS}). The direction towards the TX is marked in both cases (about 250 degrees in Scenario A and 270 degrees in Scenario B). Also the geometry of the car and the placement of the channel sounder array antenna and the user phantom (inside the car) is shown.

3.3   Channel Sounder

The channel sounder used was the RUSK Lund channel sounder from Medav. The characteristics of the sounder setup are summarized in Table 1.

3.4   Antenna Characterization

The radiation patterns and efficiencies of the handset, with and without the phantom present, have been measured previously [3, 4]. For the directional estimation we also needed a full characterization of the RxPUCA antenna. The calibration of the measurement array antenna is very important for the accuracy of the directional estimation [13, 14]. This was measured in a high quality anechoic chamber with six meter separation between the transmitting dual polarized reference horn antenna, and the rotation center of the roll-over-azimuth positioning system.

In all channel measurements used in this paper the same Tx antenna (Tx-PURA) was used. Thus, since this antenna was unchanged in the channels that is being compared, directional estimations were only required at the MS side.
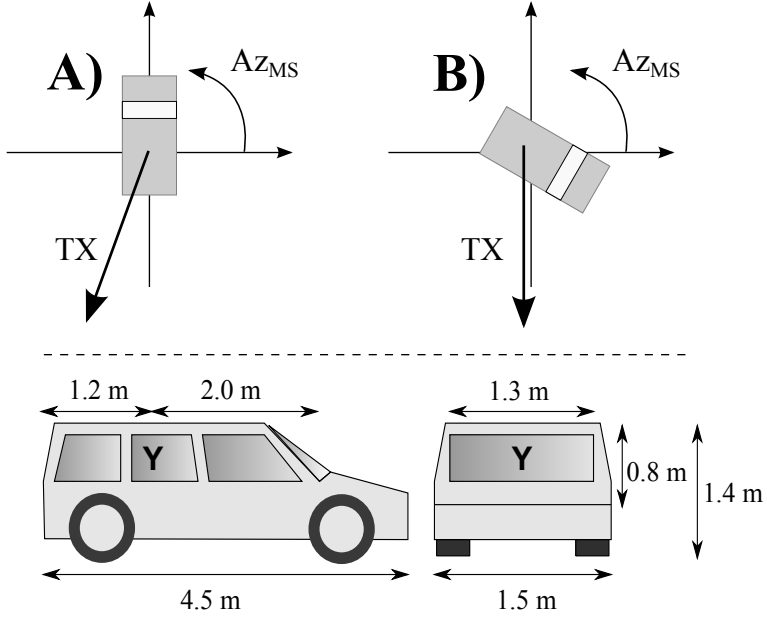
Figure 1: Orientation of the car in the two scenarios, and the car geometry with the location of the test antennas when inside the car.

Table 1: Channel sounder parameter configuration during measurements.

Center frequency, f_c	2.6 GHz
Measurement bandwidth, B	60 MHz
Delay resolution, $\Delta\tau = 1/B$	16.7 ns
Transmit power, P_t	27 dBm
Test signal length, τ_{max}	1.6 μs
Number of TxPURA antenna ports, N_t	32
Number of RxPUCA antenna ports, N_r	128
Number of Rx handset antenna elements, $N_{r'}$	4
Snapshot time, $t_{snap} = 2 * N_t * N_r * \tau_{max}$	13.1 ms
Number of snapshots at each recording	100
Number of frequency samples	97
Tx antenna height over ground, h_t	ca 9 m
Rx antenna height over ground, h_r	1.1-1.3 m

3.5   Channel Measurement Scenarios

Two measurement campaigns with two different MS location and orientation were performed at the Lund University Campus (E-building of LTH), Lund, Sweden:

Scenario A: Parked car outdoor microcell scenario with line-of-sight (LOS) obstructed by a tree. The direction to the Tx is towards the rear-left of the car with low elevation angle. Almost free sight through the rear window.

Scenario B: Parked car outdoor microcell non line-of-sight (NLOS). The direction towards the Tx is to the front-right of the car with buildings surrounding the car at three sides and obstructing the LOS.

In both scenarios the BS antenna was located at the same location (roof top of a two story building) with bore-sight towards the MS. In each scenario, two main configurations at the MS side were used. Firstly, the channel was recorded with the RxPUCA once for the purpose of directional channel characterization. Secondly, the channel was measured with the user phantom at the MS (user phantom plus handset) rotated in 90° steps to four orientations and translated to nine offset positions with $\lambda/2$ separation, i.e., 4×9 channel measurements in the latter case. These measurements were repeated twice in each scenario, once with the car absent but with the RxPUCA/phantom on a trolley at the MS location, and once with the RxPUCA/phantom placed inside the car at the nine MS locations. The measurements and scenarios are described with more details in [15].

The average receiver SNR (signal-to-noise ratio) for a single antenna to antenna (SISO) channel was between 0–17 dB in all measurements, which was improved almost 20 dB after coherent averaging over 100 channel snapshots recorded at each measurement. The measurements were taken during afternoons at a parking lot with almost no people and cars moving at the site. However, we cannot exclude that movements from a few passing pedestrians and cars in surrounding areas may have caused some interference.

4   Channel Characterization

4.1   Channel Characteristics and Estimated Parameters

With a bandwidth of 60 MHz corresponding to a standard resolution in delay of 5 meters we are not likely to resolve with good accuracy the possible impact on delay spread from the car presence by studying the power delay profile

Table 2: Channel parameters, delay spread σ_τ, azimuth spread σ_ϕ and elevation spread σ_θ, in the measurement scenarios, based on the estimated MPC parameters.

| Scenario	σ_τ (ns)	σ_ϕ (deg.)	σ_θ (deg.)
A outside	54.9	24.6	7.1
A in car	63.3	39.1	13.6
B outside	45.1	33.4	29.2
B in car	51.2	45.4	27.4

alone. However, by the high-resolution method described in Section 2.2 we can improve the result. Having performed the channel parameter estimation we studied the results in the delay and directional domains, separately. Based on these estimates we calculated the corresponding channel properties, e.g., the rms delay spread σ_τ [16, Chapter 6] and the angular spread [17] in azimuth and elevation, S_ϕ and S_θ, respectively. These results are found in Table 2 and in Figure 2 where the graphs show the directional distributions of estimated MPC parameters at the MS side for the different cases.

From Table 2 we find that the delay spread increases slightly (about 6-8 ns) and that the azimuth spread increases significantly (about 12-15 degrees) when the antenna is located inside instead of outside the car in both scenarios. The vertical elevation spread, however, increases to some extent in Scenario A (the obstructed LOS case) while it is almost unchanged in Scenario B (the NLOS case). These observations of the angular spread are apparent by looking at the angular distributions in Figure 2.

4.2   Channel Estimation Accuracy

An extensive number of uncertainties and possible error sources do inevitably affect the result of these evaluations. While some of these uncertainties are known and can be estimated, others are assumed to be negligible or small[1]. Below we discuss some of the most important error sources. Specifically, we illustrate with a few examples the consistency/in-consistency of doing plane-wave estimation in a propagation channel with near-field scattering sources, a topic that is central in this evaluation were we try to model a confined environment like the car.
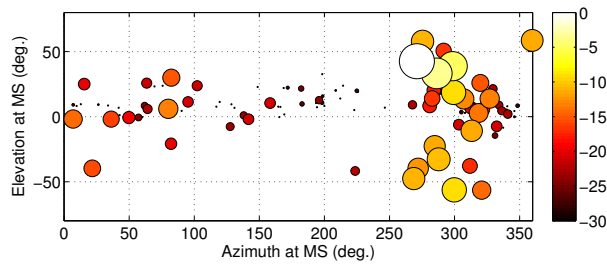
---

[1]A comprehensive investigation of experimental channel estimation limitations and various error sources can be found in [14]
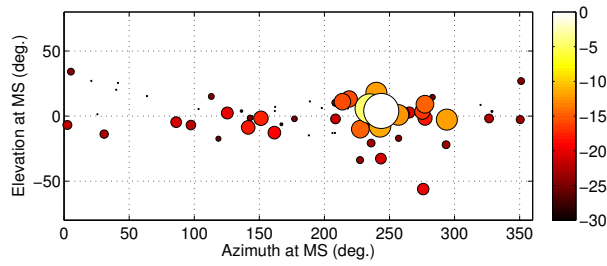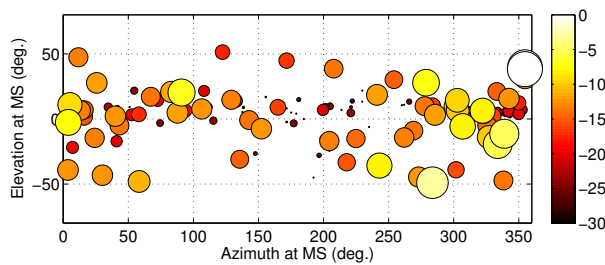
(a) Scen. A outside
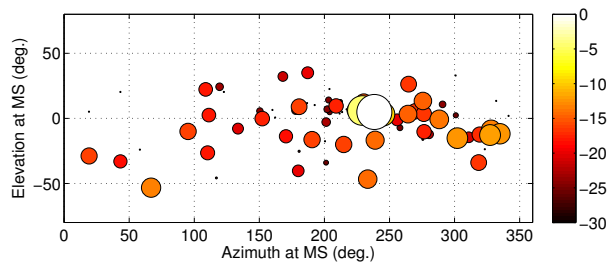
(b) Scen. A in car

(c) Scen. B outside

(d) Scen. B in car

Figure 2: Estimated MPC power vs. elevation and azimuth at the MS (DoA) in the different scenarios. The color of the circles represent the relative total power of the MPCs.

4.3   Error sources and noise

The most important practical error sources in this investigation are most certainly the limited signal power strength (SNR) and limited antenna calibration (both arrays and phantom-plus-handset) measurement accuracy. During the channel measurements with the RxPUCA the internal LNA provides the SNR_{IR} of up to 50 dB after averaging over 100 coherent snapshots which is the peak-to-noise level of the input channel data to the channel estimation process in the outdoor cases, and about 42 dB inside the car in Scenario B.

As for the antenna measurement ranges used have a potential accuracy limit well below 25 dB, but due to practical compromises with switching, bending of cables, impedance mismatch, scattering in turntables, reconfigurability of phantom-plus-handset, etc., this error level is roughly about 20 dB below the peak for the RxPUCA used for directional channel estimation, and minimum about 10 dB for the phantom-plus-handset antennas. The expected minimum accuracy level of the estimated MPCs is somewhere between 20-30 dB.

4.4   Nearfield estimation effects

Inside the car the closest obstacles or sources of scattering are within about 40 cm distance from the sounder array antenna center, see the car geometry in Figure 1. However, if we neglect the car ceiling in the direction of elevation angles above 60 deg, were this antenna is unlikely to detect MPCs, the closest obstacles are at distances beyond 60 cm. Thus, we would like to be able to estimate MPCs at least at this distance with reasonable angular and distance accuracy. To test this, we performed directional estimation with the plane-wave estimator on a synthetic test channel with a single vertically polarized point-source at zero elevation and distances between 0.3–10 meters. The result is shown in Figure 3. Here we used a theoretical model of the RxPUCA with Huygens sources and no mutual coupling.

As seen from the graph the single source estimation degrade as the source distance decreases, with artificial sources appearing in directions corresponding to a spherical wave-front expansion on a plane-wave spectrum. We also observe an apparent source distance slightly larger than the actual one as the source approaches. The face colors of the MPC circles in the graph show the estimated (apparent) additional distance to the source.

However, by looking at Figure 3 we also find that the ML estimation algorithm performs pretty good down to distances as low as 0.6 meters. This can be compared to the Rayleigh distance[2] ($2D^2/\lambda$ where D is the largest size of the antenna), which in our case is approximately 1.5 meters as marked in

---

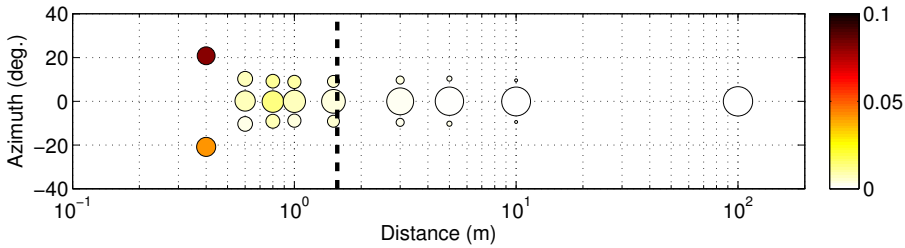[2]far-field or Fraunhofer region [18]

Figure 3: Estimated MPC azimuth angle to a single point source vs distance. The area of each circle is proportional to the MPC fractional power. The face colors of the circles show the estimated source distance minus the true test distance.

the graph. Thus, it does not seem impossible to estimate single sources with reasonable accuracy in our scenario, i.e., with a 0.3 m wide cylindrical array inside a common family car.

Now, what about angular resolution? To test this we add another source at the same distance as our first one but at a different angle. Since these two sources are at the same distance and we do not utilize the directional domain at Tx, the resolution in the far-field is simply the array beamwidth, i.e., roughly λ/D (rad.) or about 22 degrees. This effect is illustrated in Figure 4. From the graphs it is apparent that when the angular difference gets close to the resolution limit, the estimation is valid only at source distances beyond the far-field distance, but at 45 degrees angular difference the estimation resolves the two sources even somewhat closer than the far-field distance but with an increased estimation error.

4.5   Estimation residual

The residual or remaining part of the channel after subtraction of the estimated MPCs, represents antenna calibration and channel model mismatch errors that are not possible to resolve[3]. This level relative to the peak level of the impulse response is referred to as the estimation *accuracy*. With the MS array outdoors this level was about 20 dB after channel parameter estimation in both scenarios, but with the MS inside the car it was less than 10 dB. The latter depends (most certainly) on the channel model mismatch, and the question is whether these

---

[3]Non-resolvable MPC's are sometimes referred to as non-specular or diffuse multipath components (DMC) [13, 14]. In this work we make no distinction between specular and non-specular MPCs.

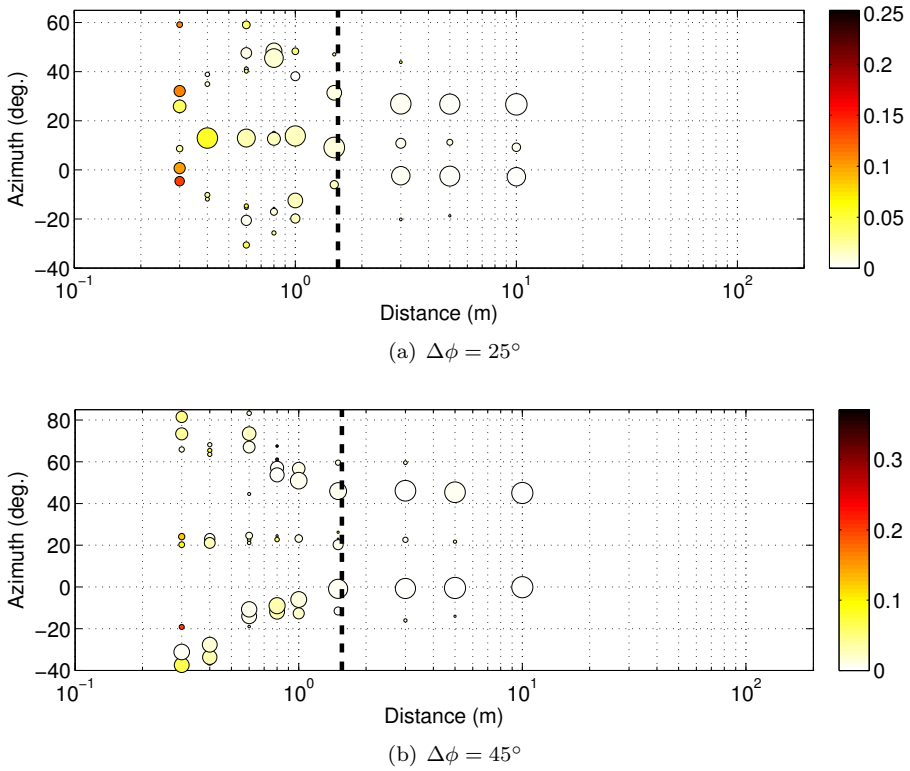(a) $\Delta\phi = 25°$

(b) $\Delta\phi = 45°$

Figure 4: Two estimated MPCs with different azimuthal separation $\Delta\phi$ vs true test source distance. The area of the circles is proportional to the fractional power. The colorbar show the estimated source distance relative the true test distance.

results are useful nevertheless. This is discussed below.

5 Comparison Between Model and Measurements

Based on the measured channels and the estimated directional channel parameters, the specific impact of the car presence in the outdoor-to-in-car channel can now be evaluated. But first we need to validate the method to be used.

5.1 Channel Matrix Element Magnitudes

A first step in the validation of both the direct measurements themselves, and the performance of the composite channel method (CCM), using the channel parameter estimations outside and inside the car, is to look at and compare the average received powers of individual antenna elements at the mobile (Rx) side. Here we let the average received power level for individual elements P_i at the receiver side be represented by the squared magnitude of the elements of the channel matrix $\mathbf{H}$ averaged over the TX antennas and the frequency as

$$P_i = \frac{1}{n_t, n_f} \sum_{j=1}^{n_t} \sum_{k=1}^{n_f} |H_{i,j,k}|^2 \tag{4}$$

In Table 3 the average power P_{col} at two selected columns of the RxPUCA is compared for the direct channel measurements P_{col}^m and the CCM calculations P_{col}^c. In general the differences between the CCM and the direct measured (DM) results are due to the truncation by the ray estimation process not catching all the measured channel energy, the limited estimation accuracy due to model errors (especially inside the car where a higher degree of cylindrical and/or spherical wave propagation are likely), and the limited antenna calibration accuracy. The preserved energies by the model were here found to be 92, 74, 83, and 59 percent in the four cases, respectively, i.e., in Scenario A outside and inside the car, and in Scenario B outside and inside the car[4]. This was found as the fraction between the synthetic and the measured overall average channel gains $\overline{P}_c/\overline{P}_m$ where

$$\overline{P}_{(m,c)} = \frac{1}{n_r, n_t, n_f} \sum_{i=1}^{n_r} \sum_{j=1}^{n_t} \sum_{k=1}^{n_f} |H_{i,j,k}^{(m,c)}|^2$$
$$= \frac{1}{n_f} \sum_{k=1}^{n_f} ||\mathbf{H}_k^{(m,c)}||_F^2 \tag{5}$$

---

[4]These figures depend to some extent on the parameter setting in the estimation process

where $\mathbf{H}_k = \mathbf{H}(f_k)$. Since we test the channel model with the same array antenna model (measurement data) that was used in the channel estimation process, the lost energy must be due to the estimation loss or residual if the antenna characterization is at least approximately correct and span the same dimensions (polarizations, number of elements and position). From Table 3 we find that the difference in average power level between the model and the measurements differs quite a bit for different test antenna columns in different channels. Naturally the error gets larger as the signal gets weaker. In the highly directive channels, i.e., A outside, A in car, and B outside, the difference is as low as 0.2 dB for co-polarized antennas when the antenna column are directed towards the main DoA (strongest signal), and as high as 3.8 dB in the worst case (cross polarization in A in car) when the column is turned away from the main DoA. In the NLOS case (B) inside the car, the difference is somewhat higher (and the signal weaker).

From these data we also observe that the cross polarization seems to increase significantly from outside to inside the car. This effect is underestimated by the model due to the inability (truncation) to estimate the weak cross polarized signals from opposite the main DoA.

In the next step this validation of the CCM is done also for the case with the phantom user and the four-antenna handset. In this case we also utilize the nine offset positions and the four horizontal rotations of the phantom outside and inside the car to improve statistics. The result is shown graphically in Figure 5 with the average power levels compared between the measured and the synthetic data on the ordinate for vertical polarization at the TX side, and with the four handset antennas and the four phantom rotations on the abscissa. Here the average power of the synthetic channels was normalized with respect to the directly measured channels outside the car. Thus, no power loss due to truncation of estimated MPC's are present.

Also here we find a good match between CCM and the direct measured data. The differences are, again, due to limited estimation accuracy, and here also the limited accuracy of the phantom-plus-handset antenna patterns due to reassembly of the user phantom and handset setup with non-identical bending of cables and positioning of the handset in the phantom hand. The mean received power, the difference, and the root-mean-square (rms) of the relative error are summed in Table 4 were the difference in mean is mainly due to the truncation loss and an additional cable loss of 2 dB from the antenna range measurement setup. The relative error is here taken as

$$\epsilon_i = \frac{P_i^c - P_i^m}{P_i^m},\tag{6}$$

where i represents a compound antenna element and phantom rotation index.

Table 3: Comparison of average received signal power between measurements and model for two array columns (weakest and strongest signal) of the test array (RxPUCA) in the four channels with separation w.r.t. co- and cross polarization of TX and RX antennas.

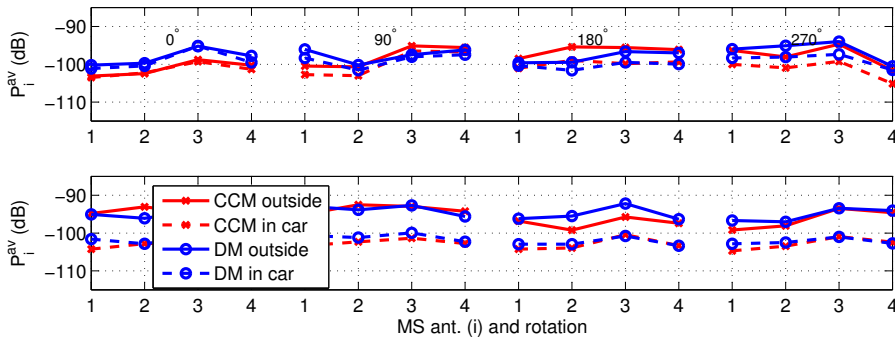| Scenario	ϕ_{col}	Pol.	P_{col}^m (dB)	P_{col}^c (dB)	Diff. (dB)
A outside	max	co	-74.3	-74.5	0.2
		cx	-91.2	-93.4	2.2
	min	co	-80.7	-81.2	0.5
		cx	-93.2	-96.3	3.1
A in car	max	co	-79.1	-79.3	0.2
		cx	-88.4	-91.7	3.3
	min	co	-83.2	-83.9	0.7
		cx	-89.3	-93.1	3.8
B outside	max	co	-76.6	-76.8	0.2
		cx	-87.1	-88.8	1.7
	min	co	-80.2	-81.0	0.8
		cx	-89.8	-92.2	2.4
B in car	max	co	-83.4	-84.6	1.2
		cx	-86.6	-90.0	3.3
	min	co	-84.3	-86.2	1.8
		cx	-88.3	-91.5	3.3

Figure 5: Average received signal powers of individual antenna elements of the phantom user with the smartphone mock-up for vertical polarization at the BS. The upper graph show the result in Scenario A and the lower in Scenario B.

Table 4: Average received power for the measurements and the model, differences, and the rms errors for the phantom-plus-handset case in the four scenarios.

Scen.	$\overline{\lvert H_{i,j}^m\rvert^2}$ (dB)	$\overline{\lvert H_{i,j}^c\rvert^2}$ (dB)	Δ_{dB}	σ_{dB}^2
A outside	-97.5	-101.8	4.3	0.15
A in car	-99.1	-104.5	5.4	0.06
B outside	-93.1	-98.9	5.8	0.04
B in car	-101.0	-107.1	6.1	0.01

The mean and the rms are calculated as

$$\overline{\epsilon} \;=\; \frac{1}{n_r n_{rot}} \sum_i^{n_r n_{rot}} \epsilon_i \tag{7}$$

$$\sigma_\epsilon^2 \;=\; \sqrt{\frac{1}{n_r n_{rot}} \sum_i^{n_r n_{rot}} (\epsilon_i - \overline{\epsilon})^2}, \tag{8}$$

and the transform to decibel is done as $\sigma_{dB}^2 = 10 \log_{10} |1 + \sigma_\epsilon^2|$. This is found to be very small which indicates a very good model match w.r.t average power of the synthetic channel, even though this apparent accuracy is partly an effect of the average power being not so sensitive to the antenna pattern and the phantom rotation. To a large extent it is still the efficiency of the individual antennas at the handset that sets the received power levels.

5.2   MIMO Eigenvalue Distribution

The most important statistical properties of a MIMO channel matrix regarding capacity performance are given by the singular values of the corresponding channel matrix. The squared singular values are equal to the eigenvalues of the channel covariance matrix

$$\boldsymbol{\lambda} = \mathrm{eig}\{\mathbf{H}\mathbf{H}^H\} \tag{9}$$

and represent signal gains of the spatial sub-channels. Again, to validate the directional channel parameter estimations and the composite channel approach, outside as well as inside the car, the sorted singular value distributions for two 32×32 test channels are plotted in Figure 6. These test matrices each array ring, 32 antenna ports of the 128 elements RxPUCA, is treated separately as four samples of the same channel. The singular value distributions are shown for both directly measured channels, and composite channel models with and without the presence of the car, in both cases with normalization to unit channel

gain (squared Frobenius norm). Naturally the composite channel data based on the estimated channel parameters are somewhat more "synthetic" with larger eigenvalue dispersion or, equivalently, less channel richness.

Apparently, there is a pretty good statistical match between the model and the measurements also inside the car for the stronger eigenvalues. The weaker eigenvalues are very unreliable and reflect measurement noise as well as measurement and model (estimation) errors. The number of estimated MPCs was here maximum $L = 100$.

In the next step this validation of the CCM is done also for the case with the phantom user holding a smartphone mock-up handset. In this case we utilize the nine offset positions and the four horizontal rotations of the phantom outside and inside the car to improve statistics. Here we allow ourselves to add an i.i.d. noise matrix $\mathbf{H}_w \sim \mathcal{CN}(\mathbf{0}, \sigma_w^2 \mathbf{I})$ to the synthetic channel matrix as

$$\mathbf{H}_c' = \mathbf{H}_c + \mathbf{H}_w. \tag{10}$$

By this procedure we compensate for inevitable receiver noise in the measurement system inherit in the direct measured data and indirect present in the synthetic channel by setting the lower limit of MPCs to be estimated. The noise power used in (10) was found from the channel measurements by comparing successive snapshots, resulting in $\sigma_w^2 = [18.5\ 16.9\ 26.9\ 19.0]$ dB below the average power of the direct measured SISO channels, i.e., $\overline{||\mathbf{H}_m||^2}_F / (n_r n_t \sigma_w^2)$. In the delay domain this corresponds to a peak-to-noise floor level of the impulse response $\mathrm{SNR}_{IR} \approx 40$ dB.

The result is shown in Figure 7. At the Tx side a selection of four vertically polarized antenna elements with $\lambda/2$ spacing was chosen from one row of the TxPURA. The match between the synthetic channel and the measured is close for all four singular values in all four scenarios. Especially inside the car the match is almost perfect in the NLOS case (Scenario B). This may partially be a consequence of that estimation errors provide an apparent realistic spatially rich channel in this specific case, the one with most rich scattering, see Figure 2. Otherwise, the additive noise has a minor effect on the result so the main difference between the synthetic and the measured channels is the lack of richness in the synthetic channel that stems from the inability to estimate enough MPCs due to limited SNR and error level. To improve these results we need higher SNR in the measurements and perhaps also higher accuracy in the antenna characterization and system calibration including cables etc.

The addition of the noise matrix $\mathbf{H}_w$ in this context shall *not* be mistaken as an additive part of the channel model. The improved match with the direct measured channel is merely a consequence of the imperfect measurement system (receiver noise), but may also compensate for error sources like antenna array
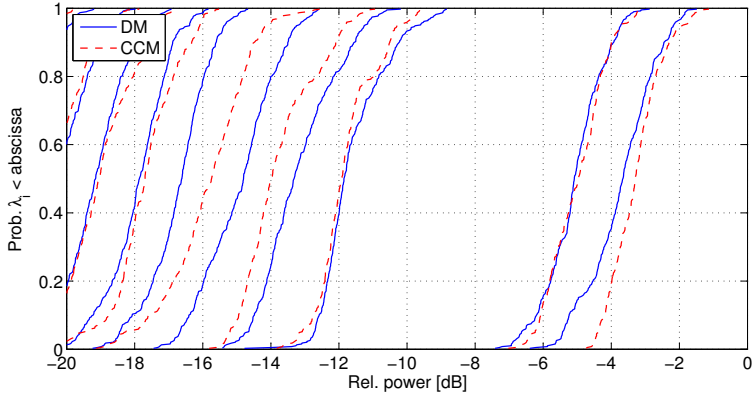
(a) Scen. A outside
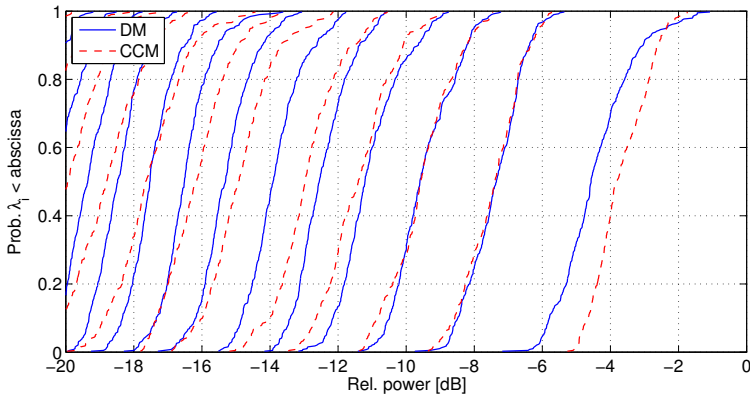
(b) Scen. B in car

Figure 6: Ordered squared singular value distributions of 32×32 channels for direct measured (solid), and CCM (dashed) with the RxPUCA in the two most different scenarios. Note that only the strongest singular values are visible.
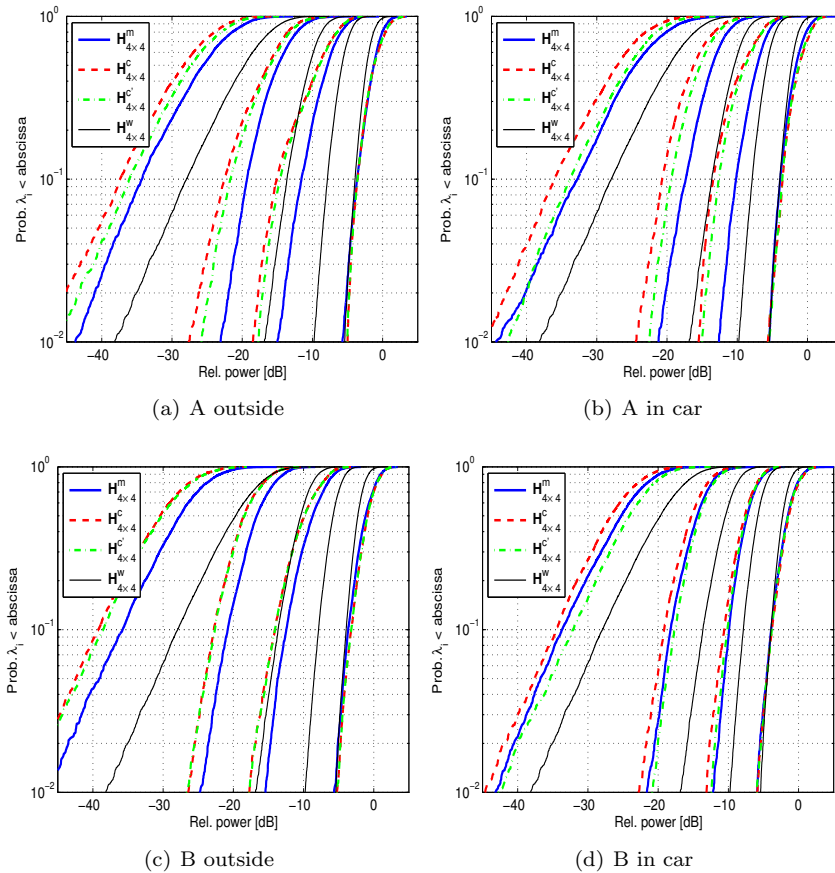
(a) A outside

(b) A in car

(c) B outside

(d) B in car

Figure 7: Ordered squared singular value distributions of 4×4 channels for direct measured (m), and synthetic with the phantom-plus-handset $(c$ and $c')$, in both scenarios outside and inside the car. For comparison the distribution of a complex Gaussian channel is shown (w).

characterization and cable calibration errors, as well as for non-resolvable *spatially white* channel components. In [13,14] the channel model itself is divided into a specular and a non-specular part, where the latter part (dense multipath) encounters possibly correlated non-specular channel components that are estimated separately. Here we persist in using the spectral channel model in (1) built up by classical independent specular components that may be resolvable or not depending on the quality of the measurement setup and the estimator algorithm. In [4] higher precision in similar measurements provided the possibility to extract a higher amount of specular channel components which showed an increased match between the synthetic and the direct measured channels as the number of specular components increased. This effect was not reached by adding spatially white noise.

6   How the User and the Car Affect System Performance

Since the composite channel model based on the MPC estimations work well in predicting the statistical properties of the MIMO channel, the tool can be used to extract and evaluate specifically how the user and the car affect system performance without further measurements. Some of these results were presented in [15], but now by utilizing the channel modeling tool it is also possible to separate the user and the car effects by comparing the synthetic channels for the handset plus user phantom with new channel calculations with previously measured handset only antenna patterns (as was done in [4] in an office environment). The handset patterns are first translated and rotated to the same position as if they were in the hand of the user phantom. In a previous investigation of user effects it was found that one of the main characteristics of the user body was an increase in correlation between received signals from the handset antennas [4], in turn affecting system properties such as diversity and channel capacity.

6.1   Antenna Correlation in Channel

The antenna (signal) correlation can be found directly from the direct measurements and was presented in [15], but here we also want to compare with the results found by CCM. The correlation matrix with entries $R_{i,j}$ denotes the correlation between signals at receive antenna ports i and j and can be estimated

as the mean over frequency samples[5] of the sample covariance matrix

$$\mathbf{R} = \frac{1}{n_f n_t} \sum_{k=1}^{n_f} \mathbf{H}(f_k)\mathbf{H}^H(f_k) \tag{11}$$

giving the estimated complex correlation coefficient with the proper normalization as

$$\rho_{i,j} = \frac{R_{i,j}}{\sqrt{R_{ii}R_{j,j}}} \tag{12}$$

Figure 8 shows the cumulative distribution of the magnitude of the complex correlation coefficients computed according to (12), where the ensemble is the slow (shadow) fading distribution, i.e., the four phantom rotations, and the nine offset locations. In the figure the correlation coefficients from the model ("CCM´´"), with and without the noise compensations from (10), and from the direct measurements for the ensemble of $\rho_{i,j}$ are compared for all $i \neq j$. The presence of the car decreases the antenna correlation in the test channels, most likely due to increased scattering "richness" inside the car [15]. This effect is also reflected by the synthetic CCM data even though these data show higher correlation in general. Nevertheless, we may conclude that the effect of the car is well caught by the model. The maximum difference in average received power between antenna elements was here about 2.5 dB, a figure sometimes referred to as antenna mismatch (not to be confused with impedance mismatch).

6.2 Diversity and Capacity Gain

A summary of the maximum-ratio combining (MRC) diversity gains and the capacity (or spatial multiplexing) gains are presented in Table 5. Here the diversity gain (DG) is taken as the ratio of the combined signal power of the two strongest (DG2) and all four (DG4) antennas, to the strongest branch single antenna signal power at the 1% outage level. This diversity gain is also referred to as the apparent diversity gain [20] and seem to slightly overestimate the actual diversity gain [21, Fig. 11], were the latter definition refers the gain to a reference case with a truly isolated single antenna and, thus, omits the influence of mutual coupling by the surrounding terminated elements in our case. This effect is here neglected.

The channel capacity is calculated from the eigenvalues of the normalized channel matrix as

$$C = \sum_{i=1}^{r} \log_2(1 + \gamma_i \lambda_i) \tag{13}$$

---

[5]assuming ergodicity in frequency and time, i.e., averaging over the ensemble is equivalent to averaging over time- and frequency-samples [19]
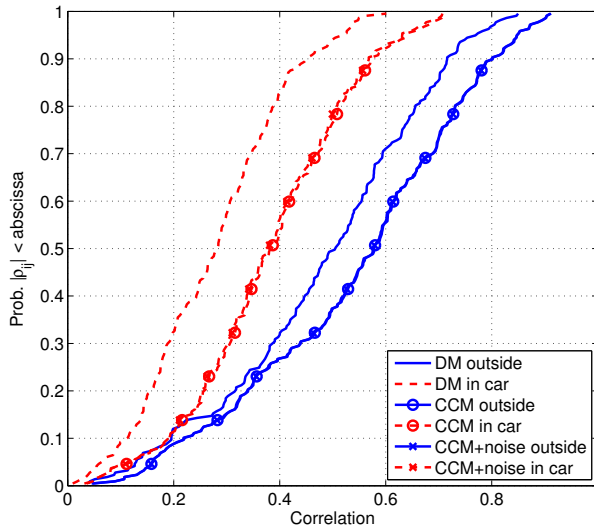
Figure 8: Cumulative distribution of the estimated MS antenna correlation coefficient for the phantom-plus-handset outside and inside the car in Scenario B (NLOS) for direct measurements (DM) and synthetic (CCM) results.

Table 5: Summary of diversity gain (dB) and capacity gain (bits/s/Hz) for the different scenarios and configurations.

Scen. A/B	Outside no user	Outside with user	In car no user	In car with user
DG2 (1%)	10.1/10.7	9.2/9.7	9.9/10.3	9.6/10.2
DG4 (1%)	16.0/17.3	14.4/15.2	16.5/17.2	14.8/16.8
ECG 4×2	2.0/2.4	1.7/2.4	2.4/2.7	2.1/2.6
OCG 4×2	2.3/2.1	1.8/1.6	2.5/2.1	1.8/2.1
ECG 4×4	4.1/4.7	3.5/4.6	4.7/5.5	4.4/5.2
OCG 4×4	3.6/4.3	3.3/4.0	4.4/4.9	4.2/4.7

where r is the rank of $\mathbf{H}$, and γ_i is the SNR after power allocation (by waterfilling assuming channel knowledge at the Tx) to the sub-channel corresponding to λ_i and with SNR= $\sum_{i=1}^{r} \gamma_i$. The channel matrix is normalized with the square-root of the SISO channel power averaged over the sample space (here the frequency samples, rotations and small-scale translations) in each scenario and handset/user/car configuration. Thus, the average user efficiency and car penetration loss is omitted and only statistical and individual antenna properties of the channel are considered.

From the distribution of C over the sample space, the ergodic capacity gain (ECG) is taken as the difference between the mean MIMO capacity and the mean of the best SIMO capacity, while the outage capacity gain (OCG) is taken at 10% outage level. The 4×4 channel matrix is formed by selecting four vertically polarized antenna elements in the bottom row with one wavelength spacing at the Tx, and in the 4×2 case the two single Rx antennas that provide the highest overall capacity is selected. The SNR was set to 10 dB.

The diversity and capacity results in Table 5 show only minor effects of the user and the car environments when the impact of body loss and car penetration loss are absent. Both the diversity gain and the capacity gain are somewhat higher in Scenario (B) compared to the Scenario (A). The user presence seems to have a negative impact on both these measures which were also found in [4], while the car environment increases the performance of spatial multiplexing up to 1.1 bits/s/Hz for the 4×4 system.

7   Conclusions

The purpose of this investigation of an outdoor-to-in-car radio channel at 2.6 GHz has mainly been two-fold: i) to investigate the validity of a MIMO composite channel model (CCM) formed by a combination of a the directional

propagation channel and the far-field radiation patterns of array antennas, with respect to MIMO performance, and ii) to evaluate the possibility to (accurately enough) perform directional channel estimation in the close confined car environment.

Two outdoor measurement campaigns have been performed where, specifically, the influence of a car is considered at the mobile side.

From the measurements with a cylindrical array antenna, directional channel parameter estimation was performed to form the propagation channel model as a part of the composite channel model. Combined with measured antenna patterns of the handset-plus-user it is found that this channel model produces channel properties such as path loss and channel statistics very similar to what are found by the direct measurements with the handset-plus-user in the channel. The composite channel model shows lower eigenvalue dispersion and higher antenna branch correlation as compared to the direct measurements. This is assumed to be an effect of the limited channel parameter resolution due to measurement noise and calibration errors.

The main challenge with the investigation was the directional estimation inside the car where parts of the car and, thus, possible sources of interaction (scattering) are within the far-field or Rayleigh distance of the antenna. Tests of the estimation algorithm on a single point source and two separated (in angle) point sources at a certain distance with a representative theoretic array antenna (to avoid antenna array calibration errors) show potential problems as the sources get within distances from the antenna about the size of the car. Despite this violation we find that the directional estimation inside the car produces reliable results, both regarding the angular distribution of the MPCs, as well as the singular value distributions of the composite channel. Thus, we conclude that the main specular components of the channel seem to account also for the most important statistical properties, and that the CCM *can* be used to model the outdoor-to-in-car channel.

Finally, with the CCM at hand, the specific influence of the car and the user was evaluated both separately and in combination. Apart from the penetration loss of the car (in average between 2-8 dB) or in an interference-limited scenario, our results show little influence of the user and the car on the channel. Both diversity gain and capacity gain are found to be slightly higher in Scenario B compared to Scenario A, the user seems to decrease these measures, while the car environment increases the capacity (at fixed SNR) by up to 1.1 bits/s/Hz for the 4×4 system.

Acknowledgment

References

[1] M. Steinbauer, A. F. Molisch, and E. Bonek, "The double-directional radio channel," *IEEE Antennas Propagat. Mag.*, vol. 43, no. 4, pp. 51–63, Aug. 2001.

[2] J. A. Fessler and A. O. Hero, "Space-alternating generalized expectation-maximization algorithm," *IEEE Trans. Signal Processing*, vol. 42, no. 10, pp. 2664–2677, Oct. 1994.

[3] F. Harrysson, J. Medbo, A. F. Molisch, A. J. Johansson, and F. Tufvesson, "The composite channel method: Efficient experimental evaluation of a realistic MIMO terminal in the presence of a human body," in *IEEE Veh. Technol. Conf. VTC 2008-Spring*, Singapore, pp. 473–477, May 2008.

[4] ——, "Efficient experimental evaluation of a MIMO handset with user influence," *IEEE Trans. Wireless Commun.*, vol. 9, no. 2, pp. 853–863, Feb. 2010.

[5] A. F. Molisch, M. Steinbauer, M. Toeltsch, E. Bonek, and R. S. Thomä, "Capacity of MIMO systems based on measured wireless channels," *IEEE J. Select. Areas Commun.*, vol. 20, no. 3, pp. 561–569, April 2002.

[6] P. S. Suvikunnas, J. Villanen, K. Sulonen, C. Icheln, J. Ollikainen, and P. S. Vainikainen, "Evaluation of the performance of multi-antenna terminals using a new approach," *IEEE Trans. Instrum. Meas.*, vol. 55, no. 5, pp. 1804–1813, Oct. 2006.

[7] J. Medbo and F. Harrysson, "Efficiency and accuracy enhanced super resolved channel estimation," in *Proceedings of the 6th European Conference on Antennas and Propagation (EuCAP)*, Prague, Czech Republic, March 2012.

[8] K. Haneda, J.-I. Takada, and T. Kobayashi, "Experimental evaluation of a SAGE algorithm for ultra wideband channel sounding in an anechoic chamber," in *Ultra Wideband Systems, 2004. Joint UWBST IWUWBS. 2004 International Workshop on*, Kyoto, Japan, pp. 66–70, May 2004.

[9] M. Landmann and T. Jun-Ichi, "On the plane wave assumption in indoor channel modelling," in *IEICE Society Conference*, Sapporo, Japan, Sept. 2005.

[10] K. Haneda, J.-I. Takada, and T. Kobayashi, "A parametric UWB propagation channel estimation and its performance validation in an anechoic

chamber," *IEEE Trans. Microwave Theory Tech.*, vol. 54, no. 4, pp. 1802–1811, June 2006.

[11] J. Medbo, M. Riback, H. Asplund, and J.-E. Berg, "MIMO channel characteristics in a small macrocell measured at 5.25 GHz and 200 MHz bandwidth," in *IEEE Veh. Technol. Conf. VTC 2005-Fall*, vol. 1, Dallas, TX, pp. 372–376, Sept. 2005.

[12] J. Medbo, H. Asplund, J.-E. Berg, and N. Jaldén, "Directional channel characteristics in elevation and azimuth at an urban macrocell base station," in *Antennas and Propagation (EuCAP), Proceedings of the 6th European Conference on*, Prague, Czech Republic, March 2012.

[13] A. Richter, "Estimation of radio channel parameters: Models and algorithms," Ph.D. dissertation, TU Ilmenau, Ilmenau, Germany, May 2005.

[14] M. Landmann, "Limitations of experimental channel characterisation," Ph.D. dissertation, TU Ilmenau, Ilmenau, Germany, May 2008.

[15] F. Harrysson, T. Hult, and F. Tufvesson, "Evaluation of an outdoor-to-in-car radio channel with a four-antenna handset and a user phantom," in *IEEE Veh. Technol. Conf. VTC 2011-Fall*, San Francisco, CA, Sept. 2011.

[16] A. F. Molisch, *Wireless Communications.* Chichester, U.K.: IEEE Press - Wiley, 2005.

[17] B. H. Fleury, "First- and second-order characterization of direction dispersion and space selectivity in the radio channel," *IEEE Trans. Inform. Theory*, vol. 46, no. 6, pp. 2027–2044, 2000.

[18] IEEE Std 145-1993, "IEEE standard definition of terms for antennas," Antenna Standards Committee of the IEEE Antennas and Propagation Society, IEEE, March 1993.

[19] R. Kattenbach, "Characterization of time-variant indoor radio channels by means of their system and correlation functions," Ph.D. dissertation, Univ. GhK Kassel, Shaker Verlag, Aachen, Germany, 1997, (in German).

[20] P.-S. Kildal and K. Rosengren, "Correlation and capacity of MIMO systems and mutual coupling, radiation efficiency, and diversity of their antennas: Simulations and measurements in a reverberation chamber," *IEEE Commun. Mag.*, vol. 42, pp. 104–112, Dec. 2004.

[21] V. Plicanic, B. K. Lau, A. Derneryd, and Z. Ying, "Actual diversity performance of a multiband diversity antenna with hand and head effects," *IEEE Trans. Antennas Propagat.*, vol. 57, no. 5, pp. 1547 –1556, May 2009.